AWARD NUMBER: W81XWH-15-2-0006

TITLE: Mechanisms of Resistance to Chemotherapies Targeting BRCA-Mutant Breast Cancer

PRINCIPAL INVESTIGATOR: Dr. Andre Nussenzweig

CONTRACTING ORGANIZATION: The Geneva Foundation
Tacoma, WA 98402

REPORT DATE: December 2016

TYPE OF REPORT: Annual

PREPARED FOR: U.S. Army Medical Research and Materiel Command
Fort Detrick, Maryland 21702-5012

REPORT DOCUMENTATION PAGE

Form Approved
OMB No. 0704-0188

1. REPORT DATE *(DD-MM-YYYY)*	2. REPORT TYPE	3. DATES COVERED *(From - To)*
December 2016	ANNUAL	01 Dec 2015 – 30 Nov 2016

4. TITLE AND SUBTITLE

Mechanisms of Resistance to Chemotherapies Targeting BRCA-Mutant Breast Cancer

5a. CONTRACT NUMBER

5b. GRANT NUMBER
W81XWH-15-2-0006

5c. PROGRAM ELEMENT NUMBER

6. AUTHOR(S)
Andre Nussenzweig, Ph.D.

Email: jmolstre@genevausa.org

5d. PROJECT NUMBER

5e. TASK NUMBER

5f. WORK UNIT NUMBER

7. PERFORMING ORGANIZATION NAME(S) AND ADDRESS(ES)

The Geneva Foundation
917 Pacific Ave, Suite 600
Tacoma, WA 98402

8. PERFORMING ORGANIZATION REPORT NUMBER

9. SPONSORING / MONITORING AGENCY NAME(S) AND ADDRESS(ES)
U.S. Army Medical Research and Materiel Command
Fort Detrick, Maryland 21702-5012

10. SPONSOR/MONITOR'S ACRONYM(S)
USAMRAA

11. SPONSOR/MONITOR'S REPORT NUMBER(S)

12. DISTRIBUTION / AVAILABILITY STATEMENT
Approved for public release; distribution unlimited

13. SUPPLEMENTARY NOTES

14. ABSTRACT

This research proposal for the BRCP Idea Expansion Award involves a detailed study of the underlying mechanisms of drug resistance in BRCA1 and BRCA2 deficient cells through the genetic manipulation of the major players that mediate homologous recombination and non-homologous end joining DNA repair pathways. These studies will serve as a foundational data set in determining the importance of DNA repair pathways in acquiring resistance to breast and ovarian cancer chemotherapies. Because drug resistance is an inescapable feature of all cancer treatments, an understanding of the causal mechanisms of resistance will undoubtedly provide new opportunities and susceptible targets in cancer therapies.

15. SUBJECT TERMS

Nothing listed

16. SECURITY CLASSIFICATION OF:			17. LIMITATION OF ABSTRACT	18. NUMBER OF PAGES	19a. NAME OF RESPONSIBLE PERSON
a. REPORT	b. ABSTRACT	c. THIS PAGE			USAMRMC
U	U	U	UU	52	19b. TELEPHONE NUMBER *(include area code)*

Standard Form 298 (Rev. 8-98)
Prescribed by ANSI Std. Z39.18

Table of Contents

Page

1. INTRODUCTION: Narrative that briefly (one paragraph) describes the subject, purpose and scope of the research.

In ongoing work being performed in support of the BCRP Idea Expansion Award, we have hypothesized that restoration of homologous recombination (HR) is a critical driver of chemo-resistance in BRCA1/2 mutated breast cancers. Earlier work provided evidence for a novel mechanism of HR restoration, through the inactivation of proteins functioning in an alternate DNA repair pathway called non-homologous end joining (NHEJ). Loss of NHEJ proteins, such as 53BP1, restored normal HR activity in BRCA1 deficient cells and rendered these cells resistant to chemotherapeutic agents. Under the aegis of the Idea Expansion Award, we have discovered a novel and unexpected mechanism of drug resistance in BRCA-deficient cancers that involves the loss of the 53BP1-interacting protein PTIP that operates independently of the re-establishment of HR. Overall, the major aim of this research is to understand the manifold routes that lead to acquired resistance in breast cancer treatment and how altering the balance between NHEJ, HR and other pathways can be exploited to overcome the Achilles heel of acquired resistance.

2. KEYWORDS: Provide a brief list of keywords (limit to 20 words).

1. 53BP1: p53 Binding Protein 1
2. Brca1 & 2: Breast cancer type 1 & 2 susceptibility protein, tumor suppressor
3. BRCT domain: BRCA1 Carboxy Terminal Domain
4. CD19: Cluster of Differentiation 19
5. CRE: Causes Recombination
6. DSB: Double Strand Breaks
7. H2AX- a variant of Histone 2A, a core chromatin protein HR: Homologous Recombination
8. MEFs: Mouse Embryonic Fibroblasts
9. NHEJ: Non-Homologous End Joining
10. PA1: PTIP-Associated protein 1
11. PALB2: PArtner and Localizer of BRCA2
12. PARP: Poly ADP-Ribose Polymerase
13. PARPi: Poly ADP-Ribose Polymerase Inhibitor
14. PTIP: Pax Transactivation Domain-Interacting Protein
15. RAP80: Receptor-Associated Protein 80
16. RIF1: RAP1 Interacting Factor 1
17. RNF8: Ring Finger protein 8
18. RNF168: Ring Finger protein 168
19. RPA: Replication Protein A
20. TCGA: The Cancer Genome Atlas

3. ACCOMPLISHMENTS: The PI is reminded that the recipient organization is required to obtain prior written approval from the USAMRAA Grants Officer whenever there are significant changes in the project or its direction.

- What were the major goals and objectives of the project?
- What was accomplished under these goals?
- What opportunities for training and professional development did the project provide?
- How were the results disseminated to communities of interest?
- What do you plan to do during the next reporting period to accomplish the goals and objectives?

What were the major goals of the project?

In this proposal, we outlined two major Specific Aims and Goals.

In **Specific Aim 1**, we proposed the use of a genetic approach to define interactions between NHEJ and HR effectors that regulate DNA repair pathway selection (24 months). In specific **Sub-Aim 1a**, we intend to test the hypothesis

that elevated levels of chromatin bound 53BP1 converts wild type cells to a 'BRCA-deficient' state in the context of drug sensitivity and genome stability. In specific **Sub-Aim 1b**, the importance of PTIP associated proteins (PA1 and MLL4) and the functional domains within PTIP necessary for HR reconstitution are to be evaluated by *in vivo* experimentation.

Overall, in **Specific Aim 2**, we proposed testing the contribution of the 53BP1 associated protein (PTIP) in influencing repair pathway selection and to also computationally interrogate clinical data sets together with data acquired from murine models to understand the mechanisms of chemo-resistance in BRCA1- and BRCA2-mutated cancers (24 months). In specific **Sub-Aim 2a**, we are testing the hypothesis that PTIP can influence repair pathway selection and drug sensitivity. In specific **Sub-Aim 2b**, we plan on using gene expression data and other genome-wide data sets from clinical databases to implicate known (and novel) proteins involved in the regulation of chemoresistance.

What was accomplished under these goals?

A. RNF168 and 53BP1 levels modulate PARP inhibitor-induced genome instability in BRCA1 deficient cells

In our 2015 Annual Report, we addressed how interactions between NHEJ and HR proteins influenced repair pathway selection (**Specific Aim 1**). Specifically, we asked whether increased expression of RNF168, a RING domain E3-ubiquitin ligase or 53BP1 impacted physiological NHEJ, such as immunoglobulin class switch recombination (CSR), versus mutagenic NHEJ (defined as NHEJ conducted during S phase which typically results in genome instability). We found that the anti-resection activities of 53BP1 are rate-limiting for mutagenic NHEJ but not for physiological CSR. An implication of our results is that deregulation of the RNF168/53BP1 pathway could alter the chemosensitivity of BRCA1 deficient tumors. The work leading to the conclusions detailed above was published in May 2015: **'*Ectopic expression of RNF168 and 53BP1 increases mutagenic but not physiological non-homologous end joining'***. Zong D, Callén E, Pegoraro G, Lukas C, Lukas J, Nussenzweig A. *Nucleic Acids Res*. 2015 May 26;43(10):4950-61.

A1. Studies being conducted currently are designed to probe functional interactions between RNF168 and BRCA1/2 in the DNA damage response and tumorigenesis. The repair of DNA double strand breaks (DSBs) by homologous recombination is mediated by a complex containing BRCA2 and PALB2 (PArtner and Localizer of BRCA2), which loads the recombinase Rad51 onto resected DNA ends in order to initiate strand invasion into the intact repair template present in the sister chromatid. We are exploring the presence of an alternative pathway for the recruitment of the PALB2/BRCA2 complex that may be dependent on the ubiquitin ligase activity of RNF168. Specifically, we are interested in characterizing the molecular interactions between RNF168 and PALB2/BRCA2 using biochemical assays and aim to identify the domains in RNF168 and PALB2 that are required for this interaction. We also plan to use mass spectrometry to identify any hitherto unknown interaction partners of RNF168 and characterize their importance to genome maintenance.

It is well known that patients with germline BRCA1 mutations are dramatically predisposed to the development of mammary and ovarian tumors. The reason(s) for this remarkable tissue specificity is not known. One possibility that has not been evaluated is whether differences in the expression of certain genes in mammary/ovarian tissues may render them especially vulnerable to the loss of a single BRCA1 allele. We are in the process of investigating whether BRCA1-associated tumors arise from lower expression of RNF168 compared to other cell types. If BRCA1 heterozygous cells deleted for RNF168 are exquisitely sensitive to clinically used chemotherapeutic agents, including PARP inhibitors and cisplatin, this raises the possibility that *BRCA1-mutated tumors* with low expression levels of RNF168 may be uniquely responsive to platinum-based and PARPi treatment. We are in the midst of testing this hypothesis through data mining of TCGA databases and the use of appropriate mouse tumor models that mimic human mammary tumorigenesis (**Specific Aim 2**, **Sub-Aim 2b**).

B. Replication fork protection by the prevention of nascent DNA strand degradation is strongly co-related with chemoresistance in BRCA1/2-deficient cells

Cells deficient in the BRCA1 and BRCA2 genes have a reduced capacity to repair DNA double-strand breaks by homologous recombination and consequently are hypersensitive to DNA-damaging agents, including cisplatin and poly(ADP-ribose) polymerase (PARP) inhibitors. In work germane to the specific aims of this grant, we showed that

loss of the MLL3/4 complex protein, PTIP, protects BRCA1/2-deficient cells from DNA damage and rescued the lethality of BRCA2-deficient embryonic stem cells. However, PTIP deficiency did not restore homologous recombination activity at double-strand breaks. Instead, its absence inhibited the recruitment of the MRE11 nuclease to stalled replication forks, which in turn protected nascent DNA strands from extensive degradation. More generally, acquisition of PARP inhibitors and cisplatin resistance was associated with replication fork protection in BRCA2-deficient tumour cells that did not develop BRCA2 reversion mutations. Disruption of multiple proteins, including PARP1 and CHD4, led to the same end point of replication fork protection, highlighting the complexities by which tumour cells evade chemotherapeutic interventions and acquire drug resistance.

In a parallel and complementary study, we examined the effect of PARPi (olaparib) on HR-proficient cells. Olaparib pretreatment, PARP1 knockdown or Parp1 heterozygosity of BRCA2cko/ko mouse embryonic stem cells (mESCs), carrying a null (ko) and a conditional (cko) allele of BRCA2, resulted in viable Brca2ko/ko cells. PARP1 deficiency did not restore HR in Brca2ko/ko cells, but instead protected stalled replication forks from MRE11-mediated degradation through its impaired recruitment. The functional consequence of PARP1 heterozygosity on BRCA2 loss is demonstrated by a significant increase in tumorigenesis in BRCA2cko/cko mice. Thus, while olaparib efficiently killed BRCA2-deficient cells, we demonstrated that it can also contribute to synthetic viability if PARP is inhibited before BRCA2 loss.

The work leading to the conclusions detailed above were published in July 2016: '*Replication fork stability confers chemoresistance in BRCA-deficient cells'*. Ray Chaudhuri A, Callen E, Ding X, Gogola E, Duarte AA, Lee JE, Wong N, Lafarga V, Calvo JA, Panzarino NJ, John S, Day A, Crespo AV, Shen B, Starnes LM, de Ruiter JR, Daniel JA, Konstantinopoulos PA, Cortez D, Cantor SB, Fernandez-Capetillo O, Ge K, Jonkers J, Rottenberg S, Sharan SK, Nussenzweig A.
Nature. 2016 Jul 20;535(7612):382-7. doi: 10.1038/nature18325. PubMed PMID: 27443740; PubMed Central PMCID: PMC4959813.

and in Aug 2016: *'Synthetic viability by BRCA2 and PARP1/ARTD1 deficiencies'*. Ding X, Ray Chaudhuri A, Callen E, Pang Y, Biswas K, Klarmann KD, Martin BK, Burkett S, Cleveland L, Stauffer S, Sullivan T, Dewan A, Marks H, Tubbs AT, Wong N, Buehler E, Akagi K, Martin SE, Keller JR, Nussenzweig A, Sharan SK.
Nat Comm. 2016 Aug 8;7:12425. doi: 10.1038/ncomms12425. PubMed PMID: 27498558; PubMed Central PMCID: PMC4979061.

The **Significant Results and Key Outcomes** summarized below highlight data germane to **Specific Aim 2** outlined in this proposal.

B1. PTIP loss protects RFs in Brca-deficient cells

Given that BRCA1 and BRCA2 have been ascribed DSB-independent functions during replication stress and since MRE11 has been implicated in mediating replication fork (RF)

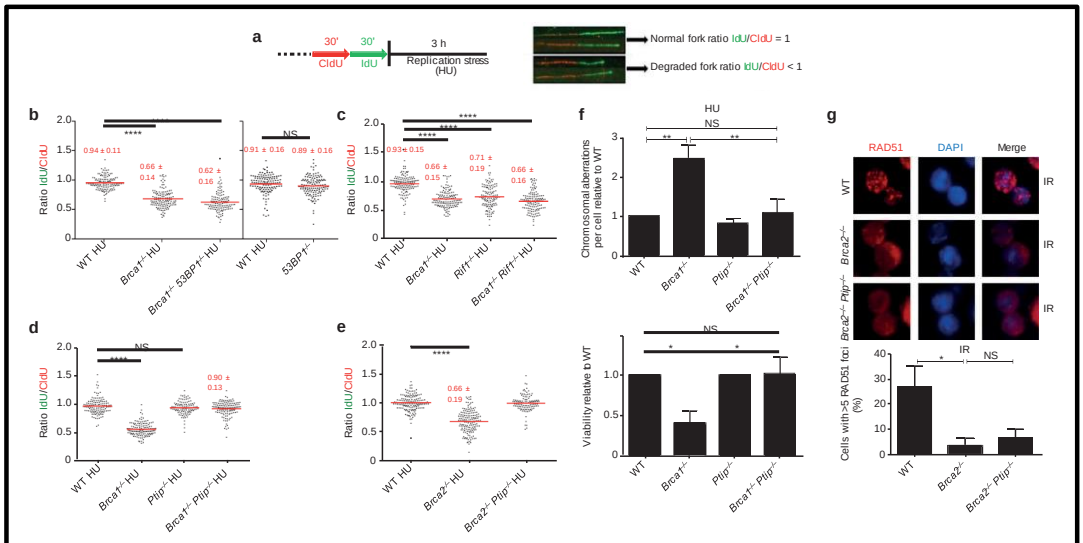

Figure 1 | Loss of *Ptip* in *Brca1/2*-deficient B cells protects nascent DNA from degradation without restoring HR. a, Schematic for labelling B cells with CldU and IdU. **b**–**e**, Ratio of IdU versus CldU upon HU treatment. Numbers in red indicate the mean ± s.d. (NS, not significant, $****P \leq 0.0001$, Mann–Whitney test). One hundred and twenty-five replication forks were analysed for each genotype. **f**, Genomic instability (top) and viability upon HU treatment (bottom) relative to WT upon 6 h of 10 mM HU treatment. ($**P \leq 0.001$, $*P \leq 0.05$, unpaired *t*-test.) Fifty metaphases were analysed. **g**, Representative images (top) and quantification (below) of irradiation (IR)-induced RAD51 foci. $*P \leq 0.05$, unpaired *t*-test ($n = 120$ cells examined). Experiments were repeated three times.

degradation in cell lines, we tested whether primary cells deficient in BRCA1 or BRCA2 also showed degradation of nascent replication tracts. We therefore conditionally inactivated BRCA1 and BRCA2 in B lymphocytes (Brca1f/fCD19Cre; Brca2f/fCd19Cre). B cells were sequentially labelled with CldU-(red) followed by IdU-(green), after which the active RFs were stalled with hydroxyurea (HU) (**Fig. 1a**). The relative shortening of the IdU tract after HU treatment serves as a measure of RF degradation (**Fig. 1a**). Upon HU treatment, wild-type (WT) cells showed a mean IdU/CldU tract ratio close to 1 (**Fig. 1b**). However, Brca1- and Brca2-deficient B cells exhibited a 30–45% reduction in the IdU tract length (**Fig. 1b–e**). Brca1/Ptip doubly deficient cells exhibited 2.4-fold fewer chromosomal aberrations and increased viability compared with Brca1−/− (**Fig. 1f**), suggesting that ***PTIP has functions at stalled RFs distinct from its DSB-dependent interactions with 53BP1 and RIF1***.

B2. PTIP loss rescues lethality of Brca2-null ESCs

Loss of Brca2 in ESCs is incompatible with cell survival. To test whether PTIP deficiency could promote ESC survival, we knocked down PTIP in mouse ESCs, which have one null and one conditional allele of Brca2 (Brca2f/−, **Fig. 2a**). After CRE transfection in Brca2f/− ESCs and selection in HAT medium, very few resistant colonies were obtained and these remained Brca2f/− rather than Brca2-null, reflecting the essential role of BRCA2 in ESC viability (**Fig. 2b**). Strikingly, 12.5% and 5% of the HAT-resistant colonies were Brca2-null when targeted by Ptip short hairpin RNAs (shRNAs) 1 and 2 respectively (**Fig. 2b**). Consistent with our analysis of Brca2−/−Ptip−/− B cells (**Fig. 1g**), irradiation-induced RAD51 foci formation was defective in Brca2/Ptip-deficient ESCs (**Fig. 2c, d**). Moreover, while efficient gene targeting to the Pim-1 locus was observed in WT ESCs using a promoterless hygromycin cassette (100% of the hygromycin-resistant WT clones were targeted integrations), we did not observe a single targeted clone in Brca2/Ptip-deficient ESCs (**Fig. 2e**) indicative of defective HR. Nevertheless, stalled RFs in PTIP-deficient Brca2−/− ESCs displayed RF protection compared with Brca2 hypomorphic mutant ESCs (Y3308X)17 (**Fig. 2f**). ***Thus, deficiency in PTIP protects RFs from degradation and rescues the lethality of Brca2 knockout ESCs without restoring DSB-induced HR***.

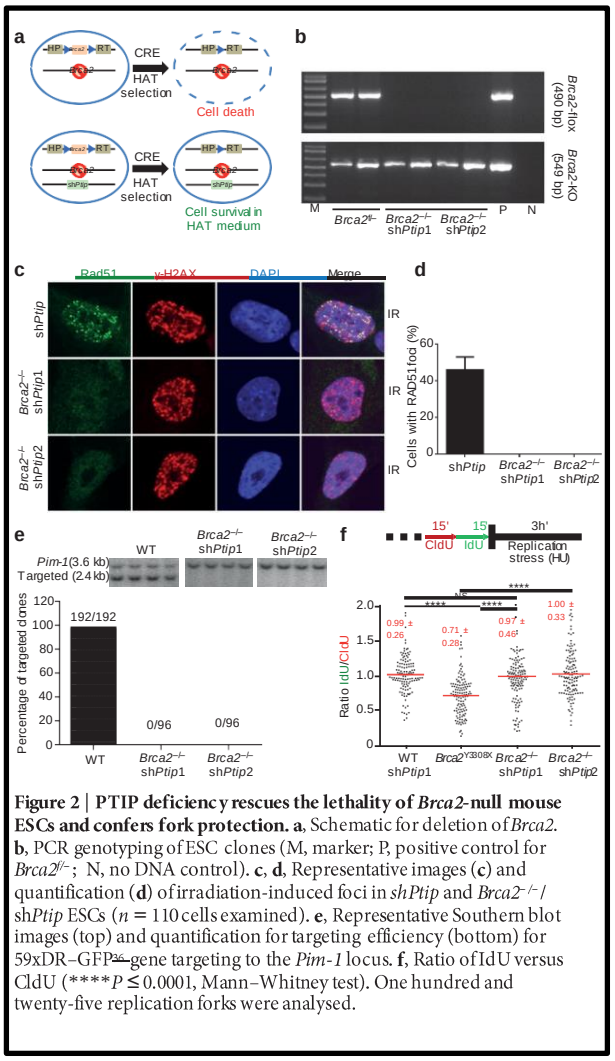

Figure 2 | PTIP deficiency rescues the lethality of *Brca2*-null mouse ESCs and confers fork protection. a, Schematic for deletion of *Brca2*. **b**, PCR genotyping of ESC clones (M, marker; P, positive control for *Brca2*$^{fl/-}$; N, no DNA control). **c**, **d**, Representative images (**c**) and quantification (**d**) of irradiation-induced foci in *shPtip* and *Brca2*$^{-/-}$/shPtip ESCs ($n = 110$ cells examined). **e**, Representative Southern blot images (top) and quantification for targeting efficiency (bottom) for 59xDR–GFP[26] gene targeting to the *Pim-1* locus. **f**, Ratio of IdU versus CldU (****$P \leq 0.0001$, Mann–Whitney test). One hundred and twenty-five replication forks were analysed.

B3. MRE11 association at RFs depends on PTIP-MLL3/4

Although the recruitment of PTIP to DSBs after irradiation is dependent on 53BP1, we hypothesized that PTIP might be recruited to sites of stalled RFs independently of its interactions with 53BP1. Consistently, we observed PTIP accumulation at sites of replication stalling marked by pan-nuclear γ-H2AX staining (**Fig. 3a**). Among cells exhibiting pan γ-H2AX signal, 71.4% of WT and 78% of 53Bp1−/− mouse embryonic fibroblasts (MEFs) exhibited PTIP foci following HU treatment (**Fig. 3a**). Even in the absence of HU treatment, PTIP exhibited extensive co-localization with proliferating cell nuclear antigen (PCNA) during late S phase both in WT and in 53BP1-deficient cells (**Fig. 3b**). ***Collectively, these data suggest that PTIP might function during normal or perturbed replication in a DSB- and 53BP1- independent manner***. Like PTIP, MRE11 also associates with chromatin in a DNA damage-independent but DNA replication-dependent manner (**Fig. 3c**). Loss of PTIP resulted in a marked decrease of MRE11 association with PCNA foci in unperturbed cycling MEFs (**Fig. 3c**). Re-introduction of WT full-length

PTIP into Ptip−/− MEFs restored MRE11 co-localization with PCNA in late S phase (**Fig. 3d**). Thus, in contrast to irradiation-induced MRE11 foci, localization of MRE11 to sites of DNA replication is PTIP-dependent (**Fig. 3c–e**). To monitor MRE11 and RAD51 association with active and stalled RFs we performed iPOND analysis in WT and Ptip−/− MEFs. WT cells showed an increase in MRE11 and RAD51 association with stalled RFs (**Fig. 3f**). Ptip-deficient cells also showed an increase in RAD51 association at RFs, but MRE11 association with nascent DNA was reduced upon HU treatment (**Fig. 3f**), consistent with our immunofluorescence analysis (**Fig. 3c**). ***Thus, MRE11 deposition on newly synthesized DNA is dependent on PTIP, which itself is recruited to stalled forks upon replication stress***.

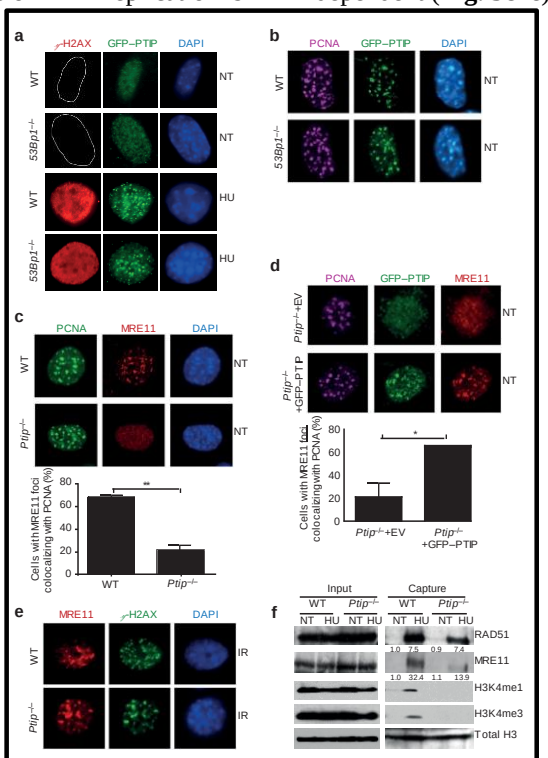

Figure 3 | PTIP localizes to sites of replication and recruits MRE11 to active and stalled replication forks. a, WT and *53Bp1*$^{-/-}$ MEFs expressing GFP-tagged PTIP were either treated or not (NT) with 4 mM HU and assessed for γ-H2AX (red) and PTIP (green). DAPI (4′,6-diamidino-2-phenylindole) indicated in blue. **b**, Co-localization of PCNA (magenta) and PTIP (green). **c**, Co-localization of PCNA (green) and MRE11 (red). Quantification in lower panel ($n = 150$ cells examined). **d**, *Ptip*$^{-/-}$ MEFs infected with either empty vector (EV, containing IRES–GFP) or full-length PTIP (GFP–PTIP) and probed for GFP (green), MRE11 (red) and PCNA (magenta). Quantification in lower panel ($n = 150$ cells examined). **e**, MRE11 (red) and γ-H2AX (green) irradiation-induced foci.

B4. RF protection confers chemoresistance

RF protection contributes to genome stability in a manner independent of DSB-induced HR. Rif1-deficient cells, characterized by extensive RF degradation (**Fig. 1c**) showed increased chromosomal aberrations in response to replication poisons PARPi, HU and cisplatin. We therefore speculated that RF stability mediated by loss of PTIP (**Fig. 1d, e**) might confer genome stability to Brca-deficient cells exposed to chemotherapeutics that poison DNA replication. Indeed, we found that Ptip deficiency reduced the levels of chromosomal aberrations both in Brca1−/− and in Brca2−/− B cells (**Fig. 4a, b**). ***Taken together, these data suggest that PTIP levels could be a biomarker for acquired resistance to platinum-based chemotherapy in Brca1/2-mutated ovarian cancers***.

An unbiased shRNA screen recently demonstrated that reduced levels of the nucleosome remodeling factor CHD4 in Brca2 mutant cancers correlated with poor patient response to chemotherapy, and increased tolerance to DNA-damaging agents without restoration of RAD51-dependent HR. To test whether the resistance mechanism in this case occurs through RF protection, we knocked down CHD4 in the Brca2 mutant ovarian cancer cell line PEO1. While CHD4 depletion in Brca2 mutant cells did not restore HR, we observed that it largely conferred protection to nascent replication tracts from degradation upon HU treatment (**Fig. 4c**). Moreover, depletion of CHD4 resulted in significantly decreased recruitment of MRE11 upon HU treatment in Brca2 mutant cells (**data not shown**). These results suggest that MRE11-mediated degradation contributes to genome instability upon treatment with replication poisons. To test this idea, we pre-incubated Brca2-deficient B cells with the MRE11 nuclease inhibitor mirin before treating with PARP inhibitor or cis-platin. Mirin treatment did not alter the frequency of replicating cells monitored by EdU incorporation (**data not shown**). However, incubation with mirin reduced the levels of PARPi-induced chromosomal aberrations approximately twofold. Similarly, Brca2-deficient cells were partly protected from cisplatin-induced DNA damage when MRE11 nuclease activity was inhibited (**data not shown**). ***We concluded that MRE11 nuclease promotes genomic instability in Brca2-deficient cells***.

Since PARP1 (ARTD1) is required for MRE11 localization to stalled replication forks and its loss rescues the embryonic lethality in Brca2- null ESCs, we tested the contribution of PARP1 to RF stability and genome integrity by generating Brca1−/−Parp1−/− B cells (Brca1f/f; Parp1−/−; Cd19Cre). Loss of Parp1 protected Brca1- deficient RFs from degradation and resulted in a significant reduction in chromosomal aberrations (**Fig. 4d, e**). Thus, despite the fact that treatment with PARP inhibitor increases levels of DNA damage in Brca1-deficient cells, loss of Parp1 before Brca1 loss protects against genome instability. To determine whether Brca2-deficient tumour cells acquire chemotherapy resistance via RF protection, we induced PARPi-resistance using the KB2P mouse model for Brca2-deficient breast cancer (**Fig. 5a**). A mammary tumour from KB2P mice was transplanted into syngeneic FVB mice and, when the tumour reached a size >200 mm3, mice were treated with PARPi (AZD2461) for 28 consecutive

days. The tumour was initially responsive to treatment but eventually grew, upon which treatment was repeated until PARPi resistance was achieved (**Fig. 5c**). The stability of acquired resistance was confirmed by re-transplanting matched naive and resistant tumours and treating the animals with vehicle or AZD2461 (**Fig. 5d**). PARPi-resistant tumours also showed cross-resistance to replication poisons topotecan and cisplatin (**Fig. 4f, g**). Both naive and resistant Brca2-deficient tumours showed impaired irradiation-induced RAD51 foci formation (**Fig. 5e, f**). We therefore assayed naive and resistant tumours ex vivo for RF stability. The mean length of the CldU and the IdU tracts were similar in all samples that were not treated with HU (**Fig. 4h** and **Fig. 5g**). While naive tumour cells showed degradation of nascent tracts upon HU treatment, resistant tumour cells were protected (**Fig. 4h**). ***These data suggest that RF protection rather than restoration of HR may be the main mechanism for acquired resistance in this mammary tumour***.

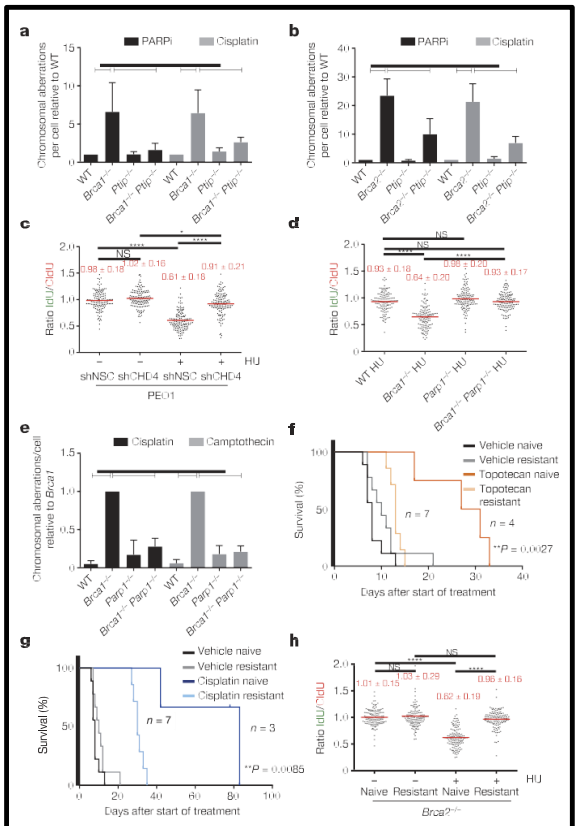

Figure 4 | Replication fork protection confers genome stability and chemotherapeutic resistance. a, **b**, Genomic instability measured in metaphase spreads from B cells ($n = 50$; $*P \leq 0.05$, $**P \leq 0.01$, $***P \leq 0.001$, $****P \leq 0.0001$, unpaired *t*-test). Experiments were repeated four times. **c**, Ratio of IdU versus CldU in *BRCA2*-mutated PEO1 cells either mock (shNSC) infected or infected with shRNA against CHD4 (shCHD4) ($*P \leq 0.05$, $****P \leq 0.0001$, Mann–Whitney test). One hundred and twenty-five replication forks were analysed. **d**, Ratio of IdU versus CldU in HU-treated B cells ($*P \leq 0.05$, $****P \leq 0.0001$, Mann–Whitney test). One hundred and twenty-five replication forks were analysed. **e**, Genomic instability in B cells ($n = 50$; $***P \leq 0.001$, unpaired *t*-test). Experiments repeated four times. **f**, **g**, Kaplan–Meier survival curves in mice implanted with either PARPi-naive or -resistant tumours and treated with either topotecan (**f**) or cisplatin (**g**) using log-rank (Mantel–Cox) test. **h**, Ratio of IdU versus CldU in untreated or HU-treated tumours (PARPi naive versus PARPi resistant) ($****P \leq 0.0001$, Mann–Whitney test). One hundred and twenty-five replication forks were analysed.

Overall Conclusions

Our study and data not shown from 'Synthetic viability by BRCA2 and PARP1/ARTD1 deficiencies' by Ding X et.al., Nat Comm. Aug 2016 provide the first examples of genetic alterations that bypass the essential requirement for DSB-induced HR, evidenced by the finding that reductions in PTIP or PARP1 levels rescues the lethality of Brca2-null ESCs. We speculate that the reason Brca2 nullizygosity is compatible with viability is because RAD51 is able to perform essential HR functions (such as SCE) by loading onto RFs independently of BRCA2, even if RAD51 loading onto processed DSBs is strictly dependent on BRCA2 (**Fig. 1g** and **Fig. 2c, d**). We also show that loss of PTIP, PARP1 and CHD4 confers resistance to a variety of DNA-damaging agents in Brca-deficient cells. Resistance to PARPi and cisplatin both in primary and in tumour cells grown *in vitro* or *in vivo* correlates with protection from RF degradation. While 53BP1 disruption rescues the viability of Brca1-deficient mice by restoration of HR, cells from these animals show residual levels of chromosomal aberrations. The significant level of RF degradation observed in Brca1−/−53Bp1−/− cells (**Fig. 1b**) may contribute to this genome instability. Since RF degradation is mediated by MRE11, we propose that persistence of MRE11 at stalled forks is toxic and normally counteracted by BRCA1/2. One possibility is that MRE11 could initially be recruited to stalled forks to mediate RF restart, and that BRCA1/2 is necessary to subsequently disengage MRE11 from already-processed DNA termini. Consistently, we have found a significant increase in chromatin-bound MRE11 in Brca2-deficient cells treated with HU or cisplatin. We therefore propose that deficiencies in PTIP, CHD4 and PARP1 could confer drug resistance in Brca- deficient cells by limiting the access of MRE11 to single-strand DNA at stalled RFs.

In summary, we have shown that protection of nascent DNA from degradation provides a mechanism that can promote synthetic viability and drug resistance in Brca-deficient cells without restoring HR at DSBs.

Summary of Methodologies Employed

Mice, MEFs, and B cell cultures. The 53Bp1−/− , Brca1f(Δ11)/f(Δ11) (NCI mouse repository), Brca2f/f (NCI mouse repository), Rif1f/f, Ptipf/f and Mll4f/f mice have been described. To generate Mll4-SET-flox/ flox mice, exons 50–51 of the Mll4/Kmt2d gene were flanked by loxP sites. Cre- mediated deletion of the floxed exons 50–51 causes frame shift and generates a stop codon in exon 52. The resulting protein lacks the carboxy (C)-terminal 276 amino acids including the entire enzymatic SET domain. Resting splenic B cells were isolated from 8- to 12-week-old WT or mutant spleen with anti-CD43 microbeads (anti-Ly48; Miltenyi Biotech) and were cultured with LPS (25 μg/ml; Sigma), IL-4 (5 ng/ml; Sigma) and RP105 (0.5 μg/ml; BD). Stimulated B cells were additionally infected with CRE to ensure a high level of gene deletion in these cells. All mice were randomly distributed in experimental groups after genotyping. WT MEFs were immortalized by SV40 retroviral infection, and SV40 immortalized Ptipf/f and Mll3 −/−Mll4f/f MEFs were infected with a CRE retrovirus to delete Ptip and Mll4 respectively. Coding sequences for mouse Ptip–GFP were cloned into the MIGR1 retroviral vector as previously described.

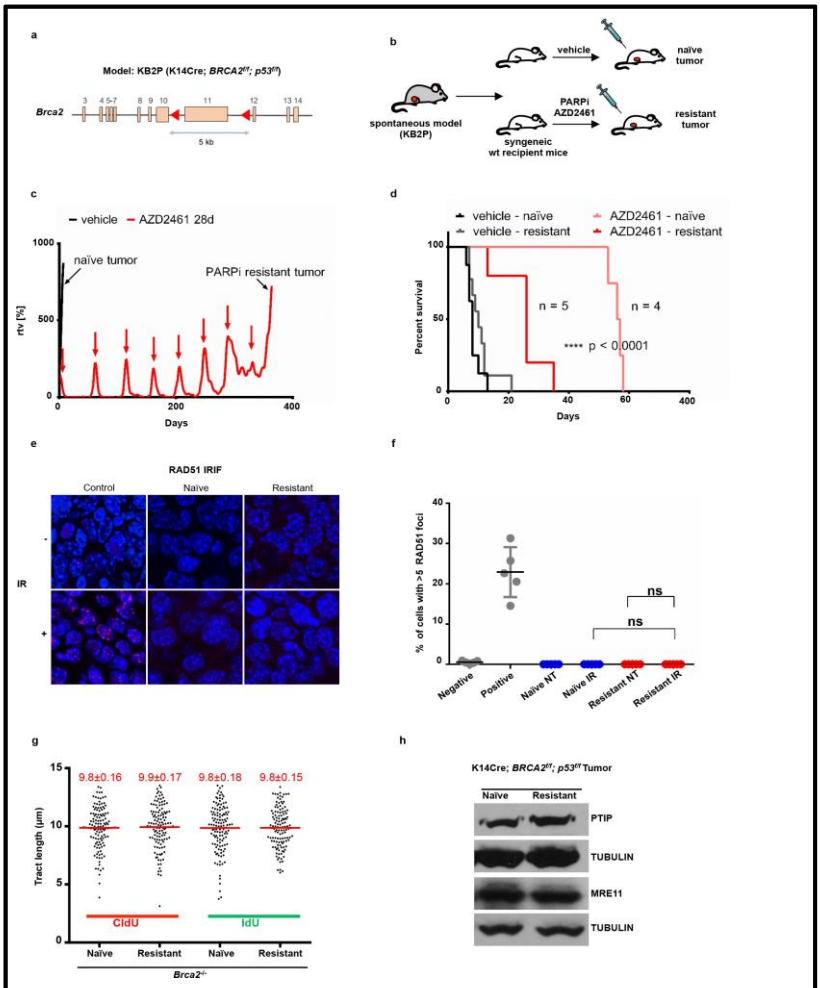

Figure 5| *Brca2*-deficient tumours acquire PARPi resistance without restoration of RAD51 foci formation. a, Schematic depicting the conditional *BRCA2* allele of the KB2P (*K14CRE;Brca2$^{f/f}$;p53$^{f/f}$*) spontaneous tumour model. **b**, Outline of the PARPi intervention study. A spontaneous BRCA2-/p53-deficient tumour was generated and re-transplated into syngeneic WT mice. When the tumours reached 200 mm^3, they were treated either with vehicle or PARPi AZD2461. **c**, PARPi response curve of the KB2P tumour (relative tumour volume (rtv) versus days). The treatment for 28 consecutive days was started when the tumour reached 200 mm^3 (rtv = 100%). In response to the treatment, the tumour shrank but eventually grew back. When it reached 100% relative tumour volume, the treatment was repeated (as indicated with red arrows) for another 28 days. This regime was continued until the tumour became resistant to PARPi (blackarrow). **d**, The stability of acquired resistance of the KB2P tumour was confirmed by re-transplanting matched naive and resistant tumours and treating animals either with vehicle or AZD2461 (only one 28-day cycle). Kaplan–Meier survival curve indicates that resistant tumours did not respond to the AZD2461 treatment, while naive tumours exhibited high sensitivity, indicative of a stable genetic mechanism of resistance. **e**, **f**, Irradiation-induced RAD51 foci were detected by immunofluorescence in the KB2P donor: RAD51 foci formation was undetectable in naive and resistant tumours, suggesting that HR restoration is not an underlying mechanism of PARPi resistance. Spontaneous tumours from *K14 Cre; p53$^{f/f}$* mice treated with irradiation were used as positive control for RAD51 foci. Unirradiated *K14 Cre; p53$^{f/f}$* cells were used as a negative control. **g**, Replication fork progression rates measured by tract lengths in micrometres of CldU (red) and IdU (green) in PARPi-naive or PARPi-resistant tumours. Numbers in red indicate the mean ± s.d. for each sample. One hundred and twenty-five replication forks were analysed for each condition. **h**, Western blot analysis for PTIP and MRE11 levels in PARPi-naive or PARPi-resistant tumours. Tubulin was used as loading control.

Generation of CHD4-deficient PEO1 lines using RNAi. BRCA2-mutated ovarian cancer cell lines PEO1 were grown in DMEM with 10% FBS and 1% Glutmax. RNAi for CHD4 was performed. ESC lines, shRNA knockdowns and rescue of BRCA2 viability. PL2F2 mouse ESCs were maintained in M15 media (Knockout DMEM with 15% fetal bovine serum, 0.00072% β-mercaptoethanol, 100 U/ml penicillin, 100 μg/ml streptomycin and 0.292 mg/ml l-glutamine) at 37 °C, 5% CO2. ESCs were plated on a monolayer of mitotically inactive feeder cells. Two different shRNAs against Ptip mRNA were cloned into pSuperior vector (Oligoengine). shRNA sequences are listed below with the targeted sequences underlined: mPtip shRNA-1 sense, 5′GATCCCC GTGGCGCTCTCCTGCCAGT TTCAAGAGA ACTGGCAGGAGAGCGCCAC TTTTTA 3′; mPtip shRNA-1 antisense, 5′ AGCTTAAAAA GTGGCGCTCTCCTGCCAGT TCTCTTGAA

ACTGGCAGGAGAGCGCCAC GGG 3′; mPtip shRNA-2 sense, 5′GATCCCC CCGTAGCAACACAGTCCTC TTCAAGAGA GAGGACTGTGTTGCTACGG
TTTTTA 3′; mPtip shRNA-2 antisense, 5′ AGCTTAAAAA CCGTAGCAACAC AGTCCTC TCTCTTGAA GAGGACTGTGTTGCTACGG GGG 3′. shRNA vectors were linearized by ScaI and electroporated into ESCs using a Bio-Rad gene pulser. Cells were selected in G418 (0.18 mg/ml) 24 h after electroporation for 5 days. Individual colonies were picked and PTIP levels were determined by western blotting. The PGK-Cre plasmid was electroporated into Ptip shRNA knockdown cells (20 μg DNA for 1×10^7 cells). Thirty-six hours after electroporation, HAT (hypoxanthine–aminopterin–thymidine) selection was performed for 5 days, after which cells were switched to HT (hypoxanthine–thymidine) media for 2 days and then transferred to normal media. Colonies were picked when visible, genomic DNA was extracted and Southern blotting was performed. For PCR genotyping, the following primers were used to amplify the Brca2 cko allele and Brca2-KO allele: Brca2-KO forward, 5′ GCCACCTCTGCCTGATTCTA; Brca2-KO reverse, 5′ AAAGAACCAGCTGGGGCTCGAG; Brca2-flox forward, 5′ TG AAGTGGACCCTGTAACCC; Brca2-flox reverse, 5′ AGTTCTCTCCTTTCA GCCTTCT.

DNA fibre analysis. Asynchronous B cells, BRCA2-mutated PEO1 cells and Brca2-deficient K2BP tumours were labelled with 30 μM CldU, washed with PBS and exposed to 250 μM IdU. After exposure to IdU, the cells were washed again in warm PBS and treated or not with HU before collection. Cells were then lysed and DNA fibres stretched onto glass slides, as described42. The fibres were denatured with 2.5 M HCl for 1 h, washed with PBS and blocked with 2% BSA in phosphate buffered saline Tween-20 for 30 min. The newly replicated CldU and IdU tracts were revealed with anti-BrdU antibodies recognizing CldU and IdU respectively. Images were taken at 60 × magnification (Zeiss Axio Observer.Z1), and statistical analysis was performed using GraphPad Prism.
DSB detection by PFGE. DSB detection by PFGE was done. Ethidium-bromide-stained gels were analysed using an UVP EC3 imaging system. Quantification was performed using ImageJ normalizing DSB signals to unsaturated DNA signals in the well. Relative DSB levels were obtained by comparing treatment results to the background DSB signals observed for untreated conditions.

Western blotting and immunofluorescence. Primary antibodies were used at the following dilutions: anti-tubulin (1:15,000, Sigma), anti-H3K4me3 (1:5,000, Millipore), anti-H3K4me1 (1:5,000, Millipore), anti-RAD51 (1:50, Santa Cruz), anti-PCNA (1:2,000, Santa Cruz), anti-total H3 (1:1,000 Millipore) and anti-Mre11 (1:10,000, gift from J. Petrini, MSKCC). MEFs were prepared for immunofluorescence by growth on 18 mm × 18 mm glass cover slips. Lymphocytes were dropped onto slides coated with CellTak (BD Biosciences). Cells were fixed with methanol and incubated with primary antibody.

iPOND and flow cytometry. iPOND was performed as follows: one hundred and fifty million WT, Ptip−/− and Mll3−/−Mll4−/− MEFs were labelled with 10 μM EdU (Life Technologies) and treated with HU as indicated. Two hundred million cells were used for iPOND experiments with ESCs. Cells were cross-linked with 1% formaldehyde for 10 min at room temperature, quenched with 0.125 M glycine and washed with PBS. For the conjugation of EdU with biotin azide, cells were permeabilized with 0.25% Triton X-100/ PBS, and incubated in click reaction buffer (10 mM sodium-l-ascorbate, 20 μM biotin azide (Life Technologies), and 2 mM CuSO4) for 2 h at room temperature. Cells were resuspended in lysis buffer (50 mM Tris-HCl, pH 8.0, and 1% SDS) supplemented with protease inhibitors (Roche), and chromatin was solubilized by sonication in a Bioruptor (Diagenode-Pico) at 4 °C for 24 min. After centrifugation, clarified supernatants were incubated for 1 h with streptavidin-MyOne C1 beads (Life Technologies). Beads were washed and captured proteins were eluted by boiling beads in 2 × NuPAGE LDS Sample Buffer (Life Technologies) containing 200 mM DTT for 40 min at 95 °C. Proteins were resolved by electrophoresis using NuPAGE Novex 4–12% Bis-Tris gels and detected by western blotting with the indicated antibodies. For flow cytometric analysis, asynchronous B cells were pulsed with 10 mM EdU for 20 min at 37 °C and stained using the Click-IT EdU Alexa Fluor 488 Flow Cytometry Assay Kit.

What opportunities for training and professional development has the project provided?

The project has presented numerous opportunities for the Principal Investigator (**Dr. Andre Nussenzweig**) and two post-doctoral fellows (**Drs. Arnab Ray Chaudhuri and Dali Zong**) to present their work in symposia at the NIH and at national and international conferences (**see details in Section 6 below**).

How were the results disseminated to communities of interest?

Results were shared with the scientific community via informal discussions, posters and presentations at scientific meetings and through publications in peer-reviewed journals

What do you plan to do during the next reporting period to accomplish the goals?

We will continue to pursue the goals outlined in Specific Aims 1 and 2, specifically focusing on dissecting the mechanisms underlying replication fork degradation/protection in BRCA1/2-deficient cells.

4. **IMPACT:** This component is used to describe ways in which the work, findings, and specific products of the project have had an impact during this reporting period. Describe distinctive contributions, major accomplishments, innovations, successes, or any change in practice or behavior that has come about as a result of the project relative to:

    - the development of the principal discipline(s) of the project;
    - other disciplines;
    - technology transfer; or
    - society beyond science and technology.

What was the impact on the development of the principal discipline(s) of the project?

Work in support of both Specific Aims of this proposal highlight mechanisms that can alter drug sensitivity or resistance in BRCA-deficient tumors. We have also observed that deregulation of the RNF168/53BP1 pathway can alter the chemosensitivity of BRCA1 deficient tumors (**Specific Aim 1**). We have also observed that PTIP or PARP1 deficiencies promote synthetic viability and drug resistance in BRCA-deficient cells without restoring HR (**Specific Aim 2**).

What was the impact on other disciplines?

Nothing to Report

What was the impact on technology transfer?

Nothing to Report

What was the impact on society beyond science and technology?

Nothing to Report

5. **CHANGES/PROBLEMS:** The Project Director/Principal Investigator (PD/PI) is reminded that the recipient organization is required to obtain prior written approval from the awarding agency Grants Officer whenever there are significant changes in the project or its direction. If not previously reported in writing, provide the following additional information or state, "Nothing to Report," if applicable:

    - Changes in approach and reasons for change.
    - Actual or anticipated problems or delays and actions or plans to resolve them.
    - Changes that have a significant impact on expenditures.
    - Significant changes in use or care of human subjects, vertebrate animals, biohazards, and/or select agents.

Changes in approach and reasons for change

Nothing to Report

Actual or anticipated problems or delays and actions or plans to resolve them

Nothing to Report

Changes that had a significant impact on expenditures

Nothing to Report

Significant changes in use or care of human subjects, vertebrate animals, biohazards, and/or select agents

Nothing to Report

6. PRODUCTS: List any products resulting from the project during the reporting period. Examples of products include:

- publications, conference papers, and presentations;
- website(s) or other Internet site(s);
- technologies or techniques;
- inventions, patent applications, and/or licenses; and
- other products.

- **Publications, conference papers, and presentations**

Journal publications.

1. ***Replication fork protection can bypass the requirement for homologous recombination.***
Nature. 2016 Jul 20;535(7612):382-7.
A. Ray Chaudhuri*, E. Callen*, X. Ding, E. Gogola, A. Duarte, J. Lee, N.Wong, V. Lafarga, J. Calvo, N. Panzarino, S. John, A. Day, A. Crespo, H. Chen, B.Shen, J. A. Daniel, P.A. Konstantinopoulos, D.Cortez, S.B. Cantor, O.Fernandez-Capetillo, K. Ge, J. Jonkers, S. Rottenberg, S.K. Sharan and A. Nussenzweig.

2. ***Synthetic viability by BRCA2 and PARP1/ARTD1 deficiencies***. X. Ding, A. Ray Chaudhuri, E. Callen, Y. Pang, K. Biswas, K.D. Klarmann, B.K. Martin, S. Burkett, L. Cleveland, S. Stauffer, T. Sullivan, A. Dewan, H. Marks, A.T. Tubbs, N. Wong, E. Buehler, K. Akagi, S.E. Martin, J.R. Keller, A. Nussenzweig, S.K. Sharan.
Nat Commun. 2016 Aug 8;7:12425.

Books or other non-periodical, one-time publications.

Nothing to Report

Other publications, conference papers, and presentations.

The project has presented numerous opportunities for the Principal Investigator (**Dr. Andre Nussenzweig**) and two post-doctoral fellows (**Drs. Arnab Ray Chaudhuri and Dali Zong**) and staff scientist (**Dr. Elsa Callen**) to present their work in symposia at the NIH and at national and international conferences.

Arnab Ray Chaudhuri: Visiting post-doctoral fellow

Invited Talks:

Sept 2016	Invited talk at the Developmental Therapeutics Branch, NCI, NIH, Bethesda, USA
July 2016	Invited talk at the Netherlands Cancer Institute, Amsterdam, Netherlands.

July 2016	Invited talk at the Department of Molecular Genetics, Erasmus Medical Centre, Rotterdam, Netherlands.
July 2016	Invited talk at the Centre for Chromosome Biology, National University of Ireland, Galway, Ireland
May 2016	Invited talk at Institute of Molecular Cancer Research, University of Zurich, Switzerland.

Poster Presentations at Meetings:

May 2016	Abcam Conference on Mechanisms of Recombination, Alicante, Spain

Dali Zong: Visiting post-doctoral fellow

No meetings attended in 2016

Elsa Callen: Staff Scientist

Invited Talks:

Dec 2016	Mount Sinai, New York City, NY, USA

Andre Nussenzweig: Principal Investigator

Invited Talks:

1. Invited Speaker, Abcam Maintenance of Genome Stability 2016, Panama City, Panama, 2016
2. Invited Speaker, Dana-Farber Cancer Institute/Harvard Cancer Center Seminars in Oncology Lecture Series, Boston, MA, 2016
3. Invited Speaker, 5th Yearly Meeting on DNA Repair, Egmond aan Zee, Netherlands, 2016
4. Invited Speaker, Samuel Waxman Cancer Research Foundation-Workshop on Aging, Hematopoiesis and Cancer, New York, NY, 2016
5. Invited Speaker, Columbia University Department of Genetics & Development Seminar Series- "Mechanisms of Genome Stability". New York, NY, 2016
6. Invited Speaker, DINGO (Dynamique Instabilité Génétique et cancer) Meeting on Replication stress, Genetic Instability & Cancer, Paris, France, 2016
7. Invited Speaker, Gordon Research Conference- 2016 Mutagenesis and Genome Alterations, Girona, Spain, 2016
8. Invited Speaker, ICGEB DNA Replication Conference- "At the intersection of DNA replication and genome maintenance: From basic mechanisms to therapeutic opportunities" Trieste, Italy, 2016
9. Invited Speaker, Cornell University –Seminar for Replication, Recombination, Repair Group, New York, NY, 2016
10. Invited Speaker, icBEST 2016 DNA Repair Meeting, Chengdu, China, 2016
11. Invited Speaker, AACR Special Conference: DNA Repair: Tumor Development and Therapeutic Response, Quebec, Canada, 2016
12. Invited Speaker, Jacques Monod Conference on Transcription-Replication Crosstalk and Genome Instability, Roscoff, France, 2016
13. Invited Speaker, Royal Tropical Institute Annual Meeting on Cancer Genomics, Amsterdam, Netherlands, 2016

- **Website(s) or other Internet site(s)**

  Nothing to Report

- **Technologies or techniques**
  Nothing to Report

- **Inventions, patent applications, and/or licenses**

  Nothing to Report

- **Other Products**

  Nothing to Report

7. PARTICIPANTS & OTHER COLLABORATING ORGANIZATIONS

Provide the following information on participants:

- what individuals have worked on the project?
- has there been a change in the other active support of the PD/PI(s) or senior/key personnel since the last reporting period? what other organizations have been involved as partners?

What individuals have worked on the project?

Provide the following information for: (1) PDs/PIs; and (2) each person who has worked at least one person month per year on the project during the reporting period, regardless of the source of compensation (a person month equals approximately 160 hours of effort).

Name:	**Dr. Andre Nussenzweig**
Project Role:	Principal Investigator
Researcher Identifier (e.g. ORCID ID):	NA
Nearest person month worked:	3
Contribution to Project:	Responsible for the overall direction of the proposed research as well as daily supervision of laboratory activities, personnel, design and interpretation of experiments, preparation of manuscripts and presentations
Funding Support:	Salary supported by the Intramural Research Program (IRP)

Name:	**Dr. Arnab Ray Chaudhuri**
Project Role:	Visiting Fellow
Researcher Identifier (e.g. ORCID ID):	NA
Nearest person month worked:	12
Contribution to Project:	Developed the replication fiber assay that measures the rates of fork progression and the extent of fork protection/degradation. He has also helped with the design and execution of primary experiments and contributed to the writing of 2 manuscripts (Nature, 2016 and Nature Communications, 2016) related to Specific Aim 2 in this proposal
Funding Support:	Salary renumeration from a fellowship with the Human Frontier Science Program

Name:	**Dr. Elsa Callen**
Project Role:	Visiting Fellow
Researcher Identifier (e.g. ORCID ID):	NA
Nearest person month worked:	4
Contribution to Project:	Responsible for genetic and biochemical assays designed to understand the contributing genetic factors in DNA repair pathway selection. Dr. Callen also helped with the design and execution of primary experiments related to replication fork protection. She also contributed to the writing of 2

	Manuscripts (Nature, 2016 and Nature Communications, 2016) related to Specific Aim 2 in this proposal
Funding Support:	Salary supported by the Intramural Research Program (IRP)

Name:	**Dr. Dali Zong**
Project Role:	Visiting Fellow
Researcher Identifier (e.g. ORCID ID):	NA
Nearest person month worked:	12
Contribution to Project:	Responsible for genetic and biochemical assays designed to understand the contributing genetic factors in DNA repair pathway selection. He made extensive contributions to the published manuscript (in Nucleic Acids Research, 2015) related to Specific Aim 1 in this proposal
Funding Support:	Supported by the Intramural Research Program (IRP)

Has there been a change in the active other support of the PD/PI(s) or senior/key personnel since the last reporting period?

Nothing to Report

What other organizations were involved as partners?

Nothing to Report

8. SPECIAL REPORTING REQUIREMENTS:

Nothing to Report

9. APPENDICES: Attach all appendices that contain information that supplements, clarifies or supports the text. Examples include original copies of journal articles, reprints of manuscripts and abstracts, a curriculum vitae, patent applications, study questionnaires, and surveys, etc.

See Pdfs of published Nature and Nature Communications Pdf

ARTICLE

doi:10.1038/nature18325

Replication fork stability confers chemoresistance in BRCA-deficient cells

Arnab Ray Chaudhuri[1]*, Elsa Callen[1]*, Xia Ding[2], Ewa Gogola[3], Alexandra A. Duarte[3], Ji-Eun Lee[4], Nancy Wong[1], Vanessa Lafarga[5], Jennifer A. Calvo[6], Nicholas J. Panzarino[6], Sam John[1], Amanda Day[1], Anna Vidal Crespo[1], Binghui Shen[7], Linda M. Starnes[8], Julian R. de Ruiter[3], Jeremy A. Daniel[8], Panagiotis A. Konstantinopoulos[9], David Cortez[10], Sharon B. Cantor[6], Oscar Fernandez-Capetillo[5], Kai Ge[4], Jos Jonkers[3], Sven Rottenberg[3,11], Shyam K. Sharan[2] & André Nussenzweig[1]

Cells deficient in the *Brca1* and *Brca2* genes have reduced capacity to repair DNA double-strand breaks by homologous recombination and consequently are hypersensitive to DNA-damaging agents, including cisplatin and poly(ADP-ribose) polymerase (PARP) inhibitors. Here we show that loss of the MLL3/4 complex protein, PTIP, protects *Brca1/2*-deficient cells from DNA damage and rescues the lethality of *Brca2*-deficient embryonic stem cells. However, PTIP deficiency does not restore homologous recombination activity at double-strand breaks. Instead, its absence inhibits the recruitment of the MRE11 nuclease to stalled replication forks, which in turn protects nascent DNA strands from extensive degradation. More generally, acquisition of PARP inhibitors and cisplatin resistance is associated with replication fork protection in *Brca2*-deficient tumour cells that do not develop *Brca2* reversion mutations. Disruption of multiple proteins, including PARP1 and CHD4, leads to the same end point of replication fork protection, highlighting the complexities by which tumour cells evade chemotherapeutic interventions and acquire drug resistance.

The role of BRCA1 and BRCA2 in the repair of double-strand breaks (DSBs) is thought to be central to their tumour-suppressor activities, and underlies the hypersensitivity of *Brca*-deficient cells to DNA-damaging agents. While cisplatin and PARP inhibitors (PARPi) have been shown to be effective chemotherapeutic agents, most *Brca*-mutant carcinomas acquire resistance[1]. Besides reduced uptake and increased efflux of drugs, the most well-described mechanism that drives chemotherapeutic resistance in *Brca1/2*-deficient tumours is through the restoration of homologous recombination (HR)[1]. Identification of additional mechanisms underlying resistance to DNA damage is crucial for improving therapies and predicting tumour responses in *Brca*-deficient cancers.

PTIP loss protects RFs in *Brca*-deficient cells

In addition to their roles in HR, recent studies have uncovered DSB-independent functions for BRCA1 and BRCA2 during replication stress[2–6]. Since MRE11 has been implicated in mediating replication fork (RF) degradation in cell lines[2–4], we tested whether primary cells deficient in BRCA1 or BRCA2 also showed degradation of nascent replication tracts. We therefore conditionally inactivated BRCA1 and BRCA2 in B lymphocytes (*Brca1*$^{f/f}$CD19Cre; *Brca2*$^{f/f}$*Cd19Cre*). B cells were sequentially labelled with CldU-(red) followed by IdU-(green), after which the active RFs were stalled with hydroxyurea (HU) (Fig. 1a). The relative shortening of the IdU tract after HU treatment serves as a measure of RF degradation (Fig. 1a). Upon HU treatment, wild-type (WT) cells showed a mean IdU/CldU tract ratio close to 1 (Fig. 1b). However, *Brca1*- and *Brca2*-deficient B cells exhibited a 30–45% reduction in the IdU tract length (Fig. 1b–e and Extended Data Fig. 1a–c).

Consistent with previous data[2,3], RF degradation in B lymphocytes was dependent on MRE11 exonuclease activity (Extended Data Fig. 1a–c). We also tested the role of DNA2 and the Werner syndrome helicase/nuclease (WRN) in degradation of forks in *Brca2*-deficient B cells. Treatment of *Brca2*-deficient cells with WRN inhibitor did not result in fork protection, whereas MRE11 and DNA2 were epistatic (Extended Data Fig. 1c).

Since 53BP1, RIF1, and PTIP counteract BRCA1-dependent HR by inhibiting MRE11-dependent DSB resection[7–15], we examined whether these factors might also function in RF stability. We thus inactivated BRCA1, BRCA2, RIF1, PTIP and 53BP1 in B lymphocytes (Extended Data Fig. 2a). Short exposure to HU did not promote significant DSB formation (Extended Data Fig. 2b), and fork progression rates were comparable across all genotypes (Extended Data Fig. 2c–f).

Absence of 53BP1 did not protect *Brca1*-deficient B cells from degradation of RFs (Fig. 1b), consistent with the finding that BRCA1 acts in RF stabilization in a manner independent of DSB repair[2,3]. Nascent strands also shortened considerably in the absence of the 53BP1 effector *Rif1* and in *Brca1/Rif1* doubly deficient cells (Fig. 1c). In striking contrast, loss of *Ptip* protected RFs from HU-induced degradation in both *Brca1*- and *Brca2*-deficient cells (Fig. 1d, e). Moreover, while *Brca1*$^{-/-}$, *Rif1*$^{-/-}$, and *Brca1*$^{-/-}$*Rif1*$^{-/-}$ B cells displayed increased genomic instability when treated with HU (Extended Data Fig. 3a), *Brca1/Ptip* doubly deficient cells exhibited 2.4-fold fewer chromosomal aberrations and increased viability compared with *Brca1*$^{-/-}$ (Fig. 1f). Similarly, loss of *Ptip* decreased the number of chromosomal aberrations in *Brca2*$^{-/-}$cells challenged with HU (Extended Data Fig. 3b), suggesting that PTIP has functions at

[1]Laboratory of Genome Integrity, National Cancer Institute, National Institutes of Health, Bethesda, Maryland 20892, USA. [2]Mouse Cancer Genetics Program, National Cancer Institute, National Institutes of Health, Frederick, Maryland 21702, USA. [3]Division of Molecular Pathology and Cancer Genomics Centre, The Netherlands Cancer Institute, Plesmanlaan 121, 1066 CX Amsterdam, The Netherlands. [4]Laboratory of Endocrinology and Receptor Biology, National Institute of Diabetes and Digestive and Kidney Diseases, National Institutes of Health, Bethesda, Maryland 20892, USA. [5]Genomic Instability Group, Spanish National Cancer Research Centre (CNIO), Madrid 28029, Spain. [6]Department of Molecular, Cell, and Cancer Biology, University of Massachusetts Medical School, UMASS Memorial Cancer Center, Worcester, Massachusetts 01605, USA. [7]Department of Radiation Biology, Beckman Research Institute of City of Hope, 1500 East Duarte Road, Duarte, California 91010, USA. [8]The Novo Nordisk Foundation Center for Protein Research, Faculty of Health and Medical Sciences, University of Copenhagen, Copenhagen 2200, Denmark. [9]Departments of Gynecologic Medical Oncology, Dana Farber Cancer Institute, Harvard Medical School, Boston, Massachusetts 02215, USA. [10]Department of Biochemistry, Vanderbilt University School of Medicine, 2215 Garland Avenue, Nashville, Tennessee 37232, USA. [11]Institute of Animal Pathology, Vetsuisse Faculty, University of Bern, Länggassstrasse 122, 3012 Bern, Switzerland.
*These authors contributed equally to this work.

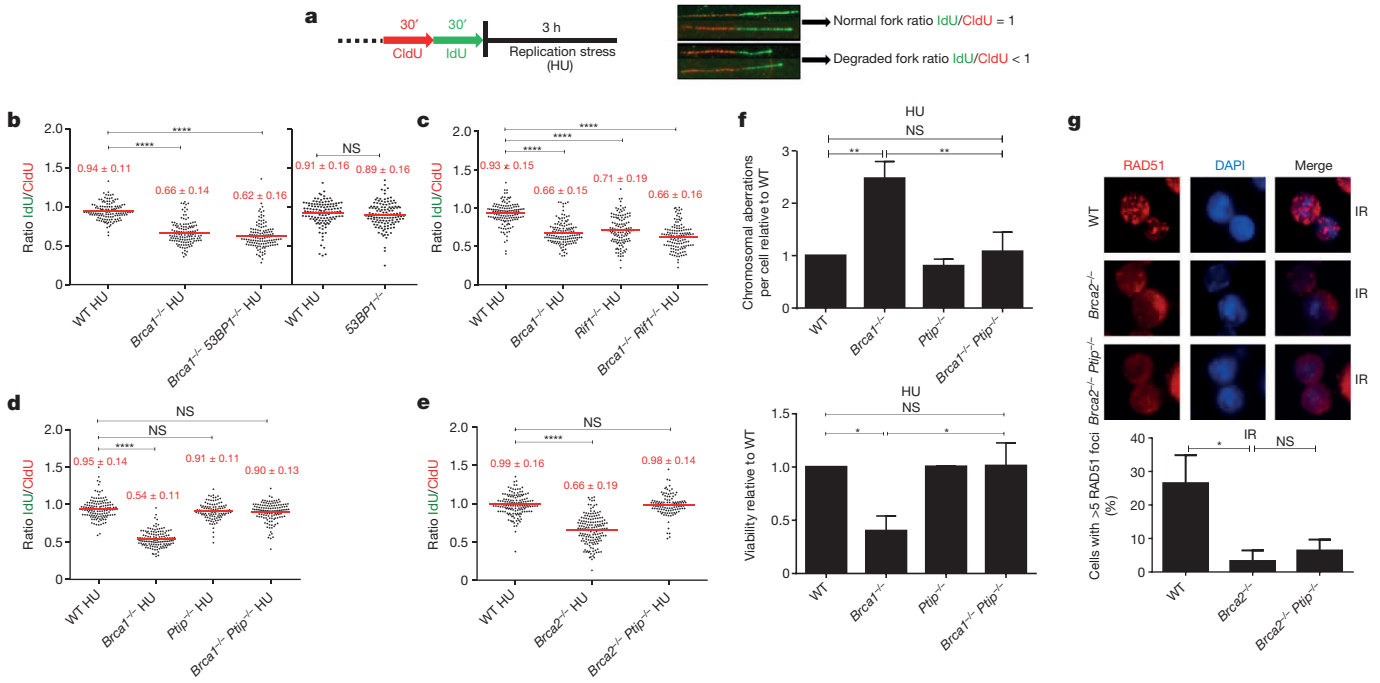

Figure 1 | Loss of *Ptip* in *Brca1/2*-deficient B cells protects nascent DNA from degradation without restoring HR. a, Schematic for labelling B cells with CldU and IdU. **b**–**e**, Ratio of IdU versus CldU upon HU treatment. Numbers in red indicate the mean ± s.d. (NS, not significant, ****$P \leq 0.0001$, Mann–Whitney test). One hundred and twenty-five replication forks were analysed for each genotype. **f**, Genomic instability (top) and viability upon HU treatment (bottom) relative to WT upon 6 h of 10 mM HU treatment. (**$P \leq 0.001$, *$P \leq 0.05$, unpaired *t*-test.) Fifty metaphases were analysed. **g**, Representative images (top) and quantification (below) of irradiation (IR)-induced RAD51 foci. *$P \leq 0.05$, unpaired *t*-test ($n = 120$ cells examined). Experiments were repeated three times.

stalled RFs distinct from its DSB-dependent interactions with 53BP1 and RIF1.

We hypothesized that HU-induced degradation would impact RF progression rates. We therefore assayed the ability of WT and mutant cells to incorporate nucleotide analogues in the presence of low concentrations of HU. We observed a significant decrease in IdU tract lengths during HU exposure across all genotypes. However, *Brca2*-deficient cells had significantly decreased progression rates upon HU treatment, whereas *Ptip*$^{-/-}$ and *Brca2*$^{-/-}$*Ptip*$^{-/-}$ cells displayed significantly longer replication tracts (Extended Data Fig. 3c). We also tested the effect of *Ptip*-deficiency on recovery after replication stalling with high concentrations of HU. We found that although the percentage of restarted RFs did not change among genotypes (Extended Data Fig. 3d), loss of *Brca2* resulted in a delayed restart, whereas *Brca2/Ptip* doubly deficient cells restarted normally (Extended Data Fig. 3e). Thus, loss of PTIP promotes RF progression and timely restart in *Brca2*-deficient cells, which correlates with decreased RF degradation.

PTIP loss rescues lethality of *Brca2*-null ESCs

Since elevated levels or stabilized RAD51 filaments could protect RFs from degradation[2,3,16], we asked whether PTIP deficiency leads to overexpression of RAD51 or enhanced RAD51 activity. RAD51 levels were similar in WT, *Ptip*$^{-/-}$, *Brca2*$^{-/-}$, and *Brca2*$^{-/-}$*Ptip*$^{-/-}$ cells (Extended Data Fig. 3f), but the ability of RAD51 to relocalize to sites of DNA DSBs was severely impaired in *Brca2/Ptip*-deficient B cells (Fig. 1g and Extended Data Fig. 3g) and embryonic stem cells (ESCs) (see Fig. 2c, d). Moreover, loss of *Ptip* did not enhance the loading of RAD51 on nascent chromatin (see Fig. 3f).

Loss of *Brca2* in ESCs is incompatible with cell survival[17]. To test whether PTIP deficiency could promote ESC survival we knocked down PTIP in PL2F7 mouse ESCs, which have one null and one conditional allele of *Brca2* (*Brca2*$^{f/-}$, Fig. 2a and Extended Data Fig. 4a)[17]. After CRE transfection in *Brca2*$^{f/-}$ ESCs and selection in HAT medium, very few resistant colonies were obtained and these remained *Brca2*$^{f/-}$ rather than *Brca2*-null, reflecting the essential role of BRCA2 in ESC viability (Fig. 2b)[17]. Strikingly, 12.5% and 5% of the HAT-resistant colonies were *Brca2*-null when targeted by *Ptip* short hairpin RNAs (shRNAs) 1 and 2 respectively (Fig. 2b and Extended Data Fig. 4b). Consistent with our analysis of *Brca2*$^{-/-}$*Ptip*$^{-/-}$ B cells (Fig. 1g), irradiation-induced RAD51 foci formation was defective in *Brca2/Ptip*-deficient ESCs (Fig. 2c, d). Moreover, while efficient gene targeting to the *Pim-1* locus was observed in WT ESCs using a promoterless hygromycin cassette (100% of the hygromycin-resistant WT clones were targeted integrations), we did not observe a single targeted clone in *Brca2/Ptip*-deficient ESCs (Fig. 2e) indicative of defective HR. Similarly, the synthetic HR reporter substrate DR–GFP revealed impaired HR in *Brca2/Ptip*-deficient ESCs (Extended Data Fig. 4c). Nevertheless, stalled RFs in PTIP-deficient *Brca2*$^{-/-}$ ESCs displayed RF protection compared with *Brca2* hypomorphic mutant ESCs (Y3308X)[17] (Fig. 2f). Thus, deficiency in PTIP protects RFs from degradation and rescues the lethality of *Brca2* knockout ESCs without restoring DSB-induced HR.

BRCA2 is dispensable for HR at RFs

It has been suggested that HR at stalled forks is regulated differently from HR at DSBs[18]. As a readout for HR at RFs, we assayed for sister chromatid exchanges (SCEs) in WT and Y3308X ESCs. Although Y3308X cells show undetectable levels of irradiation-induced RAD51 formation and loss of targeted integration, indicative of a defect in DSB-induced HR[17], the basal frequency of SCE was normal in Y3308X cells (Extended Data Fig. 4d). Moreover, RAD51 was enriched on nascent DNA in Y3308X during normal replication and in presence of HU as measured by isolation of proteins on native DNA (iPOND) analysis (Extended Data Fig. 4e). We also observed similar frequencies of spontaneously generated and DNA damage-induced SCEs in WT, *Brca2-null* and *Brca2/Ptip*-deficient B cells (Extended Data Fig. 4f). Thus, in contrast to RAD51 which is required for DSB- and replication-associated HR[19], BRCA2 appears to be dispensable for HR

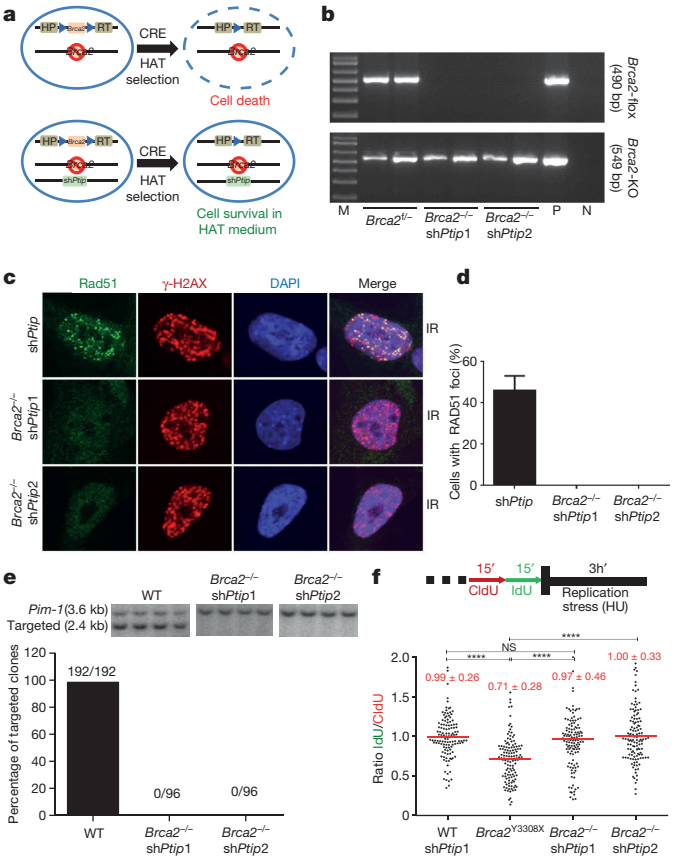

Figure 2 | PTIP deficiency rescues the lethality of *Brca2*-null mouse ESCs and confers fork protection. a, Schematic for deletion of *Brca2*. **b**, PCR genotyping of ESC clones (M, marker; P, positive control for $Brca2^{f/-}$; N, no DNA control). **c**, **d**, Representative images (**c**) and quantification (**d**) of irradiation-induced foci in *shPtip* and $Brca2^{-/-}$/sh*Ptip* ESCs ($n = 110$ cells examined). **e**, Representative Southern blot images (top) and quantification for targeting efficiency (bottom) for 59xDR–GFP[36] gene targeting to the *Pim-1* locus. **f**, Ratio of IdU versus CldU (****$P \leq 0.0001$, Mann–Whitney test). One hundred and twenty-five replication forks were analysed.

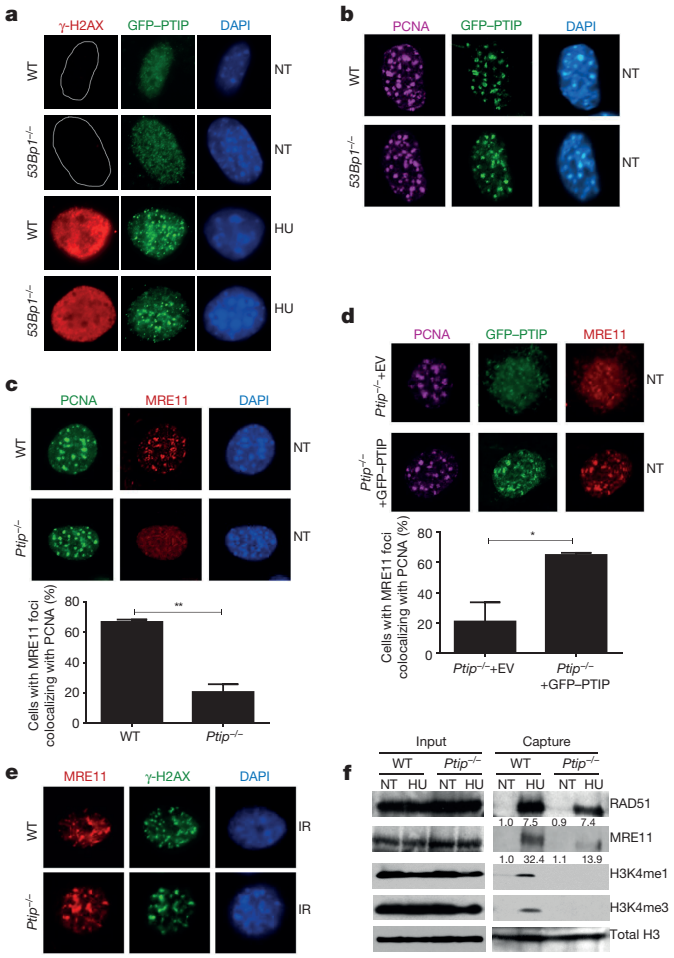

Figure 3 | PTIP localizes to sites of replication and recruits MRE11 to active and stalled replication forks. a, WT and $53Bp1^{-/-}$ MEFs expressing GFP-tagged PTIP were either treated or not (NT) with 4 mM HU and assessed for γ-H2AX (red) and PTIP (green). DAPI (4′,6-diamidino-2-phenylindole) indicated in blue. Quantification in Extended Data Fig. 5c. **b**, Co-localization of PCNA (magenta) and PTIP (green). Quantification in Extended Data Fig. 5d. **c**, Co-localization of PCNA (green) and MRE11 (red). Quantification in lower panel ($n = 150$ cells examined). **d**, $Ptip^{-/-}$ MEFs infected with either empty vector (EV, containing IRES–GFP) or full-length PTIP (GFP–PTIP) and probed for GFP (green), MRE11 (red) and PCNA (magenta). Quantification in lower panel ($n = 150$ cells examined). **e**, MRE11 (red) and γ-H2AX (green) irradiation-induced foci. Quantification in Extended Data Fig. 5g. **f**, iPOND analyses of proteins at replication forks (capture). Input represents 0.25% of the total cellular protein content. RAD51 and MRE11 levels (shown below) were normalized to total H3. Experiments were repeated three times.

that uses the nascent sister chromatid to repair DNA lesions during replication.

MRE11 association at RFs depends on PTIP–MLL3/4

Although the recruitment of PTIP to DSBs after irradiation is dependent on 53BP1 (Extended Data Fig. 5a, b)[10], we hypothesized that PTIP might be recruited to sites of stalled RFs independently of its interactions with 53BP1. Consistently, we observed PTIP accumulation at sites of replication stalling marked by pan-nuclear γ-H2AX staining[20]. Among cells exhibiting pan γ-H2AX signal, 71.4% of WT and 78% of $53Bp1^{-/-}$ mouse embryonic fibroblasts (MEFs) exhibited PTIP foci following HU treatment (Fig. 3a and Extended Data Fig. 5c). Even in the absence of HU treatment, PTIP exhibited extensive co-localization with proliferating cell nuclear antigen (PCNA) during late S phase both in WT and in *53Bp1*-deficient cells (Fig. 3b and Extended Data Fig. 5d, e). Collectively, these data suggest that PTIP might function during normal or perturbed replication in a DSB- and 53BP1-independent manner.

Like PTIP, MRE11 also associates with chromatin in a DNA damage-independent but DNA replication-dependent manner[21] (Fig. 3c). Loss of PTIP resulted in a marked decrease of MRE11 association with PCNA foci in unperturbed cycling MEFs (Fig. 3c) and defective MRE11 recruitment to ssDNA regions upon HU treatment (Extended Data Fig. 5f). Re-introduction of WT full-length PTIP into $Ptip^{-/-}$ MEFs restored MRE11 co-localization with PCNA in late S phase (Fig. 3d). Thus, in contrast to irradiation-induced MRE11 foci, localization of MRE11 to sites of DNA replication is PTIP-dependent (Fig. 3c–e and Extended Data Fig. 5g).

To monitor MRE11 and RAD51 association with active and stalled RFs we performed iPOND analysis in WT and $Ptip^{-/-}$ MEFs (Extended Data Fig. 5h)[22]. WT cells showed an increase in MRE11 and RAD51 association with stalled RFs (Fig. 3f). *Ptip*-deficient cells also showed an increase in RAD51 association at RFs, but MRE11 association with nascent DNA was reduced upon HU treatment (Fig. 3f), consistent with our immunofluorescence analysis (Fig. 3c and Extended Data Fig. 5f). Thus, MRE11 deposition on newly synthesized DNA is dependent on PTIP, which itself is recruited to stalled forks upon HU treatment (Extended Data Fig. 5i)[22].

PTIP is also known to constitutively associate with PA1 and with MLL3/MLL4 histone methyltransferases which catalyse methylation of histone H3 at lysine 4 (refs 23, 24). To identify the region of PTIP that promotes RF degradation in *Brca2*-deficient cells, we expressed EV (empty vector), FL (full-length PTIP), W165R (disrupting interactions with PA1)[25,26], W663R (disrupting interactions with 53BP1 at DSBs)[25] or Del-BRCT5-6 (disrupting interaction with MLL3/4 independently of DSBs)[23,24,26] in *Brca2/Ptip* doubly deficient cells. We observed that only reconstitution of *Brca2/Ptip*-deficient cells with PTIP-Del-BRCT5-6 maintained fork protection (Extended Data Fig. 6a).

We therefore tested whether the recruitment of MRE11 at stalled forks was dependent on MLL3/4. We observed that MRE11 association at RFs was dependent on MLL3/4 as monitored by iPOND and immunofluorescence analysis (Extended Data Fig. 6b, c). We also observed an enrichment of H3K4me1 and H3K4me3 at nascent forks upon HU treatment that was PTIP- and MLL3/4-dependent (Fig. 3f and Extended Data Fig. 6b). Thus, deposition of MRE11 on newly synthesized or stalled chromatin correlates with the establishment of H3K4me1 and H3K4me3 at RFs.

To determine whether MLL4 contributes to degradation of stalled forks in *Brca*-deficient cells, we examined RF degradation in *Brca1*$^{-/-}$ *Mll4*$^{-/-}$ and *Brca2*$^{-/-}$*Mll4*$^{-/-}$ B cells. *Brca1*$^{-/-}$*Mll4*$^{-/-}$ and *Brca2*$^{-/-}$ *Mll4*$^{-/-}$ cells displayed a partial rescue of fork degradation (Extended Data Fig. 6d, e). To test whether MLL4 methyltransferase activity is critical, we targeted the catalytic SET domain of MLL4 in *Brca1*-deficient B cells. We observed a significant rescue of fork degradation in *Brca1*$^{-/-}$ *Mll4*-SET$^{-/-}$ cells, suggesting that the methyltransferase activity is important for promoting fork degradation (Extended Data Fig. 6f).

RF protection confers chemoresistance

RF protection contributes to genome stability in a manner independent of DSB-induced HR[2,3,5]. Consistently, we observed that *Brca2*$^{-/-}$ *Mll4*$^{-/-}$ B cells showed a partial rescue of chromosomal aberrations upon PARPi and cisplatin treatment compared with *Brca2*$^{-/-}$ cells alone (Extended Data Fig. 6g). However, *Rif1*-deficient cells, characterized by extensive RF degradation (Fig. 1c) but normal irradiation-induced RAD51 foci formation (Extended Data Fig. 7a), showed increased chromosomal aberrations in response to replication poisons PARPi, HU and cisplatin (Extended Data Figs 3a and 7b, c)[27]. We therefore speculated that RF stability mediated by loss of PTIP (Fig. 1d, e) might confer genome stability to *Brca*-deficient cells exposed to chemotherapeutics that poison DNA replication. Indeed, we found that *Ptip* deficiency reduced the levels of chromosomal aberrations both in *Brca1*$^{-/-}$ and in *Brca2*$^{-/-}$ B cells (Fig. 4a, b).

To test whether differential levels of PTIP expression could be an indicator of patient responses to platinum chemotherapy, we queried clinical information from The Cancer Genome Atlas (TCGA) of patients with *Brca1/Brca2*-mutated ovarian serous adenocarcinoma treated with platinum chemotherapy (Extended Data Fig. 8a, b). Survival analysis demonstrated that platinum-treated *Brca2* mutants with high PTIP expression were correlated with a longer progression-free survival (PFS) (Extended Data Fig. 8a). Lower expression of PTIP also predicted a shorter PFS in *Brca2*-associated ovarian cancers (Extended Data Fig. 8b). Taken together, these data suggest that PTIP levels could be a biomarker for acquired resistance to platinum-based chemotherapy in *Brca1/2*-mutated ovarian cancers.

An unbiased shRNA screen recently demonstrated that reduced levels of the nucleosome remodelling factor CHD4 in *Brca2* mutant cancers correlated with poor patient response to chemotherapy, and increased tolerance to DNA-damaging agents without restoration of RAD51-dependent HR[28]. To test whether the resistance mechanism in this case occurs through RF protection, we knocked down CHD4 in the *Brca2* mutant ovarian cancer cell line PEO1 (Extended Data Fig. 8c, d). While CHD4 depletion in *Brca2* mutant cells did not restore HR[28], we observed that it largely conferred protection to nascent replication tracts from degradation upon HU treatment (Fig. 4c).

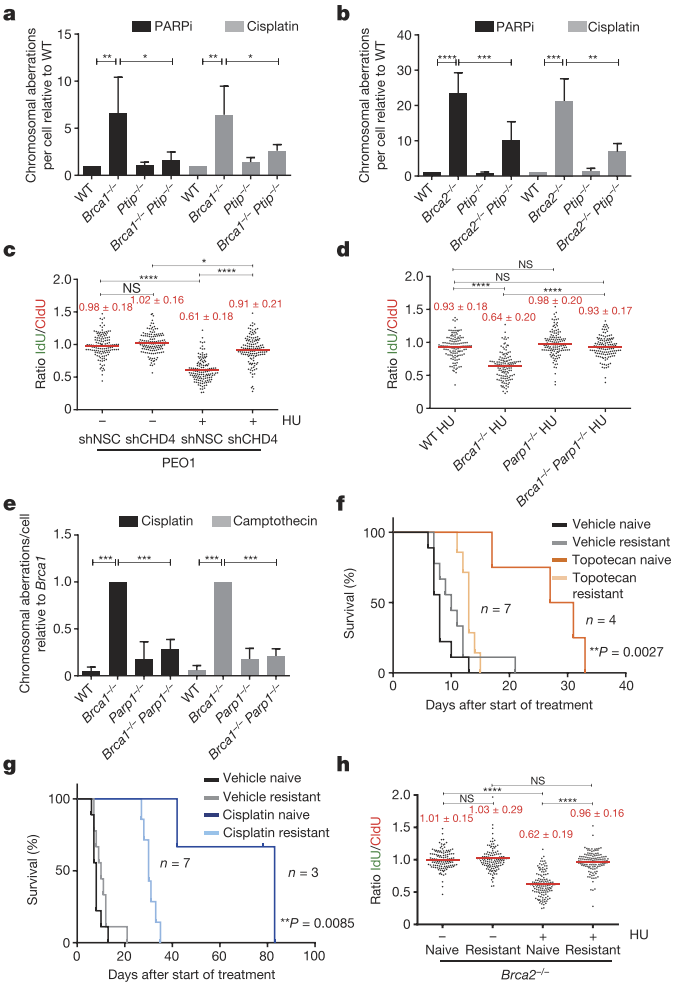

Figure 4 | Replication fork protection confers genome stability and chemotherapeutic resistance. a, **b**, Genomic instability measured in metaphase spreads from B cells ($n = 50$; $^{*}P \leq 0.05$, $^{**}P \leq 0.01$, $^{***}P \leq 0.001$, $^{****}P \leq 0.0001$, unpaired *t*-test). Experiments were repeated four times. **c**, Ratio of IdU versus CldU in *BRCA2*-mutated PEO1 cells either mock (shNSC) infected or infected with shRNA against CHD4 (shCHD4) ($^{*}P \leq 0.05$, $^{****}P \leq 0.0001$, Mann–Whitney test). One hundred and twenty-five replication forks were analysed. **d**, Ratio of IdU versus CldU in HU-treated B cells ($^{*}P \leq 0.05$, $^{****}P \leq 0.0001$, Mann–Whitney test). One hundred and twenty-five replication forks were analysed. **e**, Genomic instability in B cells ($n = 50$; $^{***}P \leq 0.001$, unpaired *t*-test). Experiments repeated four times. **f**, **g**, Kaplan–Meier survival curves in mice implanted with either PARPi-naive or -resistant tumours and treated with either topotecan (**f**) or cisplatin (**g**) using log-rank (Mantel–Cox) test. **h**, Ratio of IdU versus CldU in untreated or HU-treated tumours (PARPi naive versus PARPi resistant) ($^{****}P \leq 0.0001$, Mann–Whitney test). One hundred and twenty-five replication forks were analysed.

Moreover, depletion of CHD4 resulted in significantly decreased recruitment of MRE11 upon HU treatment in *Brca2* mutant cells (Extended Data Fig. 8e, f).

These results suggest that MRE11-mediated degradation contributes to genome instability upon treatment with replication poisons. To test this idea, we pre-incubated *Brca2*-deficient B cells with the MRE11 nuclease inhibitor mirin before treating with PARP inhibitor or cisplatin. Mirin treatment did not alter the frequency of replicating cells monitored by EdU incorporation (Extended Data Fig. 8g). However, incubation with mirin reduced the levels of PARPi-induced chromosomal aberrations approximately twofold. Similarly, *Brca2*-deficient cells were partly protected from cisplatin-induced DNA damage when MRE11 nuclease activity was inhibited (Extended Data Fig. 8h).

We conclude that MRE11 nuclease promotes genomic instability in *Brca2*-deficient cells.

Since PARP1 (ARTD1) is required for MRE11 localization to stalled replication forks[29] and its loss rescues the embryonic lethality in *Brca2*-null ESCs[30], we tested the contribution of PARP1 to RF stability and genome integrity by generating *Brca1*$^{-/-}$*Parp1*$^{-/-}$ B cells (*Brca1*$^{f/f}$; *Parp1*$^{-/-}$; *Cd19Cre*). Interestingly, loss of *Parp1* protected *Brca1*-deficient RFs from degradation and resulted in a significant reduction in chromosomal aberrations (Fig. 4d, e). Nevertheless, *Parp1* deficiency failed to rescue irradiation-induced RAD51 foci formation in *Brca1*-deficient cells (Extended Data Fig. 8i). Thus, despite the fact that treatment with PARP inhibitor increases levels of DNA damage in *Brca1*-deficient cells[31,32], loss of *Parp1* before *Brca1* loss protects against genome instability.

To determine whether *Brca2*-deficient tumour cells acquire chemotherapy resistance via RF protection, we induced PARPi-resistance using the KB2P mouse model for *Brca2*-deficient breast cancer (Extended Data Fig. 9a)[33]. A mammary tumour from KB2P mice was transplanted into syngeneic FVB mice and, when the tumour reached a size >200 mm^3, mice were treated with PARPi (AZD2461) for 28 consecutive days (Extended Data Fig. 9b, c). The tumour was initially responsive to treatment but eventually grew, upon which treatment was repeated until PARPi resistance was achieved (Extended Data Fig. 9c). The stability of acquired resistance was confirmed by re-transplanting matched naive and resistant tumours and treating the animals with vehicle or AZD2461 (Extended Data Fig. 9d). PARPi-resistant tumours also showed cross-resistance to replication poisons topotecan and cisplatin (Fig. 4f, g).

Both naive and resistant *Brca2*-deficient tumours showed impaired irradiation-induced RAD51 foci formation (Extended Data Fig. 9e, f). We therefore assayed naive and resistant tumours *ex vivo* for RF stability. The mean length of the CldU and the IdU tracts were similar in all samples that were not treated with HU (Fig. 4h and Extended Data Fig. 9g). While naive tumour cells showed degradation of nascent tracts upon HU treatment, resistant tumour cells were protected (Fig. 4h). These data suggest that RF protection rather than restoration of HR may be the main mechanism for acquired resistance in this mammary tumour. However, in this case, acquired resistance was not simply due to loss of PTIP or MRE11 proteins (Extended Data Fig. 9h).

Discussion

Our study and the accompanying paper[30] provide the first examples of genetic alterations that bypass the essential requirement for DSB-induced HR, evidenced by the finding that reduction in PTIP or PARP1 (ARTD1) levels rescues the lethality of *Brca2*-null ESCs. We speculate that the reason *Brca2* nullizygosity is compatible with viability is because RAD51 is able to perform essential HR functions (such as SCE) by loading onto RFs independently of BRCA2 (Extended Data Fig. 4e), even if RAD51 loading onto processed DSBs is strictly dependent on BRCA2 (Fig. 1g and Fig. 2c, d). We also show that loss of PTIP, PARP1 and CHD4 confers resistance to a variety of DNA-damaging agents in *Brca*-deficient cells. Resistance to PARPi and cisplatin both in primary and in tumour cells grown *in vitro* or *in vivo* correlates with protection from RF degradation. While 53BP1 disruption rescues the viability of *Brca1*-deficient mice by restoration of HR[8,9], cells from these animals show residual levels of chromosomal aberration. The significant level of RF degradation observed in *Brca1*$^{-/-}$*53Bp1*$^{-/-}$ cells (Fig. 1b) may contribute to this genome instability.

Since RF degradation is mediated by MRE11, we propose that persistence of MRE11 at stalled forks is toxic and normally counteracted by BRCA1/2. One possibility is that MRE11 could initially be recruited to stalled forks to mediate RF restart[4], and that BRCA1/2 is necessary to subsequently disengage MRE11 from already-processed DNA termini. Consistently, we have found a significant increase in chromatin-bound MRE11 in *Brca2*-deficient cells treated with HU or cisplatin (Extended Data Fig. 10 a, b)[4]. In *Saccharomyces cerevisiae*, failure to remove MRE11 from single-stranded DNA can lead to hypersensitivity to a variety of clastogens[34,35]. We therefore propose that deficiencies in PTIP, CHD4 and PARP1 could confer drug resistance in *Brca*-deficient cells by limiting the access of MRE11 to single-strand DNA at stalled RFs.

In summary, we have shown that protection of nascent DNA from degradation provides a mechanism that can promote synthetic viability and drug resistance in *Brca*-deficient cells without restoring HR at DSBs.

Online Content Methods, along with any additional Extended Data display items and Source Data, are available in the online version of the paper; references unique to these sections appear only in the online paper.

Received 30 July 2015; accepted 15 April 2016.

1. Lord, C. J. & Ashworth, A. Mechanisms of resistance to therapies targeting BRCA-mutant cancers. *Nature Med.* **19,** 1381–1388 (2013).
2. Schlacher, K. *et al.* Double-strand break repair-independent role for BRCA2 in blocking stalled replication fork degradation by MRE11. *Cell* **145,** 529–542 (2011).
3. Schlacher, K., Wu, H. & Jasin, M. A distinct replication fork protection pathway connects Fanconi anemia tumor suppressors to RAD51-BRCA1/2. *Cancer Cell* **22,** 106–116 (2012).
4. Ying, S., Hamdy, F. C. & Helleday, T. Mre11-dependent degradation of stalled DNA replication forks is prevented by BRCA2 and PARP1. *Cancer Res.* **72,** 2814–2821 (2012).
5. Pathania, S. *et al.* BRCA1 haploinsufficiency for replication stress suppression in primary cells. *Nature Commun.* **5,** 5496 (2014).
6. Pathania, S. *et al.* BRCA1 is required for postreplication repair after UV-induced DNA damage. *Mol. Cell* **44,** 235–251 (2011).
7. Bunting, S. F. *et al.* BRCA1 functions independently of homologous recombination in DNA interstrand crosslink repair. *Mol. Cell* **46,** 125–135 (2012).
8. Bunting, S. F. *et al.* 53BP1 inhibits homologous recombination in Brca1-deficient cells by blocking resection of DNA breaks. *Cell* **141,** 243–254 (2010).
9. Bouwman, P. *et al.* 53BP1 loss rescues BRCA1 deficiency and is associated with triple-negative and BRCA-mutated breast cancers. *Nature Struct. Mol. Biol.* **17,** 688–695 (2010).
10. Callen, E. *et al.* 53BP1 mediates productive and mutagenic DNA repair through distinct phosphoprotein interactions. *Cell* **153,** 1266–1280 (2013).
11. Chapman, J. R. *et al.* RIF1 is essential for 53BP1-dependent nonhomologous end joining and suppression of DNA double-strand break resection. *Mol. Cell* **49,** 858–871 (2013).
12. Escribano-Díaz, C. *et al.* A cell cycle-dependent regulatory circuit composed of 53BP1-RIF1 and BRCA1-CtIP controls DNA repair pathway choice. *Mol. Cell* **49,** 872–883 (2013).
13. Feng, L., Fong, K. W., Wang, J., Wang, W. & Chen, J. RIF1 counteracts BRCA1-mediated end resection during DNA repair. *J. Biol. Chem.* **288,** 11135–11143 (2013).
14. Di Virgilio, M. *et al.* Rif1 prevents resection of DNA breaks and promotes immunoglobulin class switching. *Science* **339,** 711–715 (2013).
15. Zimmermann, M., Lottersberger, F., Buonomo, S. B., Sfeir, A. & de Lange, T. 53BP1 regulates DSB repair using Rif1 to control 5′ end resection. *Science* **339,** 700–704 (2013).
16. Hashimoto, Y., Ray Chaudhuri, A., Lopes, M. & Costanzo, V. Rad51 protects nascent DNA from Mre11-dependent degradation and promotes continuous DNA synthesis. *Nature Struct. Mol. Biol.* **17,** 1305–1311 (2010).
17. Kuznetsov, S. G., Liu, P. & Sharan, S. K. Mouse embryonic stem cell-based functional assay to evaluate mutations in BRCA2. *Nature Med.* **14,** 875–881 (2008).
18. Willis, N. A. *et al.* BRCA1 controls homologous recombination at Tus/Ter-stalled mammalian replication forks. *Nature* **510,** 556–559 (2014).
19. Sonoda, E. *et al.* Sister chromatid exchanges are mediated by homologous recombination in vertebrate cells. *Mol. Cell. Biol.* **19,** 5166–5169 (1999).
20. Toledo, L. I. *et al.* A cell-based screen identifies ATR inhibitors with synthetic lethal properties for cancer-associated mutations. *Nature Struct. Mol. Biol.* **18,** 721–727 (2011).
21. Mirzoeva, O. K. & Petrini, J. H. DNA replication-dependent nuclear dynamics of the Mre11 complex. *Mol. Cancer Res.* **1,** 207–218 (2003).
22. Dungrawala, H. *et al.* The replication checkpoint prevents two types of fork collapse without regulating replisome stability. *Mol. Cell* **59,** 998–1010 (2015).
23. Cho, Y. W. *et al.* PTIP associates with MLL3- and MLL4-containing histone H3 lysine 4 methyltransferase complex. *J. Biol. Chem.* **282,** 20395–20406 (2007).
24. Patel, S. R., Kim, D., Levitan, I. & Dressler, G. R. The BRCT-domain containing protein PTIP links PAX2 to a histone H3, lysine 4 methyltransferase complex. *Dev. Cell* **13,** 580–592 (2007).
25. Gong, Z., Cho, Y. W., Kim, J. E., Ge, K. & Chen, J. Accumulation of Pax2 transactivation domain interaction protein (PTIP) at sites of DNA breaks via RNF8-dependent pathway is required for cell survival after DNA damage. *J. Biol. Chem.* **284,** 7284–7293 (2009).

26. Starnes, L. M. *et al.* A PTIP-PA1 subcomplex promotes transcription for IgH class-switching independently from the associated MLL3/MLL4 methyltransferase complex. *Genes Dev* **30,** 149–163 (2016).
27. Buonomo, S. B., Wu, Y., Ferguson, D. & de Lange, T. Mammalian Rif1 contributes to replication stress survival and homology-directed repair. *J. Cell Biol.* **187,** 385–398 (2009).
28. Guillemette, S. *et al.* Resistance to therapy in BRCA2 mutant cells due to loss of the nucleosome remodeling factor CHD4. *Genes Dev.* **29,** 489–494 (2015).
29. Bryant, H. E. *et al.* PARP is activated at stalled forks to mediate Mre11-dependent replication restart and recombination. *EMBO J.* **28,** 2601–2615 (2009).
30. Ding, X. *et al.* Synthetic viability by BRCA2 and PARP1/ARTD1 deficiencies. *Nature Commun*. http://dx.doi.org/10.1038/ncomms12425 (2016).
31. Bryant, H. E. *et al.* Specific killing of BRCA2-deficient tumours with inhibitors of poly(ADP-ribose) polymerase. *Nature* **434,** 913–917 (2005).
32. Farmer, H. *et al.* Targeting the DNA repair defect in BRCA mutant cells as a therapeutic strategy. *Nature* **434,** 917–921 (2005).
33. Jonkers, J. *et al.* Synergistic tumor suppressor activity of BRCA2 and p53 in a conditional mouse model for breast cancer. *Nature Genet.* **29,** 418–425 (2001).
34. Chen, H. *et al.* Sae2 promotes DNA damage resistance by removing the Mre11-Rad50-Xrs2 complex from DNA and attenuating Rad53 signaling. *Proc. Natl Acad. Sci. USA* **112,** E1880–E1887 (2015).
35. Puddu, F. *et al.* Synthetic viability genomic screening defines Sae2 function in DNA repair. *EMBO J.* **34,** 1509–1522 (2015).
36. Moynahan, M. E., Pierce, A. J. & Jasin, M. BRCA2 is required for homology-directed repair of chromosomal breaks. *Mol. Cell* **7,** 263–272 (2001).

Supplementary Information is available in the online version of the paper.

Acknowledgements We thank A. Bhandoola for discussions; K. Wolcott for flow cytometry; R. Faryabi for help with statistical analysis; T. de Lange for *Rif1*$^{f/f}$ mice, J. Tainer for PFM39, R. Brosh for WRNi and J. Petrini for Mre11 antibodies. This work was supported by the Intramural Research Program of the National Institutes of Health (NIH), the National Cancer Institute and the Center for Cancer Research, and by a Department of Defense grant to A.N. (BCRP DOD Idea Expansion Award, grant 11557134), and the Netherlands Organization for Scientific Research, the Dutch Cancer Society and the Swiss National Science Foundation to S.V. A.R.C. was supported by a Prospective Researcher Award from Swiss National Science Foundation (PBZHP3_147302) and Human Frontier Science Program Long-Term Fellowship (LT000393/2013). S.C. was supported by NIH grant R01 CA176166-01A1; B.S. was supported by NIH grant R01CA085344; and J.A.D. was supported by a grant to the Center for Protein Research from the Novo Nordisk Foundation (NNF14CC0001).

Author Contributions A.R.C., E.C., S.S. and A.N. conceived and planned the study. A.R.C., E.C. and X.D. designed, performed experiments and analysed data on B cells, MEFS and ESCs. E.G. and A.A.D. generated and performed experiments on PARPi-resistant tumours. J.J. and S.R. supervised the studies on PARPi-resistant tumours. N.W., A.D. and S.J. helped with experimentation. J.E.L. and K.G. generated *Mll4*- and *Mll4*-SET-deficient mice. L.S. and J.D. generated PTIP deletion constructs. B.S. provided reagents for experiments. D.C. provided advice on performing iPOND experiments and supervised iPOND mass spectrometry. J.C., N.P. and S.C. provided shCHD4 PEO1 cells and performed immunofluorescence experiments. P.K. analysed TCGA databases. V.F. and O.F.C. performed high-throughput image analysis of MRE11. S.S. supervised the ESC studies. A.R.C., E.C. and A.N. wrote the manuscript and all authors reviewed it.

Author Information Source tumour measurement data are provided in Supplementary Information. Reprints and permissions information is available at www.nature.com/reprints. The authors declare no competing financial interests. Readers are welcome to comment on the online version of the paper. Correspondence and requests for materials should be addressed to A.N. (andre_nussenzweig@nih.gov).

METHODS

Mice, MEFs, and B cell cultures. The *53Bp1*$^{-/-}$ (ref. 37), *Brca1*$^{f(\Delta 11)/f(\Delta 11)}$ (NCI mouse repository), *Brca2*$^{f/f}$ (NCI mouse repository), *Rif1*$^{f/f}$ (ref. 27), *Ptip*$^{f/f}$ (ref. 24) and *Mll4*$^{f/f}$ (ref. 38) mice have been described. To generate *Mll4*-SET-flox/flox mice, exons 50–51 of the *Mll4*/*Kmt2d* gene were flanked by *loxP* sites. Cre-mediated deletion of the floxed exons 50–51 causes frame shift and generates a stop codon in exon 52. The resulting protein lacks the carboxy (C)-terminal 276 amino acids including the entire enzymatic SET domain. Resting splenic B cells were isolated from 8- to 12-week-old WT or mutant spleen with anti-CD43 microbeads (anti-Ly48; Miltenyi Biotech) and were cultured with LPS (25 μg/ml; Sigma), IL-4 (5 ng/ml; Sigma) and RP105 (0.5 μg/ml; BD) as described[10]. Stimulated B cells were additionally infected with CRE to ensure a high level of gene deletion in these cells. All mice were randomly distributed in experimental groups after genotyping. WT MEFs were immortalized by SV40 retroviral infection, and SV40 immortalized *Ptip*$^{f/f}$ (ref. 39) and *Mll3* $^{-/-}$*Mll4*$^{f/f}$ MEFs[38] were infected with a CRE retrovirus to delete *Ptip* and *Mll4* respectively. Coding sequences for mouse Ptip–GFP were cloned into the MIGR1 retroviral vector as previously described[10]. All cell lines used were tested for mycoplasma using a Mycoplasma Detection Kit (Invitrogen) and relevant cell lines were authenticated either by genotyping or western blot analysis. PARP inhibitor (KU58948) was obtained from AstraZeneca. Mirin was obtained from Sigma, PFM39 and WRN inhibitors were gifts from J. Tainer and R. Brosh respectively. DNA2 inhibitor has been described[40]. Cisplatin and HU were obtained from Sigma. For FISH analysis, metaphases were prepared and imaged as described[10]. Animal experiments were approved by the Animal Care and Use Committee of NCI-Bethesda and the Animal Ethical Committee of The Netherlands Cancer Institute.

Generation of CHD4-deficient PEO1 lines using RNAi. *BRCA2*-mutated ovarian cancer cell lines PEO1 were grown in DMEM with 10% FBS and 1% Glutmax. RNAi for CHD4 was performed as previously described[28].

ESC lines, shRNA knockdowns and rescue of BRCA2 viability. PL2F2 mouse ESCs were maintained in M15 media (Knockout DMEM with 15% fetal bovine serum, 0.00072% β-mercaptoethanol, 100 U/ml penicillin, 100 μg/ml streptomycin and 0.292 mg/ml L-glutamine) at 37 °C, 5% CO_2. ESCs were plated on a monolayer of mitotically inactive feeder cells as described previously[17]. BRCA2 conditional knockout ESCs were generated as previously described[17]. Two different shRNAs against *Ptip* mRNA were cloned into pSuperior vector (Oligoengine). shRNA sequences are listed below with the targeted sequences underlined: *mPtip shRNA-1* sense, 5′GATCCCC GTGGCGCTCTCCTGCCAGT TTCAAGAGA ACTGGCAGGAGAGCGCCAC TTTTTA 3′; *mPtip shRNA-1* antisense, 5′ AGCTTAAAAA GTGGCGCTCTCCTGCCAGT TCTCTTGAA ACTGGCAGGAGAGCGCCAC GGG 3′; *mPtip shRNA-2* sense, 5′GATCCCC CCGTAGCAACACAGTCCTC TTCAAGAGA GAGGACTGTGTTGCTACGG TTTTTA 3′; *mPtip shRNA-2* antisense, 5′ AGCTTAAAAA CCGTAGCAACAC AGTCCTC TCTCTTGAA GAGGACTGTGTTGCTACGG GGG 3′.

shRNA vectors were linearized by ScaI and electroporated into ESCs using a Bio-Rad gene pulser. Cells were selected in G418 (0.18 mg/ml) 24 h after electroporation for 5 days. Individual colonies were picked and PTIP levels were determined by western blotting. The PGK-Cre plasmid was electroporated into *Ptip* shRNA knockdown cells (20 μg DNA for 1×10^7 cells). Thirty-six hours after electroporation, HAT (hypoxanthine–aminopterin–thymidine) selection was performed for 5 days, after which cells were switched to HT (hypoxanthine–thymidine) media for 2 days and then transferred to normal media. Colonies were picked when visible, genomic DNA was extracted and Southern blotting was performed as described previously[17]. For PCR genotyping, the following primers were used to amplify the *Brca2* cko allele and *Brca2*-KO allele: *Brca2*-KO forward, 5′ GCCACCTCTGCCTGATTCTA; *Brca2*-KO reverse, 5′ AAAGAACCAGCTGGGGCTCGAG; *Brca2*-flox forward, 5′ TG AAGTGGACCCTGTAACCC; *Brca2*-flox reverse, 5′ AGTTCTCTCCTTTCA GCCTTCT.

Gene targeting and the gene conversion HR assay. For gene targeting, ESCs were electroporated with 75 μg of linear targeting fragment from p59xDR–GFP, followed by selection for 5 days in 110 μg/ml hygromycin; then they were allowed to grow in normal ESC media[36]. Colonies were picked, and targeted clones were identified by Southern hybridization as described[36]. For the DSB-induced HR assay, ESCs were transiently electroporated with 20 μg of either pDR–GFP only or pDR–GFP plus I-SceI expressing vectors for 48 h. Gene conversion was read-out as the percentage of GFP-positive cells by flow cytometry analysis[41].

DNA fibre analysis. Asynchronous B cells, *BRCA2*-mutated PEO1 cells and *Brca2*-deficient K2BP tumours were labelled with 30 μM CldU, washed with PBS and exposed to 250 μM IdU. After exposure to IdU, the cells were washed again in warm PBS and treated or not with HU before collection. Cells were then lysed and DNA fibres stretched onto glass slides, as described[42]. The fibres were denatured with 2.5 M HCl for 1 h, washed with PBS and blocked with 2% BSA in phosphate buffered saline Tween-20 for 30 min. The newly replicated CldU and IdU tracts were revealed with anti-BrdU antibodies recognizing CldU and IdU respectively. Images were taken at 60 × magnification (Zeiss Axio Observer.Z1), and statistical analysis was performed using GraphPad Prism.

DSB detection by PFGE. DSB detection by PFGE was done as described[42]. Ethidium-bromide-stained gels were analysed using an UVP EC3 imaging system. Quantification was performed using ImageJ normalizing DSB signals to unsaturated DNA signals in the well. Relative DSB levels were obtained by comparing treatment results to the background DSB signals observed for untreated conditions.

Western blotting and immunofluorescence. Primary antibodies were used at the following dilutions: anti-tubulin (1:15,000, Sigma), anti-H3K4me3 (1:5,000, Millipore), anti-H3K4me1 (1:5,000, Millipore), anti-RAD51 (1:50, Santa Cruz), anti-PCNA (1:2,000, Santa Cruz), anti-total H3 (1:1,000 Millipore) and anti-Mre11 (1:10,000, gift from J. Petrini, MSKCC). MEFs were prepared for immunofluorescence by growth on 18 mm × 18 mm glass cover slips. Lymphocytes were dropped onto slides coated with CellTak (BD Biosciences). Cells were fixed with methanol and incubated with primary antibody as indicated.

iPOND and flow cytometry. iPOND was performed essentially as described[22]. One hundred and fifty million WT, *Ptip*$^{-/-}$ and *Mll3*$^{-/-}$*Mll4*$^{-/-}$ MEFs were labelled with 10 μM EdU (Life Technologies) and treated with HU as indicated. Two hundred million cells were use for iPOND experiments with ESCs. Cells were cross-linked with 1% formaldehyde for 10 min at room temperature, quenched with 0.125 M glycine and washed with PBS. For the conjugation of EdU with biotin azide, cells were permeabilized with 0.25% Triton X-100/ PBS, and incubated in click reaction buffer (10 mM sodium-L-ascorbate, 20 μM biotin azide (Life Technologies), and 2 mM CuSO4) for 2 h at room temperature. Cells were resuspended in lysis buffer (50 mM Tris-HCl, pH 8.0, and 1% SDS) supplemented with protease inhibitors (Roche), and chromatin was solubilized by sonication in a Bioruptor (Diagenode-Pico) at 4 °C for 24 min. After centrifugation, clarified supernatants were incubated for 1 h with streptavidin-MyOne C1 beads (Life Technologies). Beads were washed and captured proteins were eluted by boiling beads in 2 × NuPAGE LDS Sample Buffer (Life Technologies) containing 200 mM DTT for 40 min at 95 °C. Proteins were resolved by electrophoresis using NuPAGE Novex 4–12% Bis-Tris gels and detected by western blotting with the indicated antibodies. For flow cytometric analysis, asynchronous B cells were pulsed with 10 mM EdU for 20 min at 37 °C and stained using the Click-IT EdU Alexa Fluor 488 Flow Cytometry Assay Kit according to the manufacturer's specifications (ThermoFisher C-10425).

Generation of AZD2461-resistant KB2P tumours and *in situ* RAD51 assay. *Brca2*$^{-/-}$;*p53*$^{-/-}$ mammary tumours were generated in *K14-cre;Brca2*$^{f/f}$; *p53*$^{f/f}$ (KB2P) female mice and genotyped as described previously[33]. Orthotopic transplantations into WT FVB/N/OLA (F1) mice, tumour monitoring, and sampling were conducted as described[43]. Starting from 2 weeks after transplantation, tumour size was monitored at least three times a week. All treatments were started when tumours reached a size of approximately 200 mm^3. AZD2461 (100 mg/kg) was given orally for 28 consecutive days. If tumours did not shrink below 100% of the initial volume, treatment was continued for another 28 days. AZD2461 was diluted in 0.5% w/v hydroxypropyl methylcellulose in deionized water to a concentration of 10 mg/ml. For testing cross-resistance, mice were given a single treatment regimen of topotecan (2 mg/kg intraperitoneally, days 0–4 and 14–18) or cisplatin (Mayne Pharma, 6 mg/kg intravenously, day 0). Statistical analysis was performed using GraphPad Prism (log-rank Mantel–Cox test). The *in situ* RAD51 irradiation induced formation assay has been described[44].

Statistics. Statistics was performed by two-tailed *t*-test, Mann–Whitney test or by log-rank Mantel–Cox test unless otherwise specified. Statistical tests were justified appropriate for every figure. The data were normally distributed and the variance between groups being statistically compared was similar. No statistical methods or criteria were used to estimate sample size or to include/exclude samples. The investigators were not blinded to the group allocation during the experiments; however, the samples were coded before analysis unless otherwise specified.

37. Ward, I. M. *et al.* 53BP1 is required for class switch recombination. *J. Cell Biol.* **165,** 459–464 (2004).
38. Lee, J. E. *et al.* H3K4 mono- and di-methyltransferase MLL4 is required for enhancer activation during cell differentiation. *eLife* **2,** e01503 (2013).
39. Cho, Y. W. *et al.* Histone methylation regulator PTIP is required for PPARγ and C/EBPα expression and adipogenesis. *Cell Metab.* **10,** 27–39 (2009).
40. Liu, W. *et al.* A selective small molecule DNA2 inhibitor for sensitization of human cancer cells to chemotherapy. *EBioMedicine* **6,** 73–86 (2016).
41. Pierce, A. J., Johnson, R. D., Thompson, L. H. & Jasin, M. XRCC3 promotes homology-directed repair of DNA damage in mammalian cells. *Genes Dev.* **13,** 2633–2638 (1999).
42. Ray Chaudhuri, A. *et al.* Topoisomerase I poisoning results in PARP-mediated replication fork reversal. *Nature Struct. Mol. Biol.* **19,** 417–423 (2012).
43. Rottenberg, S. *et al.* Selective induction of chemotherapy resistance of mammary tumors in a conditional mouse model for hereditary breast cancer. *Proc. Natl Acad. Sci. USA* **104,** 12117–12122 (2007).
44. Xu, G. *et al.* REV7 counteracts DNA double-strand break resection and affects PARP inhibition. *Nature* **521,** 541–544 (2015).

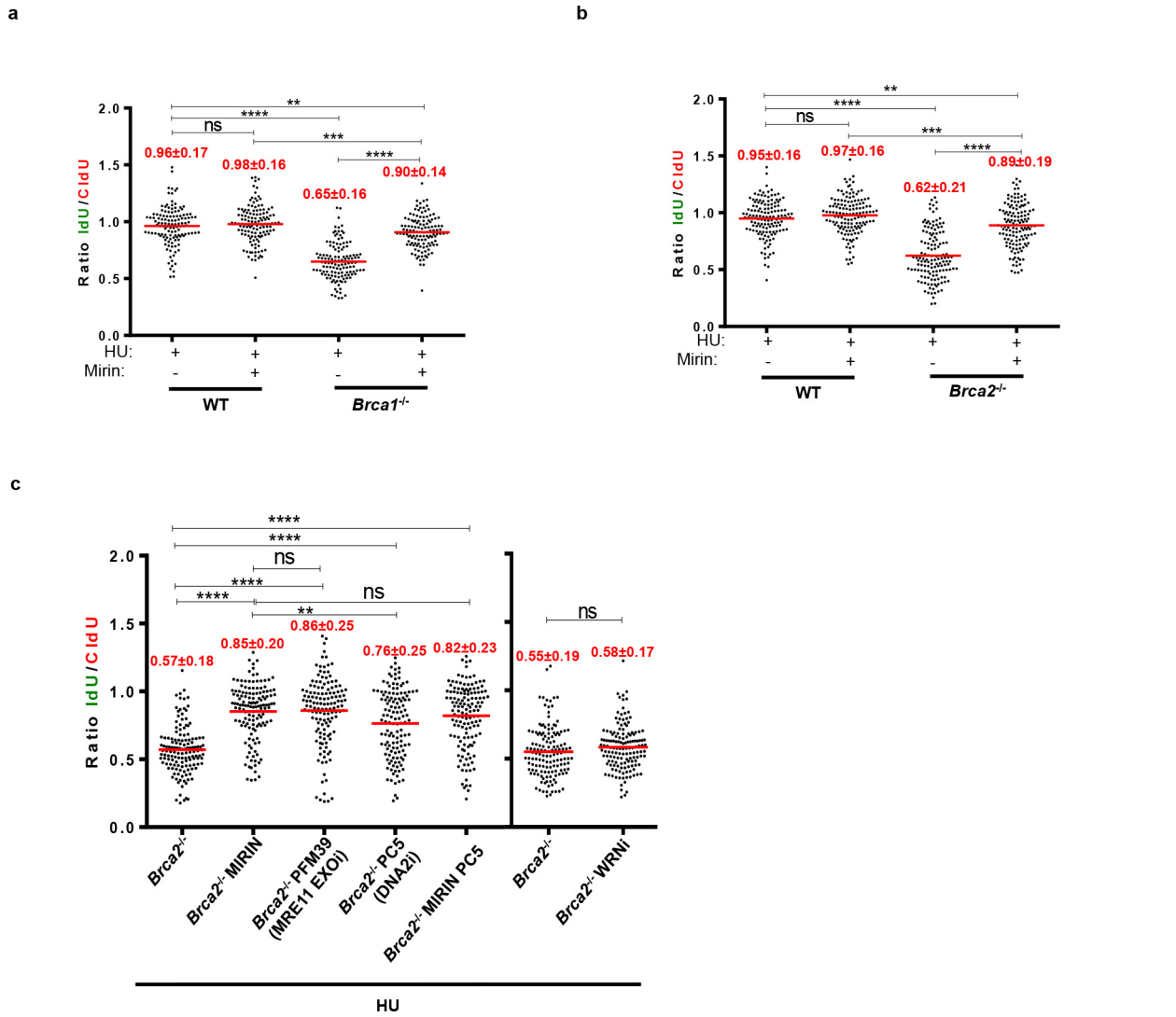

Extended Data Figure 1 | Fork degradation in *Brca*-deficient B lymphocytes is mediated by MRE11 exonuclease activity. a, **b**, Ratio of IdU versus CldU upon HU treatment in WT, *Brca1*$^{-/-}$ (**a**) and WT, *Brca2*$^{-/-}$ (**b**) B lymphocytes with or without mirin pre-treatment. Numbers in red indicate the mean ± s.d. for each sample (**$P \leq 0.05$, ***$P \leq 0.001$, ****$P \leq 0.0001$, Mann–Whitney test). One hundred and twenty-five replication forks were analysed for each genotype. **c**, Ratio of IdU versus CldU upon HU treatment in *Brca2*$^{-/-}$ B lymphocytes with or without mirin, PFM39 (MRE11 exonuclease inhibitor), PC5 (DNA2 inhibitor) or WRNi pre-treatment. Numbers in red indicate the mean ± s.d. for each sample (**$P \leq 0.05$, ****$P \leq 0.0001$, Mann–Whitney test). One hundred and twenty-five replication forks were analysed for each genotype.

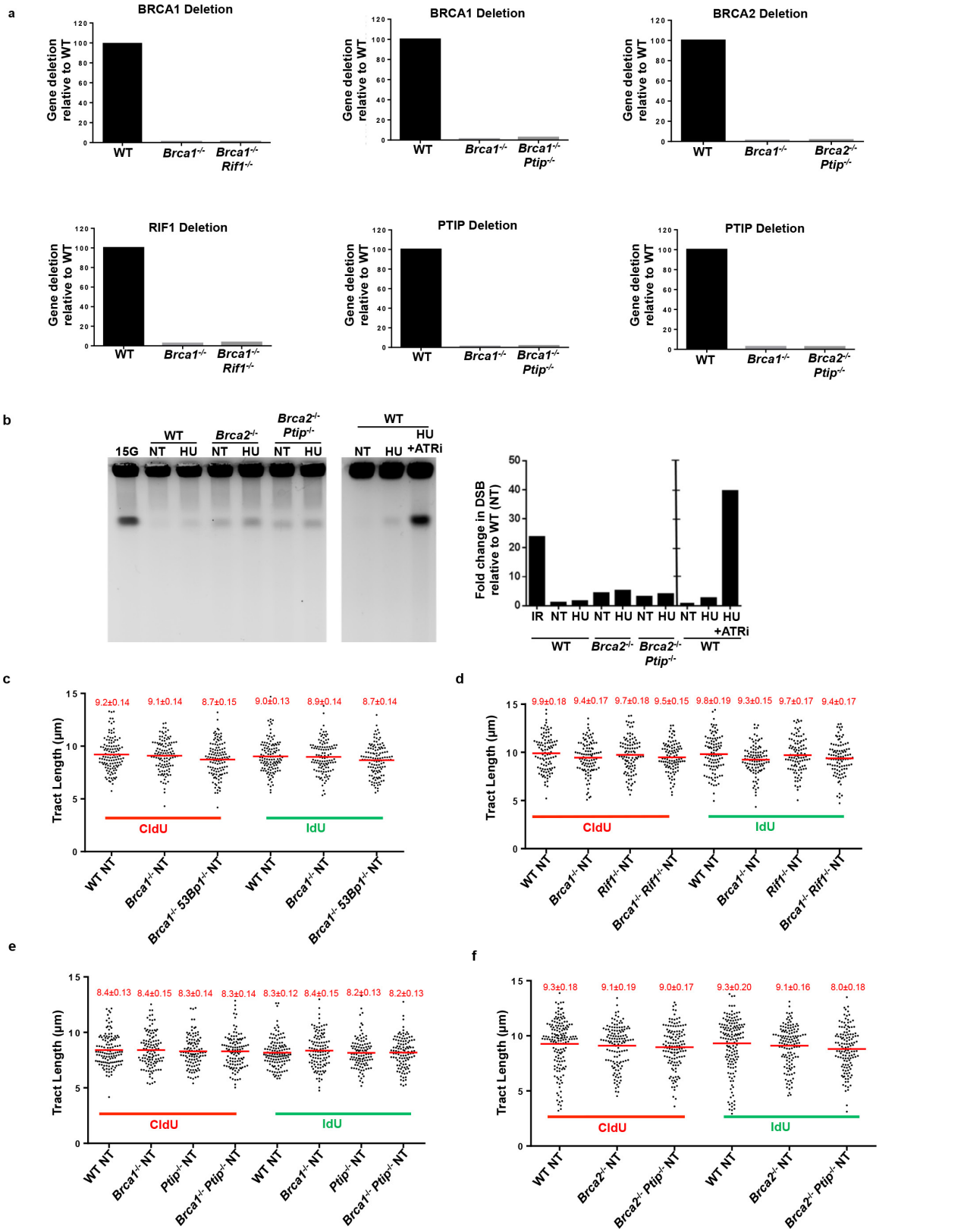

Extended Data Figure 2 | Replication fork progression rates and DSBs in B lymphocytes. a, Quantificative PCR analysis for *Brca1*, *Brca2*, *Ptip* and *Rif1* gene deletions in WT, *Brca1*$^{-/-}$, *Brca1*$^{-/-}$ *Rif1*$^{-/-}$, *Brca1*$^{-/-}$*Ptip*$^{-/-}$, *Brca2*$^{-/-}$ and *Brca2*$^{-/-}$ *Ptip*$^{-/-}$ primary B lymphocytes after infection with CRE. **b**, PFGE analysis for detection of DSBs in WT, *Brca2*$^{-/-}$ and *Brca2*$^{-/-}$ *Ptip*$^{-/-}$ B lymphocytes treated with or without 4 mM HU for 3 h. Positive control for DSBs includes treatment of 15 Gy irradiation and HU +ATRi treatment for 3 h. Quantification of fold change in DSBs across genotypes relative to non-treated WT is plotted on the right. **c**–**f**, Replication fork progression rates, measured by tract lengths in micrometres, of CldU (red) and IdU (green) in WT, *Brca1*$^{-/-}$, *Brca1*$^{-/-}$ *53Bp1*$^{-/-}$, *Rif1*$^{-/-}$, *Brca1*$^{-/-}$ *Rif1*$^{-/-}$, *Ptip*$^{-/-}$, *Brca1*$^{-/-}$ *Ptip*$^{-/-}$, *Brca2*$^{-/-}$ and *Brca2*$^{-/-}$ *Ptip*$^{-/-}$ primary B lymphocytes. Samples were not treated with HU. Numbers in red indicate the mean ± s.d. for each sample. One hundred and twenty-five replication forks were analysed for each genotype.

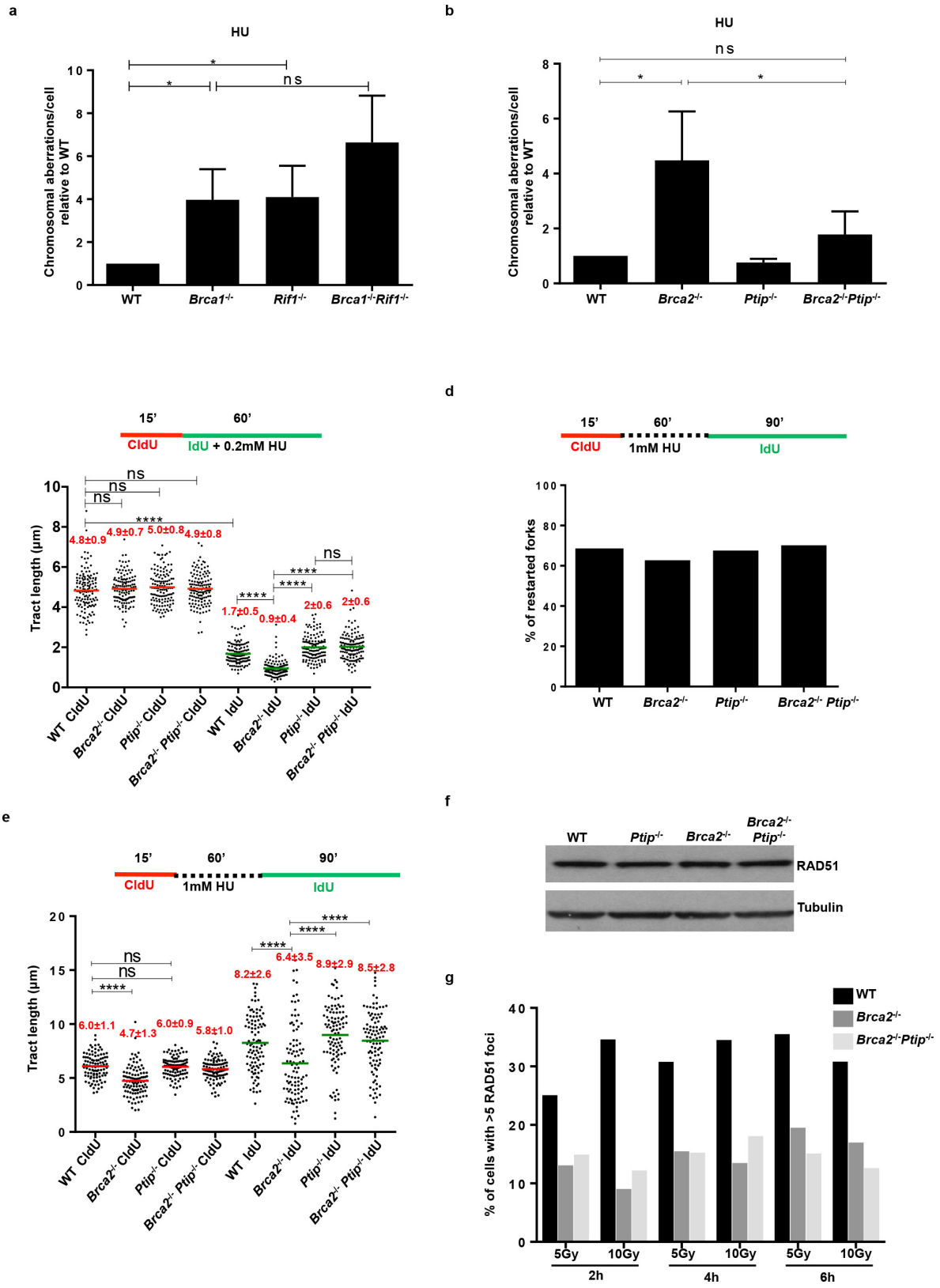

Extended Data Figure 3 | See next page for caption.

Extended Data Figure 3 | Loss of PTIP rescues fork progression and restart defects in *Brca2*-deficient B lymphocytes but does not affect RAD51 IRIF. a, Genomic instability measured in metaphase spreads from B lymphocytes derived from WT, *Brca1*$^{-/-}$, *Rif1*$^{-/-}$, *Brca1*$^{-/-}$*Rif1*$^{-/-}$ mice treated for 6 h with 10 mM HU (*$P \leq 0.05$, unpaired *t*-test). Fifty metaphases were analysed per condition. Experiments were repeated three times. **b**, Genomic instability measured in metaphase spreads from B lymphocytes derived from WT, *Brca2*$^{-/-}$, *Ptip*$^{-/-}$, *Brca2*$^{-/-}$*Ptip*$^{-/-}$ mice treated for 6 h with 10 mM HU (*$P \leq 0.05$, unpaired *t*-test). Fifty metaphases were analysed per condition. Experiments were repeated three times. **c**, Fork progression in B lymphocytes derived from WT, *Brca2*$^{-/-}$, *Ptip*$^{-/-}$, *Brca2*$^{-/-}$*Ptip*$^{-/-}$ mice treated for 1 h with 0.2 mM HU. The *y* axis represents the tract lengths in micrometres. Numbers in red indicate the mean ± s.d. for each sample (****$P \leq 0.0001$, Mann–Whitney test). One hundred and fifty replication forks were analysed for each genotype. **d**, Percentage of restarted replication forks in WT, *Brca2*$^{-/-}$, *Ptip*$^{-/-}$, *Brca2*$^{-/-}$*Ptip*$^{-/-}$ B cells treated for 1 h with 1 mM HU followed by 90 min recovery. Two hundred replication forks were analysed for each genotype. **e**, Tract lengths of restarted replication forks in WT, *Brca2*$^{-/-}$, *Ptip*$^{-/-}$, *Brca2*$^{-/-}$*Ptip*$^{-/-}$ B cells treated for 1 h with 1 mM HU followed by 90 min recovery. The *y* axis represents the tract lengths in micrometres. Numbers in red indicate the mean ± s.d. for each sample (NS, not significant, ****$P \leq 0.0001$, Mann–Whitney test). One hundred and fifty replication forks were analysed for each genotype. **f**, Western blot analysis for RAD51 levels in WT, *Ptip*$^{-/-}$, *Brca2*$^{-/-}$ and *Brca2*$^{-/-}$*Ptip*$^{-/-}$ B cell extracts. Tubulin was used as loading control. **g**, Quantification of RAD51 foci formation in WT, *Brca2*$^{-/-}$ and *Brca2*$^{-/-}$*Ptip*$^{-/-}$ B cells upon treatment with 5 and 10 Gy irradiation and recovery for 2, 4 and 6 h ($n = 150$ cells analysed).

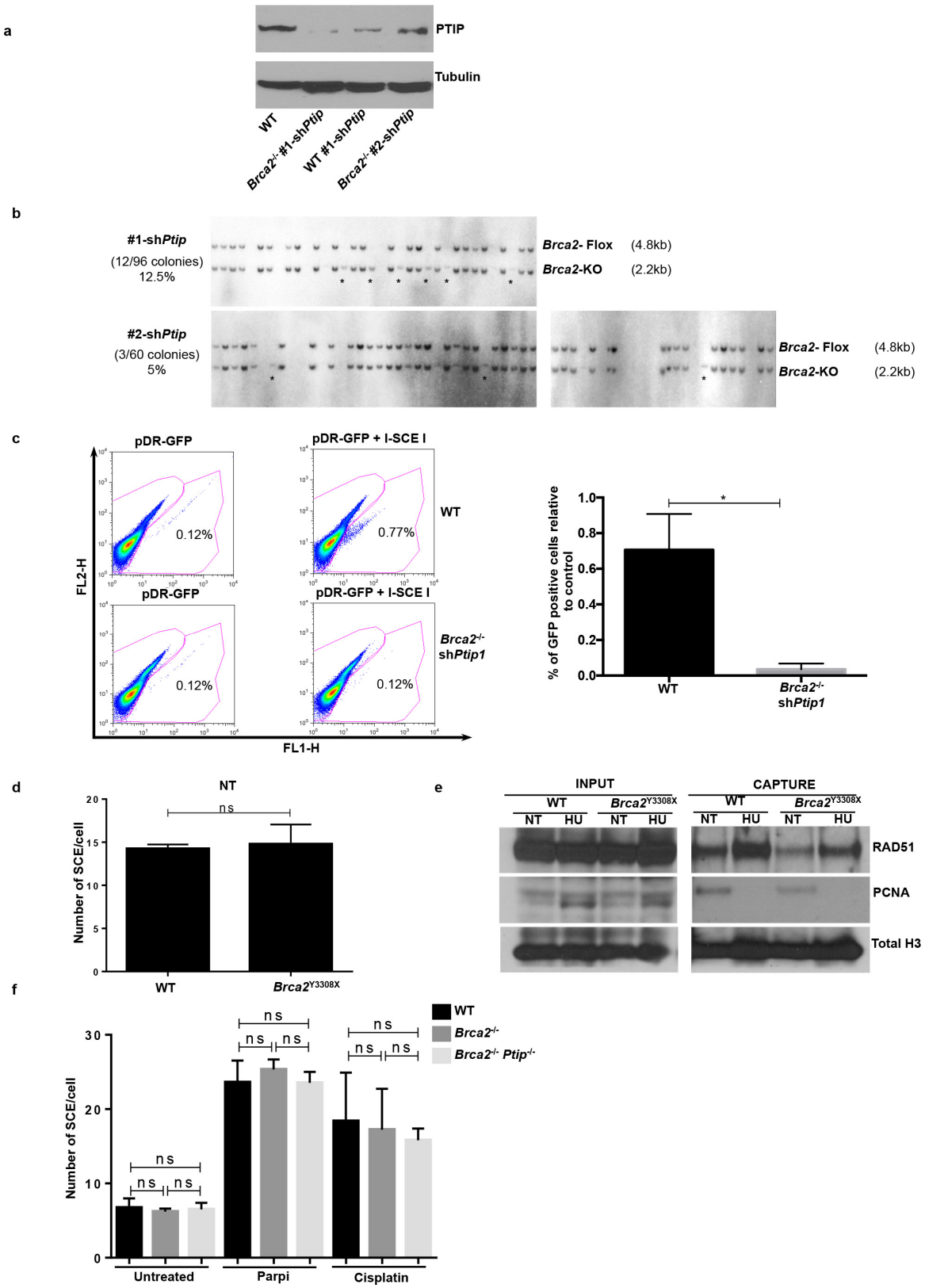

Extended Data Figure 4 | See next page for caption.

Extended Data Figure 4 | Depletion of PTIP rescues the lethality of *Brca2*-deficient ESCs. a, Western blot analysis for PTIP levels in WT and two different clones of *Brca2*$^{-/-}$ ESCs electroporated with sh*Ptip*. **b**, Southern blot analysis for determination of *Brca2* deletion in surviving clones electroporated with sh*Ptip*. Probes distinguishing the *Brca2*-flox allele (4.8 kb) (upper band) and *Brca2* KO allele (2.2 kb) (lower band) were used. *Surviving ESC clones with *Brca2* deletion and simultaneous downregulation of PTIP (12/96 *Brca2*-deleted colonies were found with sh*Ptip*1 and 3/60 colonies were found with sh*Ptip*2). Genotyping was confirmed by PCR (Fig. 2b). **c**, Top, representative FACS profiles of WT and *Brca2*$^{-/-}$/sh*Ptip* ESCs electroporated with either pDR–GFP plasmid only (control) or pDRGFP and I-SceI expressing vector for 48 h. Gene conversion of the pDR–GFP construct by HR is determined by the percentage of GFP-positive cells (FL1, green-detection filter; FL2, red-detection filter). Bottom, quantification of the percentage of GFP-positive cells in WT and *Brca2*$^{-/-}$/sh*Ptip* ESCs across three independent experiments. NS, not significant, $*P \leq 0.05$, unpaired *t*-test. **d**, Sister chromatid exchange (SCE) analysis in WT and *Brca2*^{Y3308X} hypomorphic ESCs. Twenty metaphases were analysed per condition; experiments were repeated three times. **e**, WT and *Brca2*^{Y3308X} hypomorphic ESCs were preincubated with mirin, EdU-labelled for 15 min and treated with 4 mM HU for 2 h. Proteins associated with replication forks were isolated by iPOND and detected by western blotting with the indicated antibodies. **f**, SCEs in WT, *Brca2*$^{-/-}$ and *Brca2*$^{-/-}$ *Ptip*$^{-/-}$ B cells either untreated or treated overnight with 1 μM PARPi or with 0.5 μM cisplatin (NS, not significant, $*P \leq 0.05$, $**P \leq 0.001$, unpaired *t*-test). Twenty metaphases were analysed per condition; experiments were repeated three times.

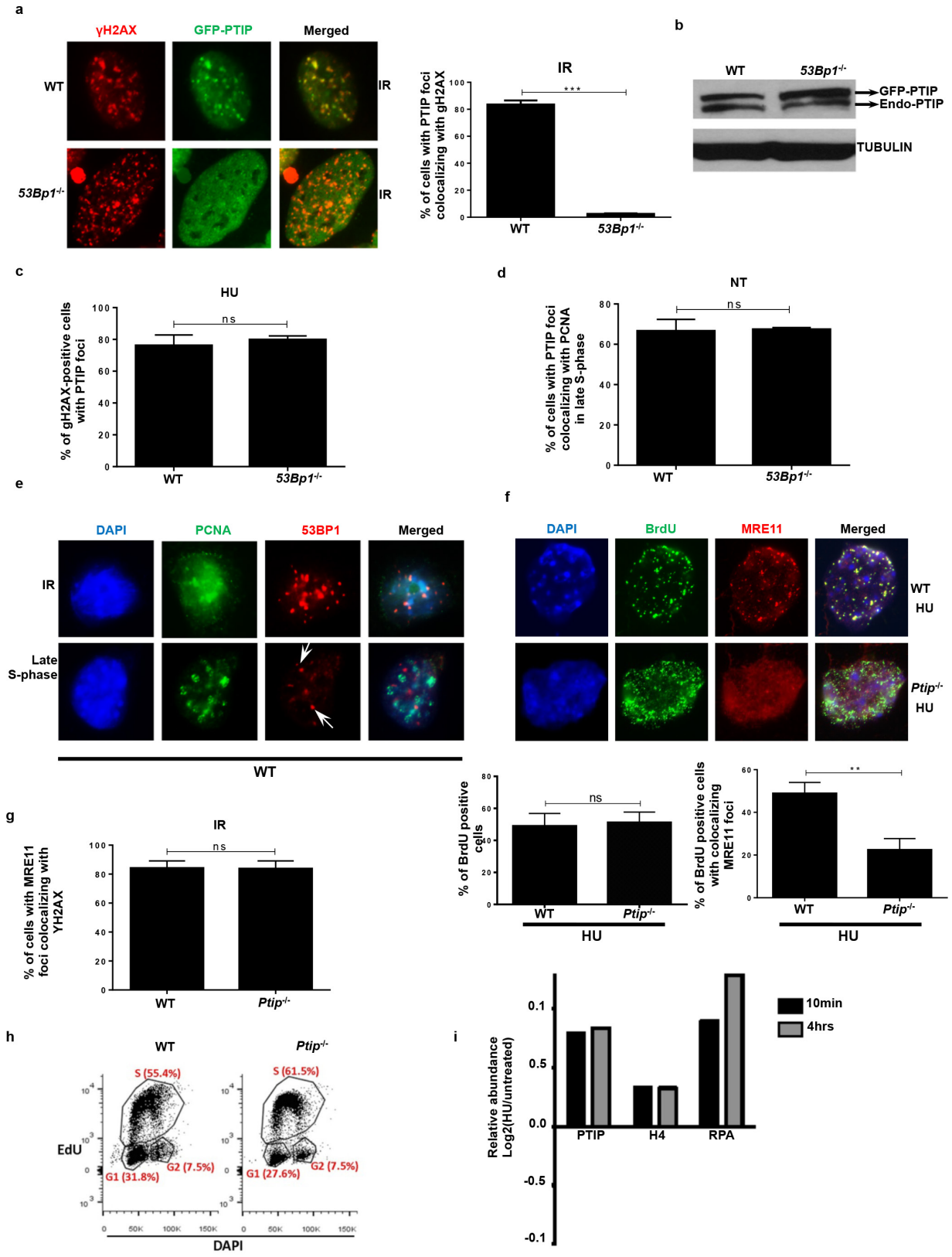

Extended Data Figure 5 | See next page for caption.

Extended Data Figure 5 | PTIP localizes to sites to DNA replication independently of DSBs. a, WT and *53Bp1*$^{-/-}$ MEFs were retrovirally infected with a GFP-tagged PTIP construct. Cells were then irradiated with 10 Gy and allowed to recover. Co-localization of γ-H2AX (red) and PTIP (green) was assessed. Adjoining graph quantifies the percentage of cells with γ-H2AX foci co-localizing with PTIP upon irradiation ($n = 150$ cells analysed). Experiments were repeated three times. **b**, Western Blot analysis for endogenous and overexpressed PTIP levels in WT and *53Bp1*$^{-/-}$ MEFs retrovirally infected with a GFP-tagged PTIP construct (GFP–PTIP). **c**, Quantification of the percentage of pan-nuclear γ-H2AX-positive cells with PTIP foci in WT and *53Bp1*$^{-/-}$ MEFs upon treatment with HU (related to Fig. 3a) ($n = 150$ cells analysed). Experiments were repeated three times. **d**, Quantification of the percentage of cells with PTIP foci co-localizing with PCNA in WT and *53Bp1*$^{-/-}$ MEFs in late S phase (related to Fig. 3b) ($n = 150$ cells analysed). Experiments were repeated three times. **e**, Representative immunofluorescence images of PCNA and 53BP1 co-staining in irradiated WT cells (10 Gy) or in late S-phase sites. White arrows indicate that the few 53BP1 foci observed in late S-phase cells do not co-localize with PCNA. ($n = 50$ cells analysed). Experiments were repeated three times. **f**, Representative immunofluorescence images of WT and *Ptip*$^{-/-}$ MEFs treated with 4 mM HU for 2 h and analysed for ssDNA (BrdU) and MRE11 co-localization. Bottom panels shows the quantification of BrdU-positive cells (left) and the percentage of MRE11 co-localization in BrdU-positive cells (right) upon HU treatment in WT and *Ptip*$^{-/-}$ MEFs. ($n = 150$ cells analysed). Experiments were repeated three times. **g**, Quantification of the percentage of cells with MRE11 foci co-localizing with γ-H2AX upon irradiation treatment (10 Gy) in WT and *Ptip*$^{-/-}$ MEFs (related to Fig. 3e) ($n = 150$ cells analysed). Experiments were repeated three times. **h**, Cell cycle profiles in WT and *Ptip*$^{-/-}$ MEFs as measured by the incorporation of EdU (*y* axis) vs. DAPI (*x* axis). **i**, iPOND coupled to SILAC Mass-Spectrometry analysis for PTIP, H4 and RPA enrichment at stalled forks in 293T cells upon 3 mM HU treatment for 10 min and 4 h (ref. 22). The *y* axes represent the relative abundance of the indicated proteins on a $\log_2$ scale.

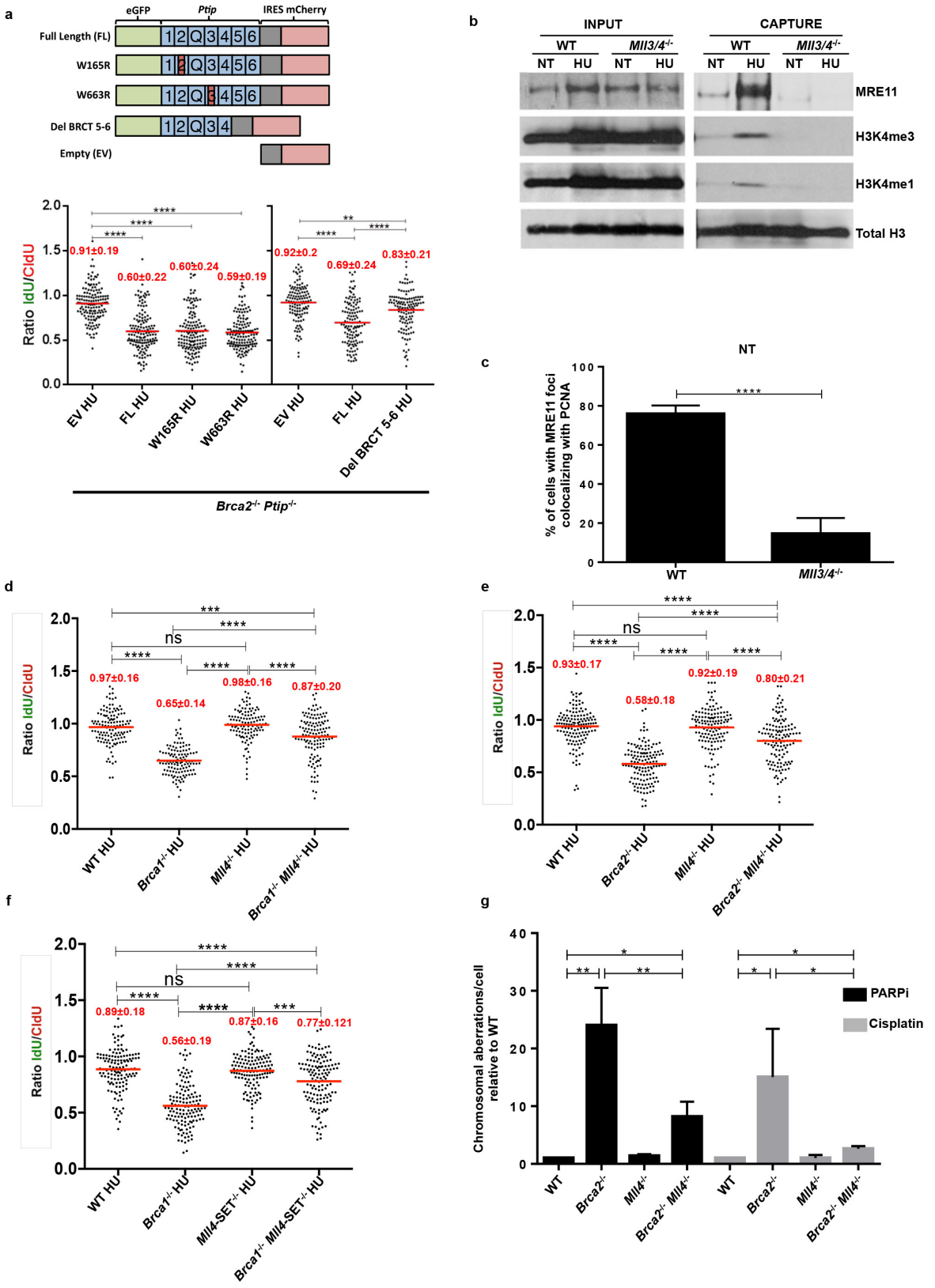

Extended Data Figure 6 | See next page for caption.

Extended Data Figure 6 | MLL3/4 promotes replication fork degradation in *Brca2*–deficient cells. a, Top, schematic of the retroviral PTIP mutant constructs used to identify the domain of PTIP involved in driving replication fork degradation. Different BRCT domains in PTIP are numbered and Q represents the glutamine rich region between the second and the third BRCT domains. Bottom, ratio of IdU versus CldU upon HU treatment of *Brca2*$^{-/-}$ *Ptip*$^{-/-}$ B lymphocytes retrovirally infected with either EV, FL, W165R, W663R and Del BRCT 5-6 PTIP-mutant constructs and sorted for GFP or mCherry expression. Numbers in red indicate the mean ± s.d. for each sample (**$P \leq 0.01$, ****$P \leq 0.0001$, Mann–Whitney test). One hundred and twenty-five replication forks were analysed for each condition. **b**, WT and *Mll3/4*$^{-/-}$ MEFs were EdU-labelled for 15 min and treated with 4 mM HU for 4 h. Proteins associated with replication forks were isolated by iPOND and detected by western blotting with the indicated antibodies. **c**, Quantification of the percentage of cells with MRE11 foci co-localizing with PCNA in late S phase in WT and *MLL3/4*$^{-/-}$ MEFs ($n = 150$ cells analysed). Experiments were repeated three times. **d**–**f**, Ratio of IdU versus CldU upon HU treatment in WT, *Brca1*$^{-/-}$, *Brca2*$^{-/-}$ *Mll4*$^{-/-}$, *Mll4*-SET$^{-/-}$, *Brca1*$^{-/-}$*Mll4*$^{-/-}$, *Brca2*$^{-/-}$*Mll4*$^{-/-}$ and *Brca1*$^{-/-}$*Mll4*-SET$^{-/-}$ B cells. Numbers in red indicate the mean ± s.d. for each sample (NS, not significant, ****$P \leq 0.0001$, Mann–Whitney test). At least 125 replication forks were analysed for each genotype. **g**, Genomic instability measured in metaphase spreads from splenic B cells derived from WT, *Brca2*$^{-/-}$, *Mll4*$^{-/-}$, *Brca2*$^{-/-}$*Mll4*$^{-/-}$ B cells treated overnight with 1 μM PARPi or with 0.5 μM cisplatin (**$P \leq 0.01$, ***$P \leq 0.001$, unpaired *t*-test). Fifty metaphases were analysed per condition. Experiments were repeated three times.

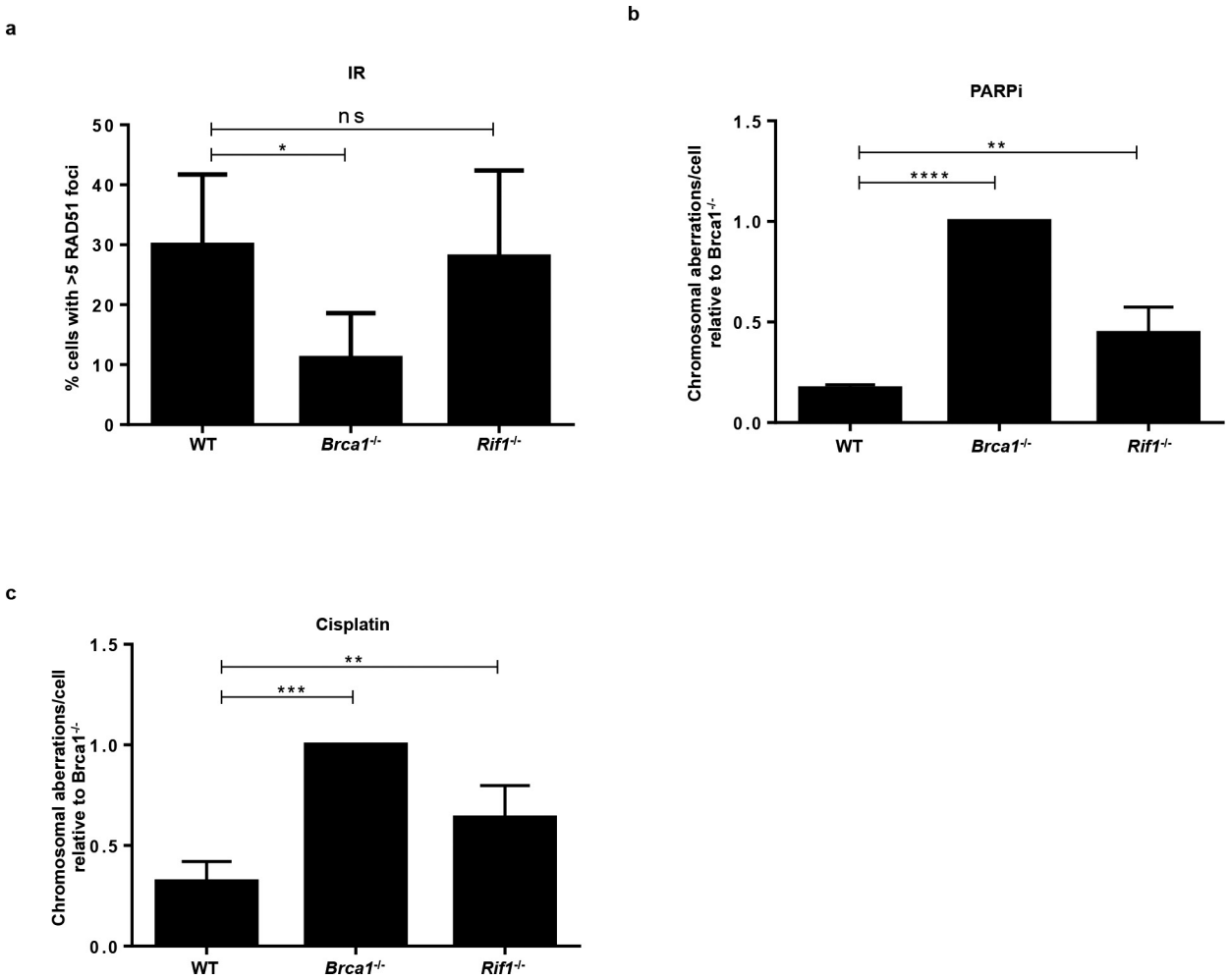

Extended Data Figure 7 | Loss of RIF1 results in chromosomal instability. a, Quantification of RAD51 foci formation in WT, *Brca1*$^{-/-}$ and *Rif1*$^{-/-}$ B cells. Cells were treated with 10 Gy and harvested 4 h after irradiation (NS, not significant, $^{*}P \leq 0.05$). At least 100 cells were analysed per condition; experiments were repeated three times. **b**, **c**, Genomic instability measured in metaphase spreads from splenic B cells derived from WT, *Brca1*$^{-/-}$ and *Rif1*$^{-/-}$ mice treated overnight with 1 μM PARPi (**b**) or with 0.5 μM cisplatin (**c**) (NS, not significant, $^{**}P \leq 0.01$, $^{***}P \leq 0.001$, $^{****}P \leq 0.0001$, unpaired *t*-test). Fifty metaphases were analysed per condition; experiments were repeated three times.

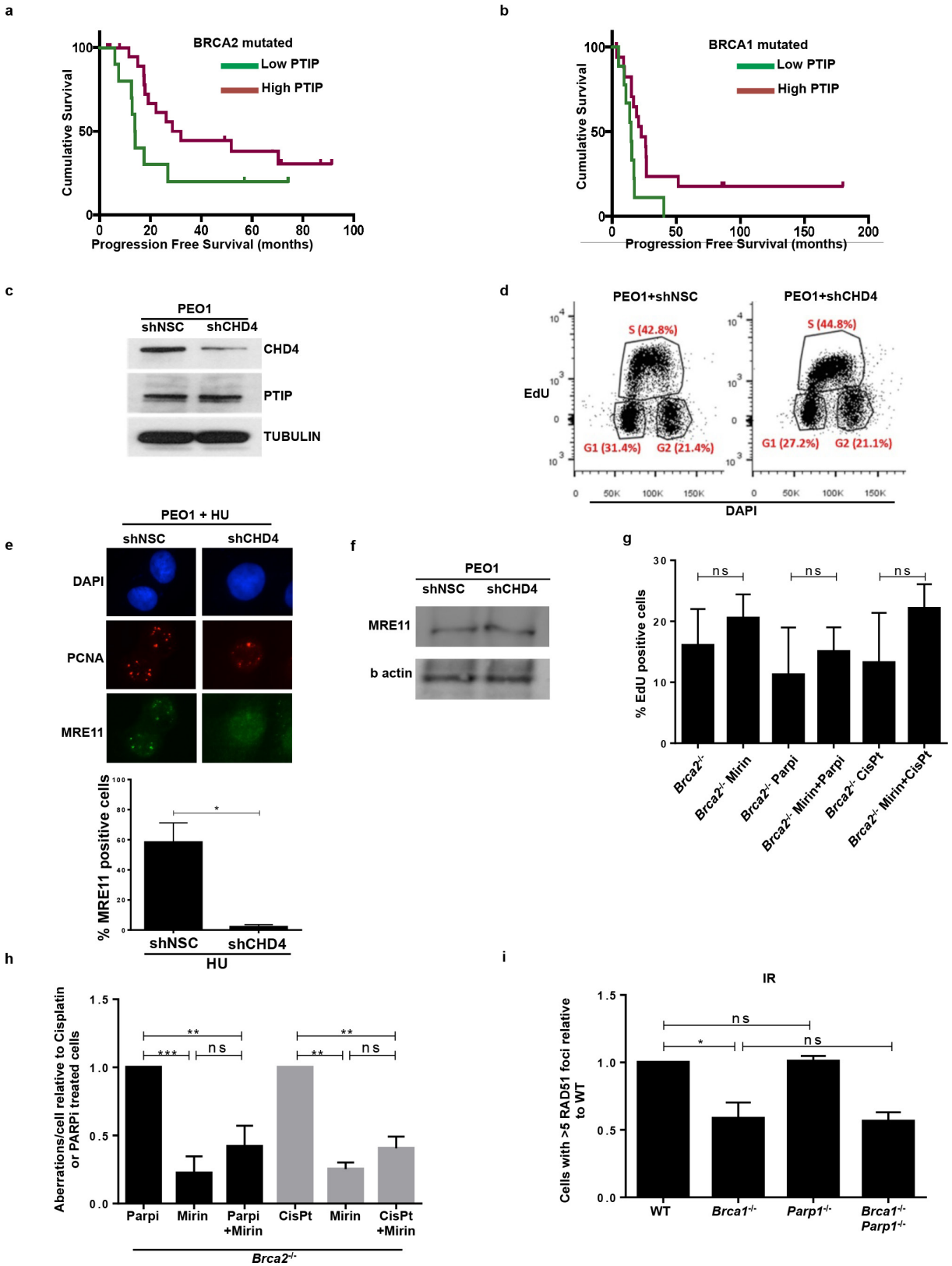

Extended Data Figure 8 | See next page for caption.

Extended Data Figure 8 | Multiple mutations can cause resistance to DNA-damaging agents in *Brca*-deficient cells. a, **b**, Difference in progression-free survival (PFS) of *BRCA2*- and *BRCA1*-mutated ovarian serous adenocarcinoma patients with standard platinum-based regimens. Data were obtained from the TCGA project. Patients were separated into PTIP low- or high-expression on the basis of the 33rd percentile of PTIP expression *z*-scores. The difference between the PFS of PTIP-low versus PTIP-high was assessed by univariate log-rank *P* value ($P < 0.072$ and $P < 0.032$ in **a** and **b**, respectively). Analysis included 38 tumours with *BRCA1* mutations and 34 tumours with *BRCA2* mutations out of 316 high-grade serous ovarian cancers that underwent whole-exome sequencing. PFS curves for PTIP-low and PTIP-high expressing tumours were generated by the Kaplan–Meier method. All reported *P* values are two-sided. **c**, Western blot analysis for CHD4 and PTIP levels in PEO1 cells infected with shNSC and shCHD4. Tubulin was used as loading control. **d**, Cell cycle profiles in PEO1 cells infected with shNSC and shCHD4 as measured by the incorporation of EdU (*y* axis) versus DAPI (*x* axis). **e**, Immunostaining for MRE11 and PCNA in PEO1 cells infected with shNSC and shCHD4 upon treatment with 4 mM HU. Bottom, quantification for MRE11 recruitment upon HU treatment. At least 100 cells were analysed per condition; experiments were repeated three times. **f**, Western blot analysis for CHD4 and MRE11 levels in PEO1 cells infected with shNSC and shCHD4. Actin was used as loading control. **g**, Percentage of EdU-positive cells was analysed 20 h after *Brca2*$^{-/-}$ B cells were treated with mirin alone, mirin+PARPi or mirin+cisplatin (NS, not significant). EdU was pulsed for 20 min before FACS analysis. Experiments were repeated three times. **h**, Genomic instability measured in metaphase spreads from B cells derived from *Brca2*$^{-/-}$ mice pretreated with 25 μM mirin for 2 h followed by overnight treatment with 1 μM PARPi or 0.5 μM cisplatin (NS, not significant, $*P \leq 0.05$, $**P \leq 0.001$, unpaired *t*-test). Fifty metaphases were analysed per condition. Experiments were repeated three times. **i**, Quantification of RAD51 foci formation in WT, *Brca1*$^{-/-}$, *Parp1*$^{-/-}$ and *Brca1*$^{-/-}$*Parp1*$^{-/-}$ B cells treated with 10 Gy irradiation and harvested 4 h after treatment. At least 100 cells were analysed per condition; experiments were repeated three times.

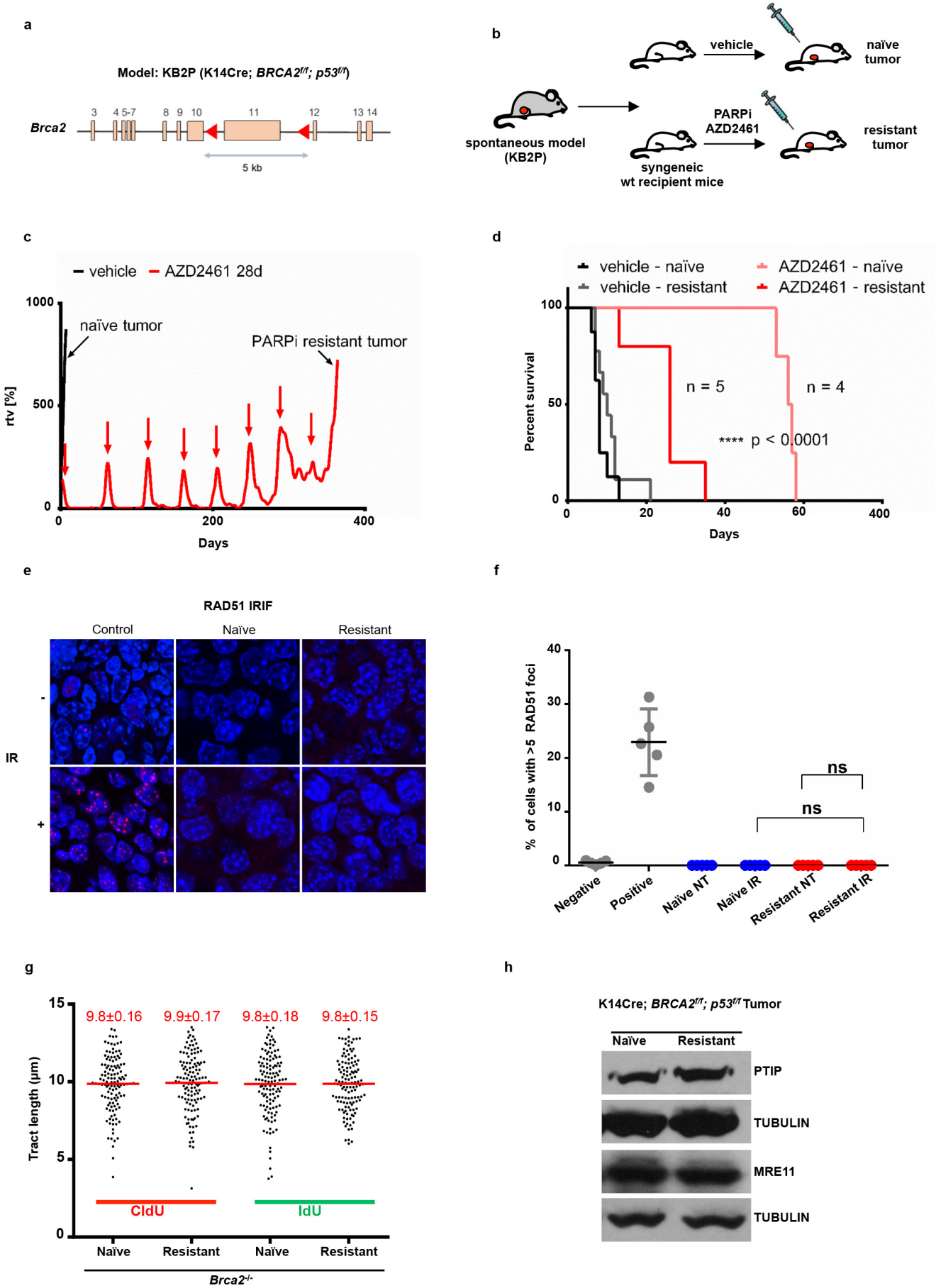

Extended Data Figure 9 | See next page for caption.

Extended Data Figure 9 | *Brca2*-deficient tumours acquire PARPi resistance without restoration of RAD51 foci formation. a, Schematic depicting the conditional *BRCA2* allele of the KB2P (*K14CRE*;*Brca2*$^{f/f}$;*p53*$^{f/f}$) spontaneous tumour model. **b**, Outline of the PARPi intervention study. A spontaneous BRCA2-/p53-deficient tumour was generated and re-transplated into syngeneic WT mice. When the tumours reached 200 mm^3, they were treated either with vehicle or PARPi AZD2461. **c**, PARPi response curve of the KB2P tumour (relative tumour volume (rtv) versus days). The treatment for 28 consecutive days was started when the tumour reached 200 mm^3 (rtv = 100%). In response to the treatment, the tumour shrank but eventually grew back. When it reached 100% relative tumour volume, the treatment was repeated (as indicated with red arrows) for another 28 days. This regime was continued until the tumour became resistant to PARPi (black arrow). **d**, The stability of acquired resistance of the KB2P tumour was confirmed by re-transplanting matched naive and resistant tumours and treating animals either with vehicle or AZD2461 (only one 28-day cycle). Kaplan–Meier survival curve indicates that resistant tumours did not respond to the AZD2461 treatment, while naive tumours exhibited high sensitivity, indicative of a stable genetic mechanism of resistance. **e**, **f**, Irradiation-induced RAD51 foci were detected by immunofluorescence in the KB2P donor: RAD51 foci formation was undetectable in naive and resistant tumours, suggesting that HR restoration is not an underlying mechanism of PARPi resistance. Spontaneous tumours from *K14 Cre; p53*$^{f/f}$ mice treated with irradiation were used as positive control for RAD51 foci. Unirradiated *K14 Cre; p53*$^{f/f}$ cells were used as a negative control. **g**, Replication fork progression rates measured by tract lengths in micrometres of CldU (red) and IdU (green) in PARPi-naive or PARPi-resistant tumours. Numbers in red indicate the mean ± s.d. for each sample. One hundred and twenty-five replication forks were analysed for each condition. **h**, Western blot analysis for PTIP and MRE11 levels in PARPi-naive or PARPi-resistant tumours. Tubulin was used as loading control.

a

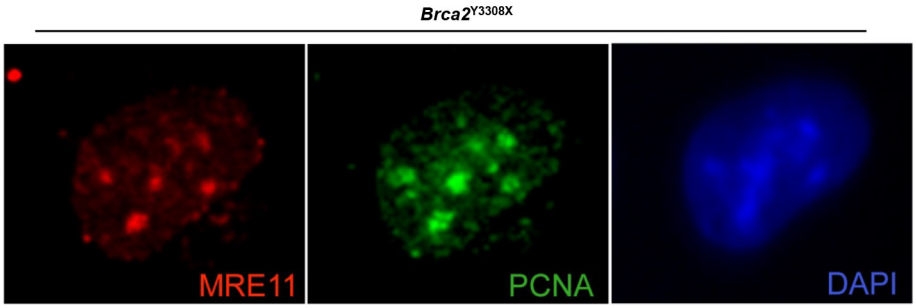

b

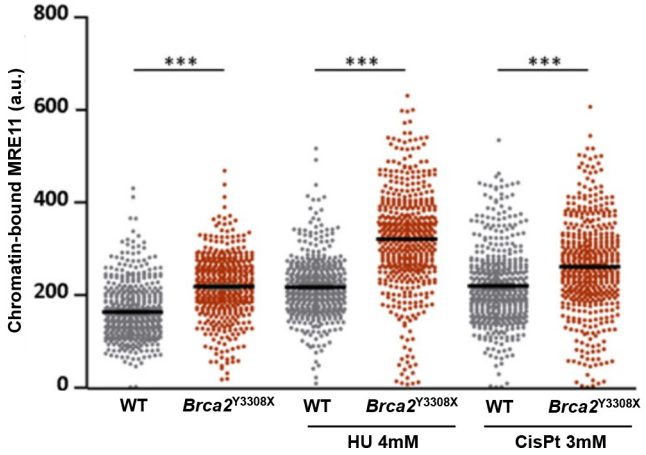

Extended Data Figure 10 | *Brca2*-deficient ESCs have higher levels of chromatin-bound MRE11. a, Representative image of a *Brca2* hypomorph mouse ESC (denoted *Brca2*^{Y3308X}) showing MRE11 foci (red) in S phase (identified by PCNA foci (green)). DNA was stained with DAPI (blue). **b**, High-throughput microscopy analysis quantifying the overall levels of chromatin-bound MRE11 per individual nucleus in WT and *Brca2*^{Y3308X} cells treated as indicated (a.u., arbitrary units).

nature COMMUNICATIONS

ARTICLE

Received 4 May 2016 | Accepted 1 Jul 2016 | Published 8 Aug 2016

DOI: 10.1038/ncomms12425 OPEN

Synthetic viability by BRCA2 and PARP1/ARTD1 deficiencies

Xia Ding[1], Arnab Ray Chaudhuri[2], Elsa Callen[2], Yan Pang[1], Kajal Biswas[1], Kimberly D. Klarmann[1,3], Betty K. Martin[1,3], Sandra Burkett[1], Linda Cleveland[1], Stacey Stauffer[1], Teresa Sullivan[1], Aashish Dewan[1], Hanna Marks[1], Anthony T. Tubbs[2], Nancy Wong[2], Eugen Buehler[4], Keiko Akagi[5], Scott E. Martin[4,†], Jonathan R. Keller[1,3], André Nussenzweig[2] & Shyam K. Sharan[1]

Poly (ADP-ribose) polymerase (PARP) inhibitor (PARPi) olaparib has been approved for treatment of advanced ovarian cancer associated with *BRCA1* and *BRCA2* mutations. *BRCA1*- and *BRCA2*-mutated cells, which are homologous recombination (HR) deficient, are hypersensitive to PARPi through the mechanism of synthetic lethality. Here we examine the effect of PARPi on HR-proficient cells. Olaparib pretreatment, PARP1 knockdown or *Parp1* heterozygosity of $Brca2^{cko/ko}$ mouse embryonic stem cells (mESCs), carrying a null (*ko*) and a conditional (*cko*) allele of *Brca2*, results in viable $Brca2^{ko/ko}$ cells. PARP1 deficiency does not restore HR in $Brca2^{ko/ko}$ cells, but protects stalled replication forks from MRE11-mediated degradation through its impaired recruitment. The functional consequence of *Parp1* heterozygosity on BRCA2 loss is demonstrated by a significant increase in tumorigenesis in $Brca2^{cko/cko}$ mice. Thus, while olaparib efficiently kills BRCA2-deficient cells, we demonstrate that it can also contribute to the synthetic viability if PARP is inhibited before BRCA2 loss.

[1] Mouse Cancer Genetics Program, National Cancer Institute, NIH, Frederick, MD 21702, USA. [2] Laboratory of Genome Integrity, National Cancer Institute, NIH, Bethesda, MD 20893, USA. [3] Leidos Biomedical Research, Inc., Frederick National Laboratory for Cancer Research, Frederick, MD 21702, USA. [4] Chemical Genomics Center, National Center for Advancing Translational Sciences, NIH, Rockville, MD 20850, USA. [5] Human Cancer Genetics Program, The Ohio State University Comprehensive Cancer Center, Columbus, OH 43210, USA. † Present address: Department of Discovery Oncology, Genentech, Inc., South San Francisco, CA 94080, USA. Correspondence and requests for materials should be addressed to A.N. (email: nussenza@exchange.nih.gov) or to S.K.S. (email: sharans@mail.nih.gov).

Women with a deleterious mutation in *BRCA1* or *BRCA2* have up to 70% risk of developing breast cancer by the age of 70 (ref. 1). It is well established that BRCA1 and BRCA2 function as tumour suppressors by maintaining genomic integrity. Both proteins are required for the repair of double-strand breaks (DSBs) by homologous recombination (HR) and also for the stability of stalled replication forks[1–3]. Their role in HR has been utilized to develop a therapeutic strategy that is based on the synthetic lethality of BRCA-deficient tumour by poly (ADP-ribose) polymerase (PARP or ADP-ribosyltransferase diphtheria toxin-like, ARTD) inhibitors[4–7].

PARPs consist of a family of enzymes that catalyse the formation of ADP-ribose polymers from NAD^+ to glutamate, aspartate or lysine residues of target proteins. At least 18 members of the PARP family have been identified based on the presence of a conserved catalytic domain. Poly ADP-ribosylation or parylation is a dynamic process as the ADP-ribose polymers can be rapidly degraded by poly (ADP-ribose) glycohydrolase and poly (ADP-ribose) hydrolase 3 (refs 8,9). PARP1, the founding member of the PARP family, has been shown to be stimulated in response to DNA damage. Parylation of target proteins by PARP1 results in decondensation of the chromatin near the site of DNA break, which is thought to facilitate the recruitment of DNA repair proteins[10]. Nevertheless, loss of PARP1 results in viable mice with no apparent defect except for the development of spontaneous tumours after a long latency and mild sensitivity to γ-radiation and alkylating agents[11].

PARP inhibitors effectively kill *BRCA*-deficient tumour cells. Originally, it was proposed that PARP inhibitors caused an increase of single-strand breaks, which are converted to DSBs during replication. Replication-associated DSBs are irreparable in the absence of HR, and are therefore toxic in the setting of BRCA deficiency[4,5]. Other plausible explanations for synthetic lethality include trapping of PARP1 at sites of DSBs or an increase in toxic non-homologous end joining in PARP1-deficient cells[12,13]. Regardless of the precise mechanism, PARP inhibitors such as olaparib continue to be the most promising and attractive treatment option for BRCA-deficient tumours because of their selectivity and apparent lack of toxicity in normal cells. Moreover, the repertoire of tumours that can be treated with PARP inhibitor (PARPi) is expanding to tumours with mutation in other genes associated with HR[14].

Although only mild side effects have been reported from PARPi treatment[6,15,16], its off-target effects are poorly understood[8]. In this study, rather than treating HR-deficient cells with a PARPi, we treated HR-proficient $Brca2^{cko/ko}$ mouse embryonic stem cells (mESCs) to examine its effect on normal cells. We primarily used mESCs because they predominantly use HR to repair damaged DNA, and also loss of PARP1 does not affect their survival[17,18]. Surprisingly, we found that chemical inhibition, as well as PARP1 knockdown and heterozygosity of *Parp1* rescued the lethality of *Brca2*-null mESC without restoring HR. PARP1 deficiency suppressed the recruitment of MRE11 nuclease to stalled replication fork, which contributed to fork protection in cells lacking BRCA2.

Results

Rescue of $Brca2^{ko/ko}$ mESC by PARP inhibition or deficiency. PARPi are selectively toxic to HR-deficient cells[4,5]. However, effects of PARPi are not limited to HR-deficient cells, as treatment of HR-proficient cells with different doses of olaparib resulted in suppression of CHK1 activation in response to replicative stress (Supplementary Fig. 1a), as reported previously[19]. To further examine the effect of olaparib on HR-proficient cells, we used PL2F7 mESCs that have one functionally null allele of *Brca2* and the other is a conditional allele ($Brca2^{cko/ko}$) (Supplementary Fig. 1b)[20]. We treated these cells with different doses of olaparib for 48–72 h and then deleted the *cko* allele by transient expression of CRE. Cell cycle analysis showed these olaparib regimens did not overall significantly affect the cell cycle distribution (Supplementary Fig. 1c,d) or TRP53 and p19ARF stress responses (Supplementary Fig. 1h).

After expression of CRE, we selected the recombinant clones in HAT (hypoxanthine, aminopterin and thymidine) media because CRE-mediated deletion of *cko* generates a functional *HPRT* minigene (Fig. 1a). Genotyping of the colonies did not reveal any $Brca2^{ko/ko}$ clones in untreated cells ($n=96$), consistent with the fact that BRCA2 is essential for viability[21]. Remarkably, olaparib pretreatment resulted in a number of viable $Brca2^{ko/ko}$ cells at all doses tested (Fig. 1b) ranging from 4 to 8% of clones.

To test whether PARP1 deficiency in $Brca2^{ko/ko}$ cells would have similar functional consequences as observed with chemical inhibition of PARP, we generated two stably knocked-down clones using two different shRNAs against *Parp1* (Fig. 1c). PARP1 stable knockdown clone had similar cell cycle distribution compared with nonsense control clone (Supplementary Fig. 1e–g). We again obtained several HAT-resistant mESC clones after *cko* deletion. Genotyping of the clones revealed that up to 86% were $Brca2^{ko/ko}$ (Fig. 1d). These results demonstrate that PARP1 deficiency rescues the viability of $Brca2^{ko/ko}$ mESC.

To further strengthen these findings, we generated *Parp1* knockout clones in PL2F7 cells by using CRISPR-Cas9 system to target exon 2 (Supplementary Fig. 2a,b). We used one *Parp1* heterozygous ($Parp1^{ko/+}$) clone and a compound heterozygous clone that was functionally null ($Parp1^{ko/ko}$) for the mESC rescue experiment (Supplementary Fig. 2c–f). We obtained several $Brca2^{ko/ko}$ mESC clones from $Parp1^{ko/+}$ PL2F7 cells (61%) confirming that the rescue of BRCA2 loss-induced mESC lethality by PARP1 deficiency (Supplementary Fig. 2g). However, no $Brca2^{ko/ko}$ mESC was obtained when we used $Parp1^{ko/ko}$ PL2F7 cells suggesting that these cells are sensitive to complete loss of both PARP1 and BRCA2, and residual PARP1 activity is required for survival of $Brca2^{ko/ko}$ mESC. Furthermore, the percentage of $Brca2^{ko/ko}$ mESC obtained on a *Parp1* heterozygous background or by stable knockdown of PARP1 is high compared with 4–8% observed when cells were transiently treated with olaparib. This suggests that either prolonged PARP1 deficiency supports viability of $Brca2^{ko/ko}$ mESC better than transient inhibition or that PARPi, in addition to rescuing the BRCA2 loss, also results in toxicity to the cells.

We further validated the genetic interaction between BRCA2 and PARP1 by examining the consequence of PARP1 deficiency on the phenotype of $Brca2^{ko/ko}$ embryos. While no viable $Brca2^{ko/ko}$ pups were obtained from $Parp1^{ko/+};Brca2^{ko/+}$ intercross, we did observe a significant rescue of the $Brca2^{ko/ko}$ embryos on $Parp1^{ko/+}$ genetic background (Supplementary Fig. 3c,d). At E8.5, $Parp1^{+/+};Brca2^{ko/ko}$ embryos were severely retarded and disorganized, whereas $Parp1^{ko/+};Brca2^{ko/ko}$ embryos had undergone gastrulation and exhibited well-developed extra embryonic structures (Supplementary Fig. 3c). At E10.5, we did not obtain any $Parp1^{ko/+};Brca2^{ko/ko}$ embryos (Supplementary Fig. 3e) indicating that these embryos die between E9.5 and E10.5. Consistent with the mESC results, we did not obtain any $Parp1^{ko/ko};Brca2^{ko/ko}$ embryos at E8.5 by either $Parp1^{ko/+};Brca2^{ko/+}$ intercross or $Parp1^{ko/+};Brca2^{ko/+}$ crossed with $Parp1^{ko/ko};Brca2^{ko/+}$ (Supplementary Fig. 3a,b), indicating that complete loss of PARP1 and BRCA2 is detrimental to mESC, as well as mouse embryos. These results suggest that PARP1 is essential for the viability of *Brca2* null cells, likely due to its wide-ranging biological functions[8].

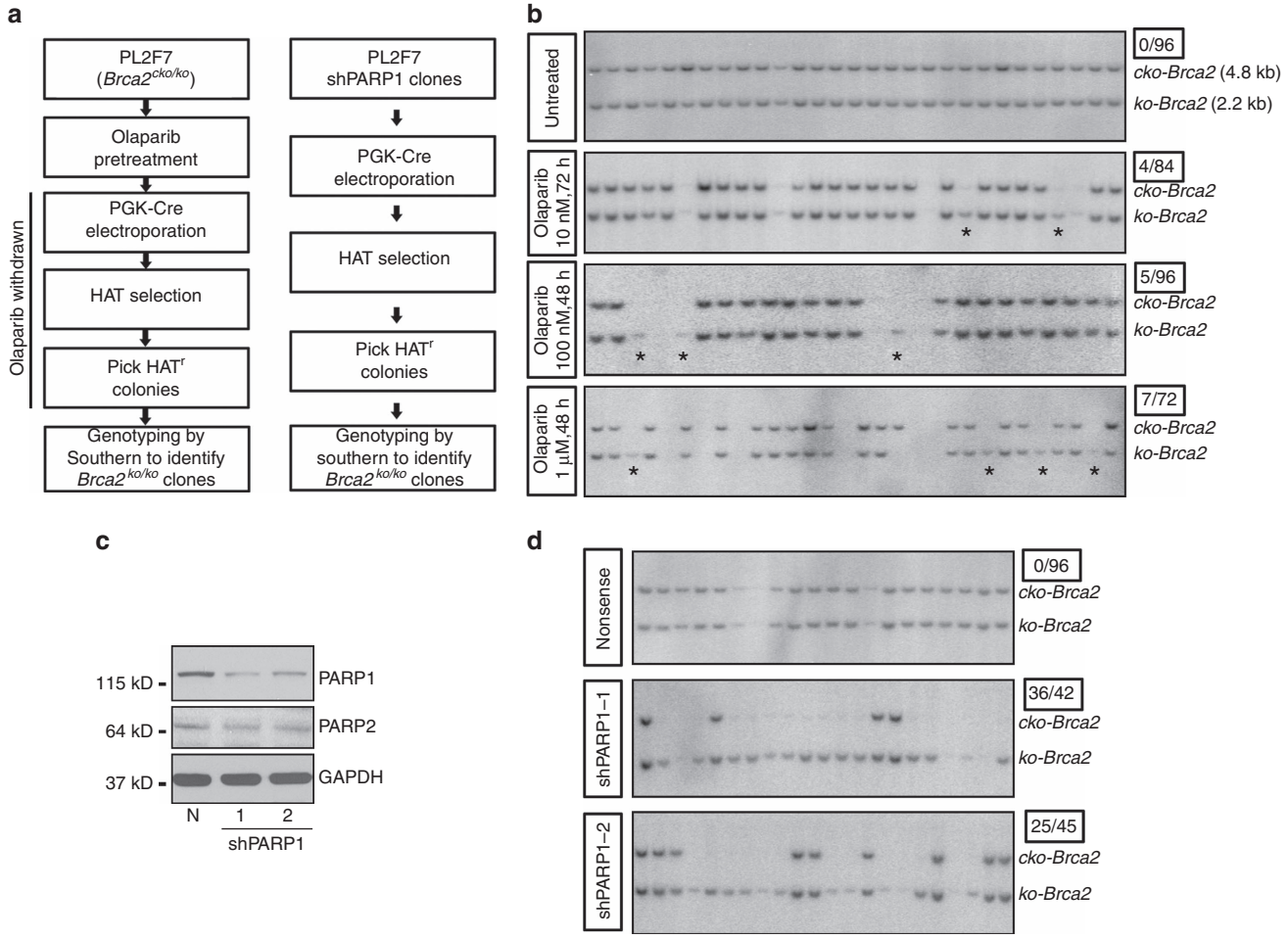

Figure 1 | PARP inhibition or PARP1 deficiency rescues lethality of *Brca2*$^{ko/ko}$ mESC. (**a**) Workflow to test the rescue of *Brca2*$^{ko/ko}$ mESC lethality. (**b**) Representative Southern blot showing rescue of *Brca2*$^{ko/ko}$ mESC by olaparib pretreatment in PL2F7 cells. Asterisks indicate the rescued clones. Ratio of the number of rescued clones and total numbers of HAT^r clones analysed are shown in the box on the right corner (same as below). (**c**) Western blot showing PARP1 level in stable knockdown clones. N, nonsense. (**d**) Representative Southern blot showing rescue of *Brca2*$^{ko/ko}$ mESC by PARP1 knockdown.

HR is not restored by PARP1 deficiency in *Brca2*$^{ko/ko}$ mESC. BRCA2 is essential for the recruitment of RAD51 at DSB to mediate HR[1,21]. We therefore examined whether RAD51 recruitment in response to DSB induction was restored in the *Brca2*$^{ko/ko}$ mESC rescued by PARP1 knockdown or by olaparib treatment. We did not observe any RAD51 foci in these cells in response to irradiation, although RAD51 was expressed at levels similar to the control cells (Fig. 2a and Supplementary Fig. 4a,b). Next, we used gene targeting to measure DSB-induced HR efficiency in the rescued cells[20]. We compared PL2F7 controls with or without PARP1 knockdown with two *Brca2*$^{ko/ko}$ mESCs rescued by PARP1 knockdown. While control and PARP1 knockdown cells exhibited a targeting efficiency of 16.7–25%, *Brca2*$^{ko/ko}$ rescued cells did not exhibit any targeted clones (Fig. 2b). Moreover, metaphase spreads revealed an increase in chromosomal aberrations in *Brca2*$^{ko/ko}$ mESC rescued by PARP1 knockdown compared with the parental PL2F7 cells (Supplementary Fig. 4c,d). Together with the defect in RAD51 foci formation, these results demonstrate that DSB-induced HR is not restored in rescued *Brca2*$^{ko/ko}$ mESC.

Rescue of *Brca2*$^{ko/ko}$ haematopoietic cells by PARPi treatment. Given the pro-survival effects of PARP1 deficiency or PARP inhibition on the viability of *Brca2*$^{ko/ko}$ mESC *in vitro*, we tested whether olaparib treatment *in vivo* can support survival of *Brca2*-deficient haematopoietic progenitor cells. Wild-type (WT) and *Brca2*$^{cko/cko}$ mice were injected with either dimethylsulfoxide (DMSO) or olaparib for 10 days and then collected the bone marrow (Fig. 3a). We then transduced the bone marrow cells with CRE-GFP lentivirus to delete the conditional allele. Green fluorescent protein (GFP)-positive cells were sorted and cultured *in vitro* for colony formation. DMSO- and olaparib-pretreated WT cells formed an average of 428 and 485 colonies per plate, respectively. In contrast, the DMSO-pretreated *Brca2*$^{cko/cko}$ cells formed very few and small colonies (average of 104 per plate). While olaparib-pretreated *Brca2*$^{cko/cko}$ cells also formed small colonies, their number was significantly higher (average of 152 colonies per plate, $P=0.0299$, *t*-test) compared with DMSO-pretreated *Brca2*$^{cko/cko}$ cells (Fig. 3b,c). In parallel, colony formation in the presence of 100 nM olaparib was also performed. The number of colonies from *in vivo* olaparib-pretreated *Brca2*$^{cko/cko}$ cells was significantly reduced by *in vitro* olaparib post treatment, whereas the colony number in DMSO-pretreated *Brca2*$^{cko/cko}$ cells remained unchanged (Fig. 3b,c). This suggests that the surviving olaparib-pretreated *Brca2*$^{cko/cko}$ clones were indeed HR-defective and BRCA2-deficient, which was confirmed by genotyping (Fig. 3d).

PARP1 deficiency protects degradation of replication forks. BRCA2 has been reported to protect replication forks from degradation, independent of its role in DSB repair by HR[2]. PARP1 has been shown to play important roles in the control of

several aspects of replication fork dynamics, including fork restart, degradation and reversal[22–24]. Since cell viability is not associated with restoration of the HR defect, we therefore asked whether PARP1 deficiency conferred replication fork stability to *Brca2*$^{ko/ko}$ mESC rescued by PARP1 knockdown. Integrity of the replication forks was examined using the DNA fibre assay, which allows single-molecule resolution of replication fork tracts[2]. Ongoing replication forks were labelled with chlorodeoxyuridine (CldU; red) and then with iododeoxyuridine (IdU; green) for 15 min each followed by fork stalling agent, hydroxyurea (HU) treatment for 3 h. We measured the track length of CldU- and IdU-labelled DNA fibres and calculated the IdU to CldU ratio. The ratio is close to 1 when the forks are protected, but <1 when the forks are degraded. While WT cells exhibited an average ratio of IdU to CldU tracts lengths close to 1, IdU tracts in mESC expressing a truncated allele of *BRCA2* (Y3308X) were considerably shorter (average IdU to CldU ratio $=0.807$, $P<0.0001$, Mann–Whitney test), indicating the degradation of nascent strands on replicative stress (Fig. 4a,b). Strikingly, in both *Brca2*$^{ko/ko}$ clones rescued by PARP1 knockdown, IdU to CldU ratios were comparable to those observed in PL2F7 cells (average IdU to CldU ratio $=1.09$ and 1.12, respectively) (Fig. 4a,b). These results indicate that deficiency of PARP1 deficiency confers protection to the replication forks in the absence of functional BRCA2.

To determine whether the observed replication fork protection due to PARP1 deficiency is observed in other cell types, we also analysed replication fork integrity in mouse B lymphocytes. For reasons not well understood, unlike mESCs, B cells are able to tolerate loss of 'essential' HR genes (for example, *BRCA1*, *BRCA2* and *CtIP*) with minimal impact on their growth *ex vivo*[25,26]. Nevertheless, these cells remain highly sensitive to agents that challenge replication forks[25,26]. We generated B lymphocytes from WT, *Parp1*$^{ko/ko}$, *Brca2*$^{cko/cko}$ and *Parp1*$^{ko/ko}$;*Brca2*$^{cko/cko}$ mice. The *cko* allele was deleted by transducing the cells with CRE-expressing retrovirus after stimulating B cells with lipopolysaccharide + interleukin-4 and RP105. Deletion of the *cko* allele was confirmed by quantitative PCR (Fig. 4c). On HU treatment, the average IdU to CldU ratios were determined to be 0.957, 0.976, 0.624 and 0.979 for WT, *Parp1*$^{ko/ko}$ and *Brca2*$^{ko/ko}$ and *Parp1*$^{ko/ko}$;*Brca2*$^{ko/ko}$ cells, respectively (Fig. 4d,e). Thus, consistent with our observation in mESC, loss of PARP1 resulted in protection of the nascent strand in *Parp1*$^{ko/ko}$;*Brca2*$^{ko/ko}$ B cells ($P=0.1147$ versus WT, Mann–Whitney test).

To test whether deficiency of PARP1 can rescue fork degradation induced by BRCA2 loss in human cells as well, we used immortalized human mammary epithelial cells MCF10A. Two independent clones with stable PARP1 knockdown were generated by transducing cells with shRNA-expressing lentivirus (Fig. 4f). We then knocked down BRCA2 by siRNA (Fig. 4g) and examined fork stability by DNA fibre assay. Average IdU to CldU ratios were 1.03, 0.64 and 0.66 in stable control clone with nonsense, BRCA2-1 and BRCA2-2 siRNA, respectively. However, the average ratios were 1.00, 0.89 and 0.95 in stable PARP1 knockdown clone with nonsense, BRCA2-1 and BRCA2-2 siRNA, respectively ($P<0.0001$, Mann–Whitney test) (Fig. 4h,i). The fact we did not observe fork degradation in MCF10A cells with stable PARP1 knockdown seems to contradict previous study in which fork degradation was observed in olaparib-treated BRCA2-proficient cells[24]. It is possible that fork protection is interfered by trapping of PARP1 by olaparib[12], whereas in the PARP1 knockdown cells trapping does not occur. Alternatively, the level of BRCA2 in the reconstituted V-C8 cells is not the same as in heterozygous cells expressing a single copy of WT *BRCA2*, making the fork sensitive to olaparib. Taken together, our data suggest that PARP1 deficiency can rescue the

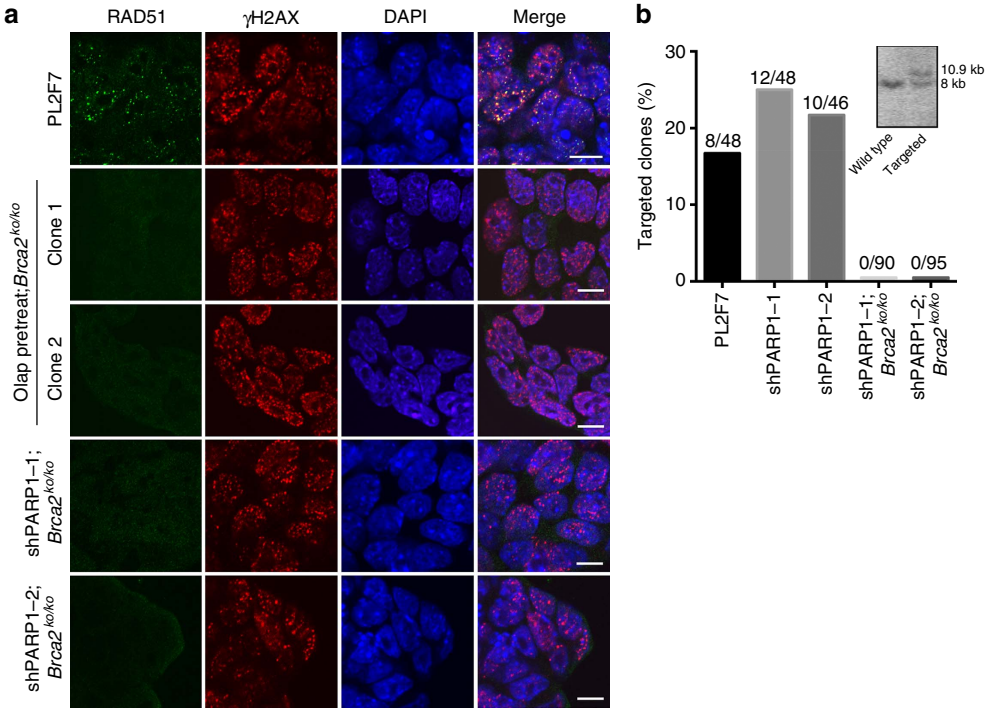

Figure 2 | HR is not restored by PARP1 deficiency in *Brca2*$^{ko/ko}$ mESC. (**a**) Immunofluorescence images showing RAD51 foci formation 5 h after 10 Gy irradiation (IR). RAD51 foci were assessed at a single time point with a single dose of irradiation (IR). Olap pretreat;*Brca2*$^{ko/ko}$ indicates *Brca2*$^{ko/ko}$ mESC rescued by olaparib pretreatment. Scale bars, 10 μm. (**b**) Histogram showing gene-targeting efficiency. shPARP1-1/2; *Brca2*$^{ko/ko}$ indicates *Brca2*$^{ko/ko}$ mESC rescued by PARP1 knockdown. Actual numbers of targeted clones and total numbers of clones are indicated above each column. Inset shows Southern blot of the gene targeting.

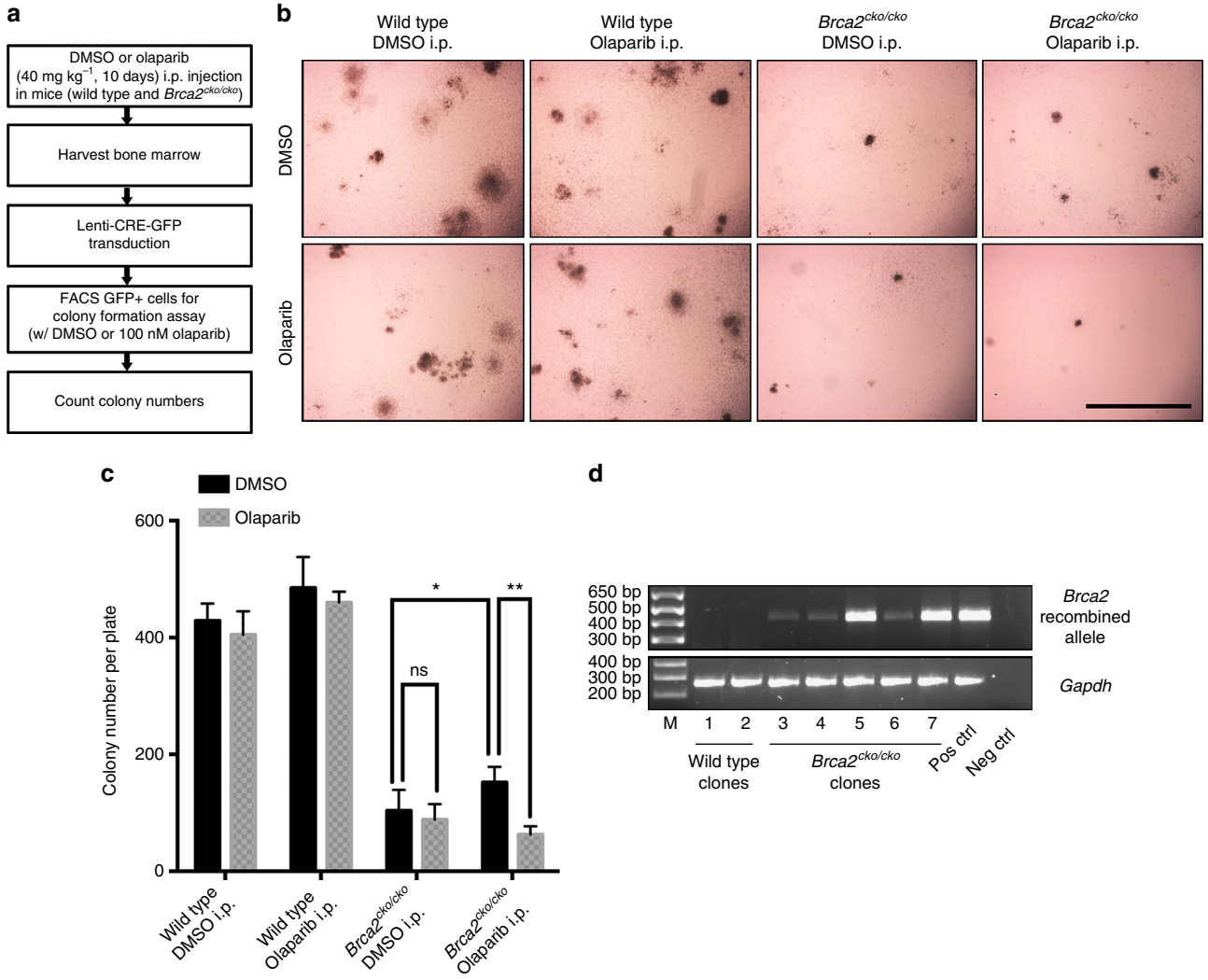

Figure 3 | Rescue of *Brca2*$^{ko/ko}$ haematopoietic cells by PARPi treatment in mice. (**a**) Workflow of clonogenic assay in haematopoietic progenitor cells. (**b**) Representative colony images of the clonogenic assay of haematopoietic progenitor cells. Scale bar, 2 mm. (**c**) Quantification on colony numbers of the clonogenic assay in haematopoietic progenitor cells. $^{*}P<0.05$, $^{**}P<0.01$ (*t*-test). (**d**) Genotyping of haematopoietic progenitor colonies from WT or *Brca2*$^{cko/cko}$ mice receiving olaparib pretreatment. Primers are listed in Supplementary Note 1.

BRCA2 loss-induced fork degradation in both mouse and human cells.

Impaired MRE11 recruitment contributes to fork protection. We next examined the molecular mechanism of the fork protection that may contribute to rescue of *Brca2*$^{ko/ko}$ mESC. MRE11 nucleolytic activity is responsible for BRCA2 loss-induced fork degradation[2,24]. MRE11 is reported to interact with PARP1 (refs 22,27). Interestingly, MRE11 has a PAR-binding RG or RGG-rich motif suggesting that it may be PARylated by PARP1 (refs 9,27). We therefore investigated whether the effect of PARP1 deficiency was mediated via MRE11. Our data confirmed previous reports that MRE11 physically interacts with PARP1 independent of replication stress and presence of DNA; however, this interaction was disrupted when PARP was inhibited by olaparib (Fig. 5a and Supplementary Fig. 5d). We further identified the N-terminal region of PARP1 containing two Zn finger domains but not the catalytic domain to interact with MRE11. Our findings suggest that PARP1 and MRE11 interaction was dependent on PARP activity (Supplementary Fig. 5a–c). Since the interaction is mediated by PARP1 N-terminal instead of its catalytic domain, we also speculate that auto-PARylation of PARP1 may be important for PARP1 and MRE11 interaction. The fact that interaction between PARP1 N-terminal domain and MRE11 can also be disrupted by olaparib (Supplementary Fig. 5c) suggests that the N-terminal domain might be auto-PARylated.

Consistent with previous studies[2], we observed rescue of the fork degradation in Y3308X *BRCA2*-expressing mESC by MRE11 inhibitor, mirin (Supplementary Fig. 6a), indicating MRE11 indeed mediates the fork degradation in BRCA2-deficient mESC.

To determine whether PARP inhibition or PARP1 deficiency affected recruitment of MRE11 to stalled replication forks, we examined the presence of MRE11 at the fork in mESC treated with HU (4 mM, 4 h) or HU with olaparib (1 μM, 2 h pretreatment followed by HU combination for another 4 h) by iPOND (isolation of proteins on nascent DNA)[28]. HU treatment induced marked increase in MRE11 recruitment to stalled replication forks. However, olaparib reduced the association of MRE11 to stalled replication forks (Fig. 5b). To examine the effects of PARP1 deficiency, we performed iPOND by using mESC with PARP1 knockdown (Supplementary Fig. 6e), as well as *Parp1*$^{ko/ko}$-immortalized mouse embryonic fibroblasts (MEFs) (Fig. 5c and Supplementary Fig. 6b). Consistently, we observed a marked reduction of MRE11 recruitment in these

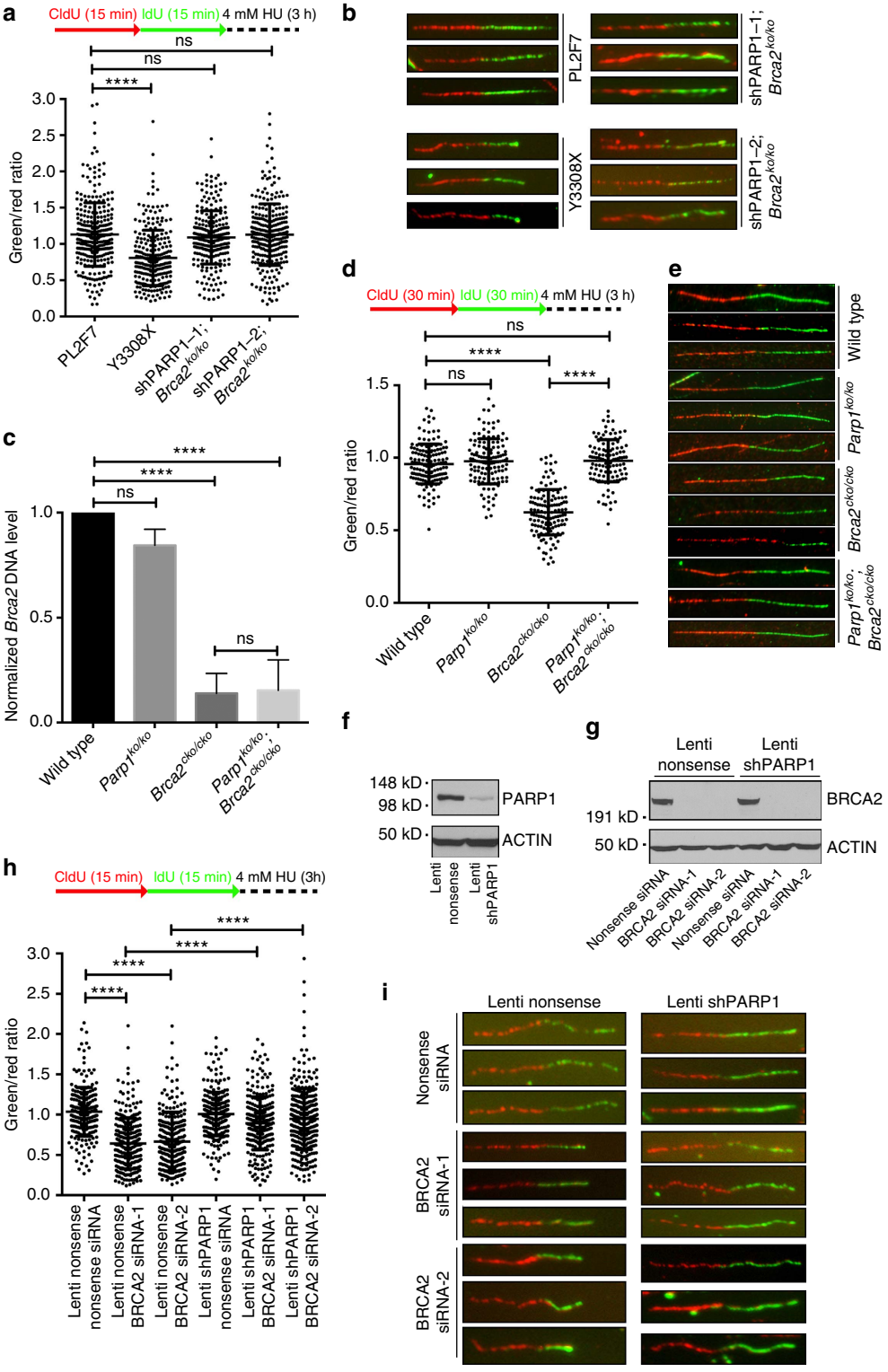

Figure 4 | PARP1 deficiency protects BRCA2 loss-induced replication fork degradation. (**a**) Scattered plot showing DNA fibre analysis of indicated cell lines. ****$P<0.0001$, ns, not significant (Mann–Whitney test). (**b**) Representative images of DNA fibres as quantified in **a**. (**c**) qPCR showing the deletion of genomic *Brca2* DNA in B cells with the indicated genotypes. All the cells were infected by retrovirus-Cre. Primers are listed in Supplementary Note 1. ****$P<0.0001$, ns, not significant (*t*-test). (**d**) Scattered plot showing DNA fibre analysis in B cells. (**e**) Representative images of DNA fibres as quantified in **d**. (**f**) Western blot showing PARP1 level in MCF10A stable knockdown cells. (**g**) Western blot showing BRCA2 knockdown level by siRNA in PARP1 stable knockdown MCF10A clones. (**h**) Scattered plot showing DNA fibre analysis in MCF10A cells, ****$P<0.0001$ (Mann–Whitney test). (**i**) Representative images of DNA fibres quantified in **h**.

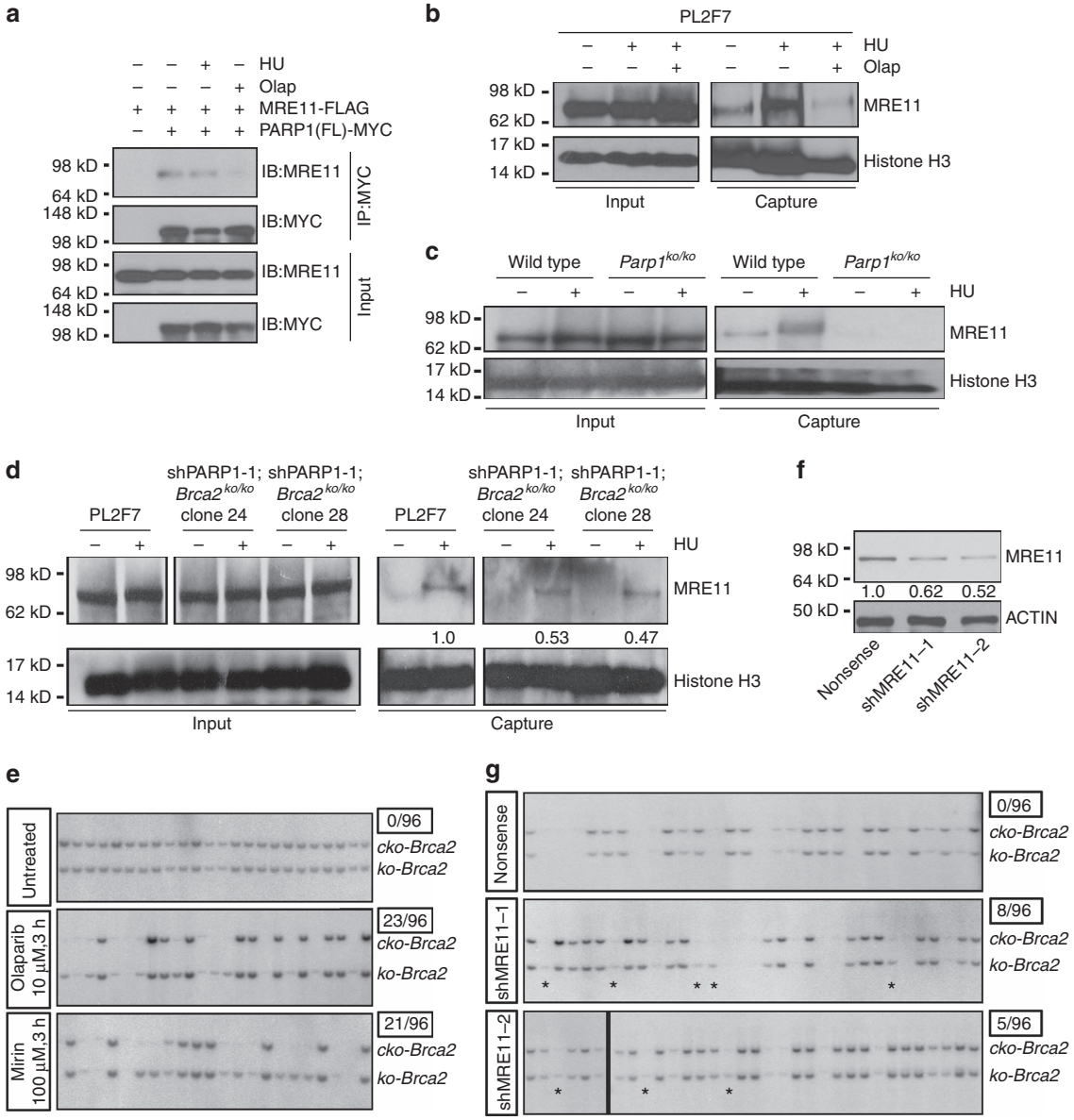

Figure 5 | Impaired MRE11 recruitment contributes to fork protection and cell survival after BRCA2 loss. (**a**) Western blot of immunoprecipitation in HEK293T cells showing interaction of MRE11 and PARP1. (**b**) Western blot of iPOND samples in PL2F7 cells showing MRE11 and Histone H3 levels at the replication fork. HU, 4 mM, 4 h (same as below). Olaparib (Olap), 1 μM, 2 h pretreatment, with HU for 4 h. (**c**) Western blot of iPOND samples in MEF cells showing MRE11 and Histone H3 levels at the replication fork. (**d**) Western blot of iPOND samples from indicated cell lines showing MRE11 and Histone H3 levels at the replication fork. Numbers indicate quantification of relative band intensity of MRE11 normalized to Histone H3. These band intensities were compared with the intensity of MRE11 in PL2F7 cells, which was considered to be 1. (**e**) Representative Southern blot showing rescue of *Brca2*$^{ko/ko}$ mESC by transient olaparib or mirin pretreatment. (**f**) Western blot showing MRE11 level in stable knockdown mESC clones. Numbers indicate quantification of relative band intensity of MRE11 normalized to corresponding ACTIN band intensity. These band intensities were compared with the intensity of MRE11 in Nonsense, which was considered to be 1. (**g**) Representative Southern blot showing rescue of *Brca2*$^{ko/ko}$ mESC in two MRE11 stable knockdown clones. Asterisks indicate the rescued clones.

PARP1-deficient cells. Furthermore, compared with PL2F7 cells, we detected a clear reduction in MRE11 recruitment at the fork in two independent *Brca2*$^{ko/ko}$ mESC clones rescued by PARP1 knockdown (Fig. 5d and Supplementary Fig. 6c). On the basis of the above results, we conclude that impaired recruitment of MRE11 to stalled replication forks by PARP inhibition or PARP1 deficiency contributes to fork protection in *Brca2*$^{ko/ko}$ mESC.

If fork protection indeed contributes to the rescue of *Brca2*$^{ko/ko}$ mESC survival, it is difficult to reconcile the survival of *Brca2*$^{ko/ko}$ mESC rescued by olaparib, because the olaparib-mediated inhibitory effect is transient. We therefore tested whether transient PARPi treatment was indeed sufficient to rescue *Brca2*$^{ko/ko}$ mESC lethality. We pretreated PL2F7 cells with 10 μM olaparib for only 3 h and then performed the rescue experiment as described in Fig. 1a. Surprisingly, even such transient exposure to olaparib resulted in a number of viable *Brca2*$^{ko/ko}$ mESC clones (24%) (Fig. 5e). This is in line with the iPOND analysis, which revealed that olaparib disrupts the MRE11 recruitment to the stalled fork (Fig. 5b). Unlike the *Brca2*$^{ko/ko}$ mESC rescued by PARP1 knockdown, *Brca2*$^{ko/ko}$ mESC rescued by olaparib resulted in fork degradation (Supplementary Fig. 6d,g). These cells also had significantly

more breaks and gaps than the cells rescued by PARP1 knockdown (Supplementary Fig. 4c,d). These results suggest transient fork protection during the deletion of *Brca2* may contribute to rescue the survival of $Brca2^{ko/ko}$ mESC, however, the subsequent survival of $Brca2^{ko/ko}$ cells is not dependent on fork protection.

Rescue of $Brca2^{ko/ko}$ mESC by MRE11 inhibition or deficiency. To directly test whether MRE11 inhibition can rescue the lethality of $Brca2^{ko/ko}$ mESC, we pretreated PL2F7 cells with 100 μM mirin (the same dosage that can rescue fork degradation as shown in Supplementary Fig. 6a) for 3 h and then performed the rescue experiment described in Fig. 1a. We obtained a number of $Brca2^{ko/ko}$ mESC (22%, Fig. 5e). Like other BRCA2-null rescued mESC described above, these cells lacked irradiation-induced RAD51 foci (Supplementary Fig. 6f,h), indicating that HR was not restored. To rule out any off-target effects of mirin, we generated MRE11 stable knockdown clones by shRNA in PL2F7 cells (Fig. 5f). Consistent with the rescue by mirin, MRE11 stable knockdown resulted in the survival of $Brca2^{ko/ko}$ mESC as evident in two independent MRE11 knockdown clones (Fig. 5g). Although we cannot rule out the possibility that other genetic and epigenetic alterations or effects on cell cycle regulation induced by PARP or MRE11 inhibition or knockdown may contribute to viability, our findings suggest that fork protection may play an important role in rescue of cellular viability. We also conclude that while transient fork protection by either PARPi or MRE11 inhibition contributes to the initial survival of $Brca2^{ko/ko}$ mESC, it is not essential to maintain the growth of these cells (Fig. 6).

$Brca2^{cko/cko}$ mice are tumour prone in a $Parp1^{ko/+}$ background. It is known that mESC lethality due to BRCA1 loss can be rescued by 53BP1 loss, which restores end resection and HR, and suppresses tumorigenesis in mice[25,29]. In contrast PARP1 deficiency does not restore HR but results in fork protection. Although the fork protection promotes genomic stability relative to cells that lack fork protection (Supplementary Fig. 4c,d), the level of genomic instability is higher than the cells expressing WT BRCA2. We predict that viable cells exhibiting genomic instability are likely to contribute to tumorigenesis. To directly test whether PARP inhibition or PARP1 deficiency can facilitate tumorigenesis in BRCA2-deficient mice, we generated *K14-Cre;*$Brca2^{cko/cko}$ mice on $Parp1^{+/+}$ and $Parp1^{ko/+}$ genetic backgrounds. We observed a marked increase in the incidence of epithelial tumours in *K14-Cre;*$Brca2^{cko/cko}$ mice in a $Parp1^{ko/+}$ genetic background (23 out of 56 mice, 41.1%) compared with that in $Parp1^{+/+}$ genetic background (2 out of 18 mice, 11.1%; $P = 0.0226$, Fisher's exact test; Fig. 7a, Supplementary Fig. 7 and Supplementary Table 1), suggesting PARP1 deficiency indeed facilitates BRCA2 loss-induced tumorigenesis.

Discussion

PARylation by PARP1 affects the cellular localization and site-specific recruitment, such as recruitment to DNA damage sites, of a number of proteins involved in a wide-range of biological processes[8]. Here we have investigated the functional consequence of PARP inhibition on HR-proficient cells that express functional BRCA2. PARPi is toxic to BRCA2-deficient cells, however, we show that PARP inhibition can paradoxically promote their survival. We show that knockdown or heterozygous loss of *Parp1*, as well as olaparib treatment before BRCA2 loss rescues the lethality of $Brca2^{ko/ko}$ mESC. We speculate that the order of two genetic events, PARP inhibition or PARP1 deficiency and BRCA2 loss, dictates the outcome of either synthetic lethality or synthetic viability (Fig. 6). Inactivation of PARP1 before loss of BRCA2 is likely to promote survival by preventing MRE11-mediated toxicity linked to DNA replication and subsequent cell death. In contrast, in BRCA2-null cells, MRE11 may persist at the replication forks and degrade it, causing persistent DNA damage. This genomic instability would be exacerbated and result in cell death by the subsequent PARPi due to the additional block in single-strand break repair or perhaps due to the PARP1 trapping[12,30].

The role of MRE11 in cell viability by PARP inhibition or PARP1 deficiency is demonstrated by the rescue of $Brca2^{ko/ko}$ mESC by knockdown of *MRE11*, as well as by treatment of cells with mirin before BRCA2 loss. Although our findings suggest that the MRE11-mediated fork protection by PARP inhibition or PARP1 deficiency may contribute to the rescue of $Brca2^{ko/ko}$ mESC, is not essential for maintaining cell survival even in the absence of HR. For example, a short treatment of olaparib or mirin rescues $Brca2^{ko/ko}$ mESC. What contributes to the viability in this case is puzzling because the rescued cells are unable to protect the fork in response to replication stress. We hypothesize that when PARP or MRE11 are inhibited and the conditional allele of *Brca2* is deleted, cells are able to overcome the

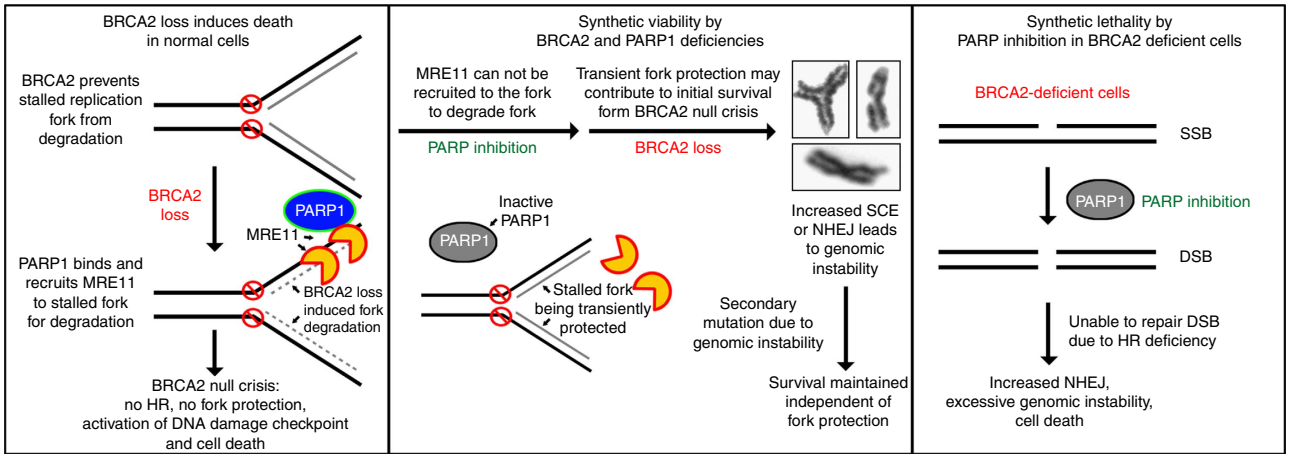

Figure 6 | Cell model of synthetic viability between BRCA2 and PARP1 deficiency. Model to explain the difference between synthetic viability and synthetic lethality associated with BRCA2 and PARP1 loss. The outcome is dependent on the order of events. When BRCA2 loss is followed by PARP inhibition or PARP1 deficiency, it results in synthetic lethality (right). In contrast, when PARP inhibition or PARP1 deficiency is followed by BRCA2 loss, it results in synthetic viability (middle).

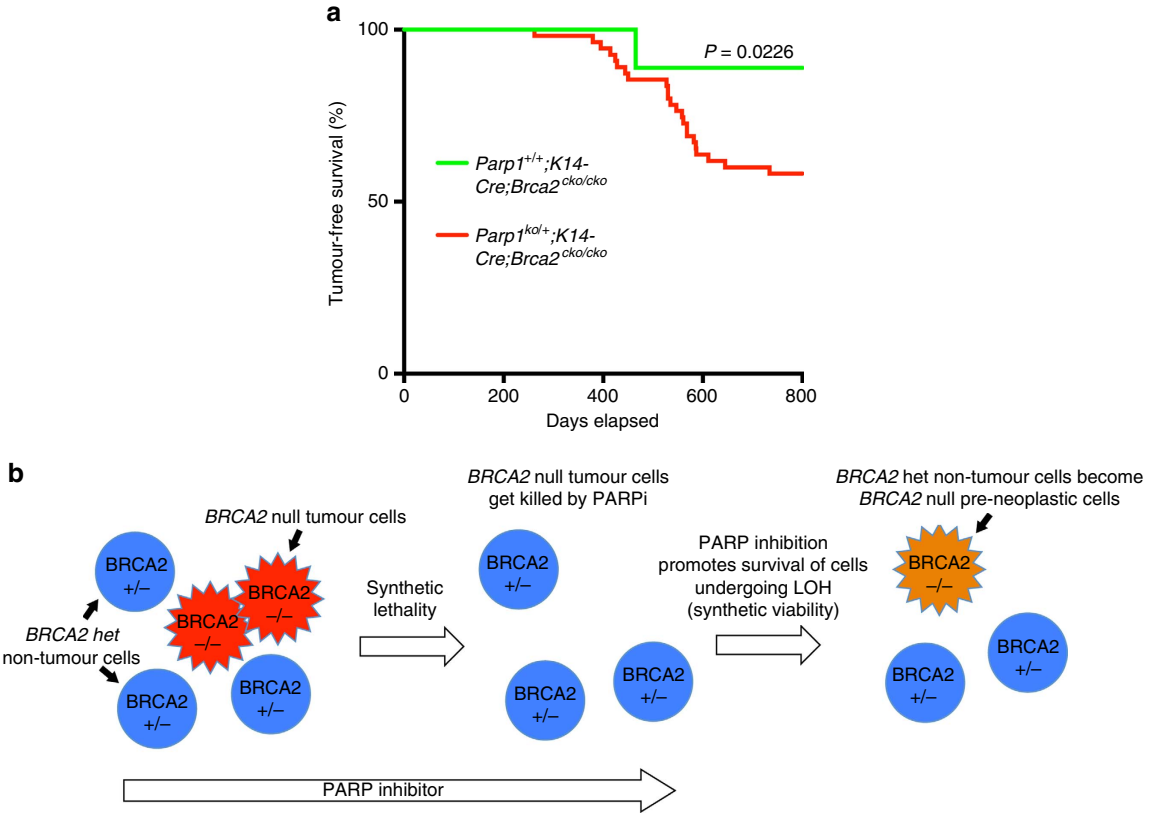

Figure 7 | *Brca2*$^{cko/cko}$ mice with *K14-Cre* are tumour prone in a *Parp1*$^{ko/+}$ background. (**a**) Kaplan–Meier curves showing tumour-free survival percentage of *K14-Cre; Brca2*$^{cko/cko}$ mice under *Parp1*$^{+/+}$ or *Parp1*$^{ko/+}$ genetic background. (**b**) Model to explain the targeting of BRCA2-deficient tumours by PARPi and the potential concern related to its role in cell survival.

BRCA2-null crisis (that is, BRCA2 loss-induced excessive fork degradation, fork collapse resulting in un-repairable DSBs causing cell death) because the replication forks are transiently protected due to defect in MRE11 recruitment. We propose that this transient fork protection may be sufficient for the initial survival. Once the cells survive the BRCA2-null crisis, their survival is no longer dependent on PARP inhibition or fork protection (Fig. 6). These results therefore suggest that the rescued cells may acquire epigenetic changes or secondary mutations perhaps through mutagenic non-homologous end joining or sister chromatid exchanges, which are indeed enhanced by PARP inhibition or PARP1 deficiency (Supplementary Fig. 4c–e)[13,31,32].

Interestingly, in an independent study, MRE11 recruitment to nascent DNA strands was shown to be dependent on PTIP and the associated histone methyltransferases MLL3 and MLL4 (ref. 33). Similar to PARP1 deficiency, PTIP loss inhibits degradation of stalled forks and rescues the viability of *Brca2*$^{ko/ko}$ mESC. An important functional consequence of fork protection associated with PTIP loss is resistance to PARPi and cisplatin in *Brca2*-deficient tumour cells that is independent of the presence of secondary reversion mutations. Similar association between fork protection and PARPi or cisplatin resistance was also observed with CHD4 loss[33,34]. Together, this study and our present study highlight the importance of fork protection in rescuing BRCA2 loss-associated phenotypes without restoration of HR.

Our ability to rescue the lethality of *Brca2*$^{ko/ko}$ cells may have important implications. We predict that in addition to killing the tumour cells, PARPi may facilitate the survival of normal *BRCA2* heterozygous cells that undergo loss of heterozygosity. These cells that will otherwise undergo apoptosis may be able to survive and have the potential to become neoplastic (Fig. 7b). Taken together, our findings provide evidence that PARPi, although lethal to HR-deficient cancers, is not innocuous in HR-proficient normal cells.

Methods

mESC culture. All mESCs were cultured on mitotically inactive SNL feeder cells in M15 media, which is Knockout DMEM media (Life Technologies) supplemented with 15% fetal bovine serum (FBS; Life Technologies), 0.00072% beta-mercaptoethanol, 100 U ml^{-1} penicillin, 100 μg ml^{-1} streptomycin and 0.292 mg ml^{-1} L-glutamine at 37 °C, 5% CO_2. PL2F7 cells were generated from AB2.2 mouse embryonic stem cell line by knocking out one copy of *Brca2* and flanking the other allele of *Brca2* with two *LoxP* sites[20].

Generation of PARP1 stable knockdown mESC clones. Two different shRNAs against mouse *Parp1* mRNA and one control shRNA (nonsense) were cloned into pSUPERIOR.retro.neo vector (Oligoengine) into BglII and HindIII restriction sites. shRNA sequences are listed in Supplementary Note 1. shRNA vectors were linearized by ScaI, 20 μg of the linearized vectors were electroporated into 1×10^7 mESCs suspended in 0.9 ml PBS using Gene Pulser (Bio-Rad) at 230 V, 500 μF. After electroporation, 2×10^4 cells were plated into 10 cm plate, and G418 selection (0.18 mg ml^{-1}) was started 24 h after electroporation. G418 was withdrawn after 5 days of selection for colonies to become visible. Individual colonies were picked into 96-well plate and PARP1 knockdown level of each clone was determined by western blot.

Generation of *Parp1* knockout clones in mESC by CRISPR-Cas9n. Small guide RNA (sgRNA) was designed within exon 2 of mouse *Parp1* gene by using CRISPR design tool at http://crispr.mit.edu. The oligonucleotide sequences are listed in Supplementary Note 1. Oligonucleotides were cloned into Cas9 nickase (Cas9n) expression vector pX335-U6-Chimeric_BB-CBh-hSpCas9n (D10A) (Addgene, plasmid #42335). Oligonucleotides were cloned into the vector to generate sgRNAs. SURVEYOR nuclease assay was performed by transfecting sgRNA into NIH3T3 cells and PCR amplifying the edited genomic region. Nuclease S was used to digest the re-annealed PCR products[35]. Primers for SURVEYOR nuclease assay are listed in Supplementary Note 1.

For sgRNA transfection in mESC, 3×10^5 mESCs were plated in 6-well plates 24 h before transfection. sgRNAs (1 μg of each) were co-transfected with pcDNA3.1 (1 μg) plasmid (Life Technologies) by using 12 μl FuGENE 6 transfection reagent (Promega). Cells were trypsinized and 1×10^4 cells were re-plated into 10 cm plate 24 h after transfection. G418 selection (0.18 mg ml^{-1}) was started 24 h after re-plating. G418 selection was performed for 5 days followed by growth in M15 media for colonies to become visible. Individual colonies were picked into 96-well plate and PCR was performed to amplify the targeted region. PCR primers are listed in Supplementary Note 1. PCR products of clones having band sizes different from WT band were purified and sequenced. PARP1 protein expression of each clone was determined by western blot.

Deletion of *Brca2 cko* allele and selection of *Brca2$^{ko/ko}$* mESC. A unit of 20 μg of PGK-Cre plasmid DNA were electroporated into 1×10^7 mESCs suspended in 0.9 ml PBS by Gene Pulser (Bio-Rad) at 230 V, 500 μF. HAT selection was started 36 h after electroporation and lasted for 5 days, followed by selection in HT media for 2 days and then normal M15 media until colonies became visible. Colonies were picked into 96-well plate. For extracting genomic DNA, colonies were lysed in 50 μl mESC buffer (10 mM Tris-HCl (pH 7.4), 10 mM EDTA, 10 mM NaCl, 5 mg ml^{-1} sodium lauroyl sarcosinate, 1 mg ml^{-1} proteinase K) at 55 °C overnight, and DNA was precipitated by 100 μl 75 mM NaCl in absolute ethanol. Genomic DNA was rinsed by 70% ethanol and digested by EcoRV at 37 °C overnight for Southern blot.

Southern blot. EcoRV-digested DNA was electrophoresed on 1% agarose gel in 1 × TBE (0.1 M Tris, 0.1 M boric acid and 2 mM EDTA, pH 8.0) and transferred to nylon membrane. DNA probe for distinguishing conditional *Brca2* allele (*cko-Brca2*, 4.8 kb) and *Brca2* knockout allele (*ko-Brca2*, 2.2 kb)[20] was labelled by [α-^{32}P]-dCTP by Prime-It II Random Primer Labeling Kit (Agilent Technologies) and hybridized with Hybond-N + nylon membrane (GE Healthcare) at 65 °C overnight. Membrane was washed twice with saline sodium citrate phosphate (SSCP) buffer containing 0.1% SDS in and exposed in phosphor image screen overnight and subsequently developed in Typhoon image scanner.

Mice and tumour pathology. *Brca2$^{ko/+}$* mice carrying a null allele of *Brca2* and *CD19-Cre* mice expressing Cre transgene under the control of CD18 promoter were used[21,36]. *K14-Cre* and *Brca2$^{cko/cko}$* mice were obtained from NCI-Frederick mouse repository (strain number:01XF1 and 01XB9, respectively)[37], *Parp1$^{ko/ko}$* mice were obtained from Jackson Laboratory (stock number: 002779)[11]. All genotyping primers are listed in Supplementary Note 1. These mice were crossed to generate mice of desired genotypes. Mice of each genotype were randomly selected for experiments. Mice necropsy was performed by NCI-Frederick Pathology and Histotechnology Laboratory. Tumours were evaluated by blindly a board-certified veterinary pathologist, who was blinded to the group allocation.

All animal studies were performed as per the guidelines outlined in the Guide for the Care and Use of Laboratory Animals and protocols approved by the NCI-Frederick Animal Care and Use Committee.

Embryo dissection and laser capture microdissection. Timed pregnancy in mice was set-up and embryos were collected at E8.5 or E10.5. Embryos were dissected according to established protocol[38]. Dissected embryos were lysed in 50 μl mESC lysis buffer at 55 °C overnight. Genomic DNA was precipitated using 3 M sodium acetate (1/10 volume) and 2 volumes of ethanol. Precipitated DNA was rinsed with 70% ethanol, resuspended in 1 × TE buffer and used for genotyping PCR. Genotyping PCR primers are listed in Supplementary Note 1.

For laser capture microdissection (LCM), whole embryos were fixed in 10% neutral buffered formalin solution (Sigma). Embryos were embedded in paraffin and were serially sectioned at 5 μm. The section adjacent to haematoxylin and eosin was mounted on LCM slide (MMI CellCut Plus from Molecular Machines & Industries) for embryo collection. LCM workflow, LCM slide preparation, target dissection and collection were carried following standard procedures[39,40]. Collected embryos were incubated in 25 μl DNA lysis buffer (Arcturus PicoPure DNA extraction Kit, Life Technologies) for 48 h at 55 °C. Genomic DNA was precipitated by adding 1 μl glycogen (Sigma), 3 M sodium acetate (1/10 volume) and 2 volumes of ethanol. DNA was precipitated at − 20 °C for at least 1.5 h. Precipitated DNA was rinsed with 70% ethanol, resuspended in 1 × TE buffer and used for genotyping PCR. Genotyping PCR primers were listed in Supplementary Note 1.

B-cell culture. Resting splenic B cells were isolated from 8- to 12-week-old mice with anti-CD43 microbeads (anti-Ly48; Miltenyi Biotech) and were cultured with lipopolysaccharide (25 μg ml^{-1}; Sigma) and interleukin-4 (5 ng ml^{-1}; Sigma) and RP105 (0.5 μg ml^{-1}; BD)[41]. Stimulated B cells were infected with retrovirus-CRE to ensure high level of deletions of *Brca2* in these cells.

MEF isolation. MEF cells were isolated from 13.5-day embryos from WT and *Parp1$^{ko/ko}$* mice. Head and liver were removed and remaining tissues were digested by 0.05% trypsin for 10 min. Embryo tissue was forced through 21 G needle and was pipetted three times for dissociation. Cells were then plated and cultured in high-glucose DMEM with 10% FBS, 100 U ml^{-1} penicillin, 100 μg ml^{-1} streptomycin and 0.292 mg ml^{-1} L-glutamine at 37 °C, 5% CO_2, 3% O_2. MEF cells were immortalized by SV40 retroviral infection.

***PARP1* and *BRCA2* knockdown in MCF10A cells.** Immortalized human mammary epithelial MCF10A cell line is a kind gift from Dr Esta Sterneck (NCI-Frederick, NIH). Cells were maintained in DMEM-F12 media (Life Technologies) containing 10% FBS, 100 U ml^{-1} penicillin, 100 μg ml^{-1} streptomycin, 0.292 mg ml^{-1} L-glutamine, 10 μg ml^{-1} insulin, 100 ng ml^{-1} choleratoxin, 20 ng ml^{-1} epidermal growth factor and 0.5 μg ml^{-1} hydrocortisone at 37 °C, 5% CO_2. Lentiviral shRNA vector against human *PARP1* (TRCN0000007930) and control shRNA (SHC202) was purchased from Sigma (MISSION shRNA). For packaging lentivirus, HEK293T cells (American Type Culture Collection) at 80% confluency were co-transfected with shRNA vector, pRSV-Rev, pMDLg-pRRE and pHCMVG. Packaging vectors were kind gifts from Dr Steven Hou (NCI-Frederick, NIH). After 72 h transfection, supernatant was collected and 0.45 μm filtered before being used for infecting MCF10A cells. After 48 h infection, MCF10A cells were subjected to 3.3 μg ml^{-1} puromycin selection for 2 days. Puromycin-resistant cells were expanded and tested for PARP1 expression. Two siRNAs against human *BRCA2* were purchased from Dharmacon (siGenome D-003462-01 and D-003462-02) and were transfected into PARP1 stable knockdown MCF10A cells by Lipofectamine 2000 (Life Technologies). After 48 h transfection, cells were used for DNA fibre assay, as well as for analysing BRCA2 protein expression by western blot.

iPOND. To perform iPOND, 1.5×10^8 cells were labelled with 10 μM EdU (Life Technologies) and treated with 4 mM HU for 4 h as indicated[42]. Cells were crosslinked with 1% formaldehyde for 10 min at room temperature, quenched with 0.125 M glycine and washed with PBS. For the conjugation of EdU with biotin azide, cells were permeabilized with 0.25% Triton X-100 in PBS buffer, and incubated in click reaction buffer (10 mM sodium-L-ascorbate, 20 μM biotin azide (Life Technologies) and 2 mM $CuSO_4$) for 2 h at room temperature. Cells were resuspended in lysis buffer (50 mM Tris-HCl (pH 8.0) and 1% SDS) supplemented with protease inhibitors (Roche), and chromatin was solubilized by sonication in a Bioruptor (Diagenode-Pico) at 4 °C for 24 min. After centrifugation, supernatants were incubated for 1 h streptavidin-MyOne C1 beads (Life Technologies). Beads were washed and captured proteins were eluted by boiling beads in 2 × NuPAGE LDS Sample Buffer (Life Technologies) containing 200 mM dithiothreitol for 40 min at 95 °C. Proteins were resolved by electrophoresis using NuPAGE Novex 4–12% Bis-Tris gels and detected by western blot with the indicated antibodies.

HR assay. HR assay was performed by gene-targeting assay[20]. Briefly, mESCs were electroporated by the targeting vector and were selected in hygromycin. Colonies were picked and targeted clones were identified by Southern hybridization.

DNA fibre assay. Cells were sequentially pulsed by 8 μg ml^{-1} CldU for 15 min for mESC and MCF10A cells, or 30 min for B cells followed by 90 μg ml^{-1} IdU for 15 min for mESC and MCF10A cells, or 30 min for B cells. Cells were then treated with 4 mM HU for 3 h before they were resuspended in PBS. A volume of 3 μl of cell suspension containing ~3×10^5 cells were mixed with 7 μl lysis buffer (200 mM Tris-HCl (pH 7.4), 50 mM EDTA, 0.5% SDS) on glass slides and incubated at room temperature for 8 min before DNA fibre was spread. Fibres were fixed in methanol and acetic acid (3:1) at 4 °C overnight, rehydrated by PBS and denatured in 2.5 M HCl for 1 h. After rinsing away HCl by PBS, slides were blocked in PBS with 5% bovine serum albumin (BSA) for 1 h and incubated with anti-BrdU antibody (Mouse, #347580, Becton Dickinson, 1:100 dilution) and anti-BrdU antibody (Rat, ab6326, Abcam, 1:500 dilution) at 4 °C overnight. Slides were rinsed with PBS with 0.1% Tween-20 (PBST) and incubated with AlexaFluo488-conjugated anti-mouse IgG secondary antibody and AlexaFluo594-conjugated anti-rat IgG secondary antibody for 1 h at room temperature. Slides were rinsed with PBST and mounted by mounting media (Prolong Gold, Invitrogen). Images were taken in Zeiss Axio Imager Z1 microscope and fibre length was measured by ImageJ software (NIH).

Protein expression and interaction studies. The following antibodies were used: anti-PARP1 (Rabbit, #9542, Cell Signaling Technology); anti-PARP2 (Rabbit, ab93416, Abcam); anti-GAPDH (Rabbit, #2118, Cell Signaling Technology); anti-ACTIN (Goat, sc-1616, Santa Cruz); anti-RAD51 (Rabbit, PC130, Calbiochem); anti-γH2AX (Mouse, 05–636, Millipore); anti-pS317 CHK1 (Rabbit, #12302, Cell Signaling Technology); anti-CHK1 (Mouse, sc-8408, Santa Cruz); anti-MRE11 (Goat, sc-5859, Santa Cruz); anti-MRE11 (Rabbit, Callen and Nussenzweig, unpublished); anti-MYC (Mouse, 631206, Clontech); anti-MYC (Rabbit, 2272, Cell Signaling Technology); anti-p53 (Mouse, 2524, Cell Signaling Technology); anti-pS15 p53 (Rabbit, 9284, Cell Signaling Technology); anti-Histone H3 (Rabbit, 9715, Cell Signaling Technology); anti-PCNA (Rabbit, 13110, Cell Signaling Technology); anti-p19ARF (Rabbit, ab80, Abcam); and anti-BRCA2 (Mouse, OP95, Millipore). For western blot, cells were lysed in SDS lysis buffer (2% SDS, 10% glycerol, 0.1 M dithiothreitol and 0.2 M Tris-HCl (pH6.8)) and subjected to SDS–PAGE gel electrophoresis, and subsequently

transferred to nitrocellulose membrane. Blots were incubated with the indicated primary antibodies at 4 °C overnight, washed by PBST and probed with corresponding horseradish peroxidase-conjugated secondary antibodies at room temperature for 2 h and subjected to ECL (Amersham). For immunofluorescence, cells were fixed with 4% paraformaldehyde, permeabilized by 0.25% Triton X-100 and blocked with 3% BSA. Cells were incubated with the indicated primary antibodies at 4 °C overnight. After washing four times with PBST, cells were incubated with AlexaFluo488-conjugated anti-rabbit IgG antibody and AlexaFluo568-conjugated anti-mouse IgG antibody (Life Technologies) at room temperature for 2 h. Nucleus was counterstained by 4,6-diamidino-2-phenylindole. Images were taken on Zeiss LSM 510 confocal microscope.

For immunoprecipitation, cells were lysed in IP buffer (30 mM Tris-HCl (pH 8.0), 75 mM NaCl, 10% glycerol and 0.5% Triton X-100) containing protease inhibitors (Complete Mini protease inhibitor cocktail tablets, Roche) at 4 °C for 15 min and subjected to centrifugation at 15,000*g* for 15 min at 4 °C. Supernatant was transferred and added 30 µl beads (Protein G sepharose 4 Fast Flow, GE Healthcare) together with 2 µg indicated antibodies and incubated on rocker at 4 °C for 4 h. Beads were rinse four times by IP buffer at 800*g* for 1 min each time. Proteins were dissociated from the beads by SDS lysis buffer and boiled at 95 °C for 10 min. For the immunoprecipitation with DNase treatment, DNase I (2 U µl^{-1}, New England Biolabs) was added to the IP buffer with the EDTA-free protease inhibitors (Complete EDTA-free protease inhibitor cocktail tablets, Roche) and IP procedures were the same as mentioned above. Uncropped images of western blot are shown in Supplementary Fig. 8.

Generation of constructs expressing mouse PARP1 fragments. Mouse full-length *Parp1* cDNA and all other fragments (N, M, WGR and CAT)[43] were PCR amplified from MGC mouse *Parp1* cDNA clone (GE Healthcare, clone ID: 2648390) and was subcloned into pcDNA3.1 (+) vector and fused with a MYC tag in the C terminus. PCR primers were listed in Supplementary Note 1. For immunoprecipitation, HEK293T cells were used for transfection. All groups were transfected by MRE11-Flag plasmid (a kind gift from Dr John Petrini, MSKCC), together with pcDNA3.1 (+) empty vector or full-length or other fragments of PARP1 by Lipofectamine 2000. After 48 h transfection, immunoprecipitation was performed by pulling down with anti-MYC antibody (Mouse, 631206, Clontech), subsequent detection by western blot was performed by indicated antibodies.

Haematopoietic stem cell assay. WT and *Brca2*$^{cko/cko}$ mice (two mice per group) were injected either by DMSO or 40 mg kg^{-1} olaparib (Selleckchem) for 10 days before their bone marrow was collected from the femur and tibia. Bone marrow was cultured in DMEM media containing 10% FBS, 100 ng ml^{-1} murine stem cell factor, 100 ng ml^{-1} human thrombopoietin, 100 ng ml^{-1} human Flt-3 ligand (hFlt-3L) and 50 ng ml^{-1} murine interleukin-6. Bone marrow cells were transduced by lentivirus expressing CRE-ires-GFP. For lentivirus packaging, HEK293T cells were transfected by lentiviral CRE-ires-GFP vector together with HIV gag-pol and VSVG vectors. After 48 h transfection, viral supernatant was collected and 0.45 µm filtered and was added to RetroNectin (25 µg ml^{-1}, T100B, Takara)-coated six-well plates. Plates were centrifuged at 2,600*g* for 2 h at 4 °C in order for the virus to attach. Supernatant was removed and plates were ready to be used for transducing bone marrow cells. Three hours after bone marrow was collected from the mice, bone marrow cells were added to the lentiviral plates. Bone marrow cells were transferred every 12 h to fresh lentiviral plates to achieve higher transduction efficiency. Four rounds of transduction were performed before the GFP-positive cells were subjected to sorting on BD FACSAria II cell sorter. Immediately after sorting, the transduced GFP-positive bone marrow cells were plated in MethoCult (StemCell Technologies, Vancouver, Canada) as per the manufacturer's instructions. The following haematopoietic growth factors were added: 100 ng ml^{-1} murine stem cell factor; 100 ng ml^{-1} human thrombopoietin; 100 ng ml^{-1} human Flt-3 ligand (hFlt-3L); 50 ng ml^{-1} murine interleukin-6 and 30 ng ml^{-1} murine interleukin-3 (Peprotech Inc. Rocky Hill, NJ, USA). DMSO or olaparib (100 ng ml^{-1}) was also added. Cells were plated at a density of 1.375×10^4 cells per ml per plate in 35 mm cell dishes (Nunc) in triplicates and were incubated at 37 °C, 5% CO_2 for 7–10 days. In all, 15–20 random images per plate were taken under ×2 objective and colony number was counted manually. Average colony number per image was calculated and was multiplied by 50 to get the total colony number per plate. For genotyping the colonies, individual colonies were picked and lysed by the mESC buffer as mentioned above at 55 °C overnight. Genomic DNA was precipitated by adding 1 µl glycogen, 3 M sodium acetate (1/10 volume) and 2 volumes of ethanol. DNA was precipitated at −20 °C for at least 1.5 h. Precipitated DNA was rinsed with 70% ethanol, resuspended in water and used for genotyping PCR. Genotyping PCR primers were listed in Supplementary Note 1.

Cell cycle analysis. Cells were trypsinized, resuspended and fixed in 70% ethanol at 4 °C for 30 min. Cells were then rinsed by PBS, resuspended and incubated in PI and RNase staining buffer (BD) at 37 °C for 30 min. Cell cycle distribution was analysed in BD FACSCalibur flow cytometer.

Karyotyping of mESC. The metaphases were arrested by incubation with Colcemid (KaryoMax Colcemid Solution, Invitrogen, Carlsbad, Calif., USA) (10 µg ml^{-1}) 3 h before harvest. Cells were collected and treated with hypotonic solution (KCl 0.075 M) for 15 min at 37 °C and fixed with methanol:acetic acid 3:1. Slides were prepared and chromosomal aberrations were analysed.

Quantitative PCR. qPCR to determine *Brca2* genomic deletion in B cells was performed by using iTaq Universal SYBR Green Supermix (Bio-Rad). qPCR reaction was run on Mx3000P qPCR system (Agilent Technologies). Primers are listed in Supplementary Note 1.

Statistics. Statistics was performed by two-tailed *t*-test, Mann–Whitney test, two-tailed Fisher's exact test or χ^2-test unless otherwise specified. All error bars represent s.d. Statistical tests were justified appropriate for every figure. The data are normally distributed, and the variance between groups that are being statistically compared is similar. $P<0.05$ was considered statistically significant. No statistical methods or criteria were used to estimate sample size or to include or exclude samples. The investigators were not blinded to the group allocation during the experiments unless otherwise specified.

Data availability. This is to confirm that all relevant data are available from the authors on request.

References

1. Venkitaraman, A. R. Linking the cellular functions of BRCA genes to cancer pathogenesis and treatment. *Annu. Rev. Pathol.* **4,** 461–487 (2009).
2. Schlacher, K. *et al.* Double-strand break repair-independent role for BRCA2 in blocking stalled replication fork degradation by MRE11. *Cell* **145,** 529–542 (2011).
3. Schlacher, K., Wu, H. & Jasin, M. A distinct replication fork protection pathway connects Fanconi anemia tumor suppressors to RAD51-BRCA1/2. *Cancer Cell* **22,** 106–116 (2012).
4. Bryant, H. E. *et al.* Specific killing of BRCA2-deficient tumours with inhibitors of poly(ADP-ribose) polymerase. *Nature* **434,** 913–917 (2005).
5. Farmer, H. *et al.* Targeting the DNA repair defect in BRCA mutant cells as a therapeutic strategy. *Nature* **434,** 917–921 (2005).
6. Fong, P. C. *et al.* Inhibition of poly(ADP-ribose) polymerase in tumors from BRCA mutation carriers. *N. Engl. J. Med.* **361,** 123–134 (2009).
7. Kaelin, Jr W. G. The concept of synthetic lethality in the context of anticancer therapy. *Nat. Rev. Cancer* **5,** 689–698 (2005).
8. Rouleau, M., Patel, A., Hendzel, M. J., Kaufmann, S. H. & Poirier, G. G. PARP inhibition: PARP1 and beyond. *Nat. Rev. Cancer* **10,** 293–301 (2010).
9. Teloni, F. & Altmeyer, M. Readers of poly(ADP-ribose): designed to be fit for purpose. *Nucleic Acids Res.* **44,** 993–1006 (2016).
10. Luijsterburg, M. S. *et al.* PARP1 Links CHD2-Mediated chromatin expansion and H3.3 deposition to DNA Repair by non-homologous end-joining. *Mol. Cell* **61,** 547–562 (2016).
11. Wang, Z. Q. *et al.* Mice lacking ADPRT and poly(ADP-ribosyl)ation develop normally but are susceptible to skin disease. *Genes Dev.* **9,** 509–520 (1995).
12. Murai, J. *et al.* Trapping of PARP1 and PARP2 by clinical PARP inhibitors. *Cancer Res.* **72,** 5588–5599 (2012).
13. Patel, A. G., Sarkaria, J. N. & Kaufmann, S. H. Nonhomologous end joining drives poly(ADP-ribose) polymerase (PARP) inhibitor lethality in homologous recombination-deficient cells. *Proc. Natl Acad. Sci. USA* **108,** 3406–3411 (2011).
14. Lord, C. J. & Ashworth, A. BRCAness revisited. *Nat. Rev. Cancer* **16,** 110–120 (2016).
15. Ledermann, J. *et al.* Olaparib maintenance therapy in platinum-sensitive relapsed ovarian cancer. *N. Engl. J. Med.* **366,** 1382–1392 (2012).
16. Ledermann, J. *et al.* Olaparib maintenance therapy in patients with platinum-sensitive relapsed serous ovarian cancer: a preplanned retrospective analysis of outcomes by BRCA status in a randomised phase 2 trial. *Lancet Oncol.* **15,** 852–861 (2014).
17. Ogino, H. *et al.* Loss of Parp-1 affects gene expression profile in a genome-wide manner in ES cells and liver cells. *BMC Genomics* **8,** 41 (2007).
18. Tichy, E. D. *et al.* Mouse embryonic stem cells, but not somatic cells, predominantly use homologous recombination to repair double-strand DNA breaks. *Stem Cells Dev.* **19,** 1699–1711 (2010).
19. Min, W. *et al.* Poly(ADP-ribose) binding to Chk1 at stalled replication forks is required for S-phase checkpoint activation. *Nat. Commun.* **4,** 2993 (2013).
20. Kuznetsov, S. G., Liu, P. & Sharan, S. K. Mouse embryonic stem cell-based functional assay to evaluate mutations in BRCA2. *Nat. Med.* **14,** 875–881 (2008).
21. Sharan, S. K. *et al.* Embryonic lethality and radiation hypersensitivity mediated by Rad51 in mice lacking Brca2. *Nature* **386,** 804–810 (1997).
22. Bryant, H. E. *et al.* PARP is activated at stalled forks to mediate Mre11-dependent replication restart and recombination. *EMBO J.* **28,** 2601–2615 (2009).
23. Ray Chaudhuri, A. *et al.* Topoisomerase I poisoning results in PARP-mediated replication fork reversal. *Nat. Struct. Mol. Biol.* **19,** 417–423 (2012).

24. Ying, S., Hamdy, F. C. & Helleday, T. Mre11-dependent degradation of stalled DNA replication forks is prevented by BRCA2 and PARP1. *Cancer Res.* **72,** 2814–2821 (2012).
25. Bunting, S. F. *et al.* 53BP1 inhibits homologous recombination in Brca1-deficient cells by blocking resection of DNA breaks. *Cell* **141,** 243–254 (2010).
26. Polato, F. *et al.* CtIP-mediated resection is essential for viability and can operate independently of BRCA1. *J. Exp. Med.* **211,** 1027–1036 (2014).
27. Haince, J. F. *et al.* PARP1-dependent kinetics of recruitment of MRE11 and NBS1 proteins to multiple DNA damage sites. *J. Biol. Chem.* **283,** 1197–1208 (2008).
28. Sirbu, B. M. *et al.* Analysis of protein dynamics at active, stalled, and collapsed replication forks. *Genes Dev.* **25,** 1320–1327 (2011).
29. Bouwman, P. *et al.* 53BP1 loss rescues BRCA1 deficiency and is associated with triple-negative and BRCA-mutated breast cancers. *Nat. Struct. Mol. Biol.* **17,** 688–695 (2010).
30. Dantzer, F. *et al.* Involvement of poly(ADP-ribose) polymerase in base excision repair. *Biochimie* **81,** 69–75 (1999).
31. Schreiber, V. *et al.* A dominant-negative mutant of human poly(ADP-ribose) polymerase affects cell recovery, apoptosis, and sister chromatid exchange following DNA damage. *Proc. Natl Acad. Sci. USA* **92,** 4753–4757 (1995).
32. Wang, Z. Q. *et al.* PARP is important for genomic stability but dispensable in apoptosis. *Genes Dev.* **11,** 2347–2358 (1997).
33. Ray Chaudhuri *et al.* Replication Fork stability confers chemoresistance in BRCA-deficient cells. *Nature* **535,** 382–387 (2016).
34. Guillemette, S. *et al.* Resistance to therapy in BRCA2 mutant cells due to loss of the nucleosome remodeling factor CHD4. *Genes Dev.* **29,** 489–494 (2015).
35. Ran, F. A. *et al.* Genome engineering using the CRISPR-Cas9 system. *Nat. Protoc.* **8,** 2281–2308 (2013).
36. Rickert, R. C., Roes, J. & Rajewsky, K. B lymphocyte-specific, Cre-mediated mutagenesis in mice. *Nucleic Acids Res.* **25,** 1317–1318 (1997).
37. Jonkers, J. *et al.* Synergistic tumor suppressor activity of BRCA2 and p53 in a conditional mouse model for breast cancer. *Nat. Genet.* **29,** 418–425 (2001).
38. Nagy, A. in *Manipulating the Mouse Embryo: A Laboratory Manual* 3rd edn (Cold Spring Harbor Laboratory Press, 2003).
39. Golubeva, Y. & R. K. in *Methods in Molecular Biology* (ed. Kozlov, S. V.) (Humana, 2009).
40. Golubeva, Y., Salcedo, R., Mueller, C., Liotta, L. A. & Espina, V. in *Cell Imaging Techniques Methods and Protocols* (ed. Taatjes, D. J. & Roth, J.) 213–257 (Humana, 2013).
41. Callen, E. *et al.* ATM prevents the persistence and propagation of chromosome breaks in lymphocytes. *Cell* **130,** 63–75 (2007).
42. Sirbu, B. M., Couch, F. B. & Cortez, D. Monitoring the spatiotemporal dynamics of proteins at replication forks and in assembled chromatin using isolation of proteins on nascent DNA. *Nat. Protoc.* **7,** 594–605 (2012).
43. Xie, S. *et al.* Timeless interacts with PARP-1 to promote homologous recombination repair. *Mol. Cell* **60,** 163–176 (2015).

Acknowledgements

We thank members of our laboratory for helpful discussions and suggestions. We also thank the staff of NCI-Frederick Pathology and Histotechnology Laboratory for help with tumour analysis. We thank Dr Terry Yamaguchi (NCI-Frederick, NIH) for help with phenotypic analysis of mouse embryos. We thank Dr John Petrini and Shawn Fox (MSKCC) for MRE11 expression construct. This research was sponsored by the Intramural Research Program, Center for Cancer Research, National Cancer Institute, US National Institutes of Health. X.D. received Department of Defense, Breast Cancer Research Program, Postdoctoral Fellowship (W81XWH-13-1-0362).

Author contributions

X.D. designed and performed experiments, analysed data and wrote the manuscript; A.R.C. and E.C. designed and performed experiments and analysed data; K.B. performed experiments and analysed data; K.D.K. and J.R.K. helped with HSC experiments and data analysis; Y.P., L.C., S.S., T.S., A.D., H.M., A.T.M. and N.W. helped with experiments; B.K.M. assisted with animal studies; S.B. performed cytogenetic analysis; E.B., K.A. and S.E.M. helped with data analysis; A.N. contributed to experimental design, data analysis and manuscript writing; S.K.S. conceived and supervised the study, analysed data and wrote the manuscript.

Additional information

Supplementary Information accompanies this paper at http://www.nature.com/naturecommunications

Competing financial interests: The authors declare no competing financial interests.

Reprints and permission information is available online at http://npg.nature.com/reprintsandpermissions/

How to cite this article: Ding, X. *et al.* Synthetic viability by BRCA2 and PARP1/ARTD1 deficiencies. *Nat. Commun.* 7:12425 doi: 10.1038/ncomms12425 (2016).